Copyright

by

Katrina Marie Czenkusch

2014

The Dissertation Committee for Katrina Marie Czenkusch Certifies that this is the approved version of the following dissertation:

Evaluation of Transport and Transport Stability in Glassy Polymer Membranes

Committee:

Don Paul, Supervisor

Benny Freeman, Co-Supervisor

Christopher Ellison

Isaac Sanchez

Wei Li

Evaluation of Transport and Transport Stability in Glassy Polymer Membranes

by

Katrina Marie Czenkusch, B.S.

Dissertation

Presented to the Faculty of the Graduate School of

The University of Texas at Austin

in Partial Fulfillment

of the Requirements

for the Degree of

Doctor of Philosophy

The University of Texas at Austin

May 2014

Dedication

To my family and friends without whom this would not have been possible.

Acknowledgements

A journey this long would have been impossible without the assistance of numerous people. This simple acknowledgement is insufficient thanks for the gifts they have given me. Nevertheless, I want to address them here.

First, I want to thank my parents, Jim and Jan, who have supported me through all of life's twists and turns. Your guidance and unwavering love are an inspiration to me and remind me of how I want to live my life. No matter what I needed, or what time of night I needed it, you were always there. I hope, always, to make you proud. My baby brother, Kevin, also deserves a mention. No matter how much we argue and compete, you've always had my back, and I hope you know that I've got yours. I could not hope for a better family and I could not have done this without you.

I cannot calculate the worth of the friends I've had over the years. Whether through playing games, hanging out, going dancing, or dragging me off into the wilds of Connecticut, you have kept me sane. There is no way I can list all of the people who have been dear to me, but a couple of special thanks are in order. First, to Julie and Edgar, who reminded me of what true friendship is like: always supportive, always ready to listen, always prepared to remind me what's important. Without you, I would not be here. Second, to Kelly, my oldest friend, effectively my sister, throughout all of our years, you've always been ready to share the good times and the bad, even if it was hard sometimes to follow behind you. To Chris and Hector, you gave me so much of the best in yourselves, and I will always remember the joy you gave me. To all of my friends, I wish you nothing but the best, now and forever.

I have been further blessed with amazing colleagues over the last several years. You have made this process infinitely better just by being yourselves. I could not have asked for better research partners, or lunch partners. I will miss working with you all, but I know you have great things waiting for you. Although I cannot thank you each individually, know that I truly appreciate your friendship. To Claudio, Kris, and Norman, thank you for your wisdom and your assistance over the years, I would have been lost without you. Finally, thanks to my advisors, Dr. Freeman and Dr. Paul, for the advice they gave me and their patience and wisdom.

Evaluation of Transport and Transport Stability in Glassy Polymer Membranes

Katrina Marie Czenkusch, Ph.D.

The University of Texas at Austin, 2014

Supervisors: Don Paul and Benny Freeman

Both novel membrane materials with better separation characteristics and a better fundamental understanding of membrane transport stability are needed to improve the competitiveness of commercial membrane separations. In this work, the effect of a novel moiety, hexafluoroalcohol, on the gas transport properties of an aromatic polyimide membrane are evaluated. The hexafluoroalcohol group increases the membrane's fractional free volume, which increases the membrane's permeability to all gases. Additionally, the HFA-containing polyimide shows resistance to plasticization by carbon dioxide. However, ideal selectivity for several gas pairs is unchanged by the inclusion of hexafluoroalcohol and the increase in the polymer's fractional free volume. This lack of selectivity loss with increasing free volume is attributed to hydrogen bonding between the hexafluoroalcohol and imide groups, which reduces chain mobility.

The ethanol dehydration characteristics of a so-called "TR" polymer are also evaluated in this work. TR polymers are heterocyclic, aromatic polymers synthesized by a solid-state, high temperature condensation from ortho-functional polyimides. Pervaporation studies on a representative TR polymer film demonstrate that the material has separation properties that exceed those of a commercial ethanol dehydration membrane. The transport properties of the TR film, combined with high thermal and

chemical stability characteristic of these materials, make TR polymers promising materials for high-temperature, high-water content ethanol dehydration.

Finally, the physical aging and plasticization of cellulose triacetate, the dominant natural gas purification membrane, is presented. Although this material has been used industrially for over 30 years, the physical aging and plasticization of the material, particularly in sub-micron films, has never been studied. Although cellulose triacetate does show physical aging behavior, as observed by permeability decreases over time, cellulose triacetate thin films do not show accelerated aging. Furthermore, the plasticization of thin cellulose triacetate films is reduced, rather than increased as seen in other polymers. The unusual transport stability of thin cellulose triacetate films may be due to their complex, semi-crystalline morphology, which, due to the thermal instability of the material, may not be thermally controlled.

Table of Contents

List of Tables xv

List of Figures xvi

Chapter 1 Introduction 1

1.1 Introduction 1

1.2 Goals and Organization of this Thesis 2

1.3 References 4

Chapter 2 Background 7

2.1 Membrane Separations 7

2.1.1 Gas Separations 7

2.1.2 Pervaporation and Vapor Permeation 10

2.1.3 General Membrane Design Considerations 13

2.1.4 Effect of Chemical Structure on Transport Properties 17

2.1.4.1 Glass Transition Temperature 17

2.1.4.2 Backbone Structure 18

2.1.4.3 Side Chain and Backbone Substitution 19

2.2 Polymer Properties and Phenomena 20

2.2.1 The Glassy State and Physical Aging 20

2.2.1.1 Definition of the Glass Transition Temperature and the Glassy State 20

2.2.1.2 Introduction to Physical Aging 21

2.2.1.3 Physical Aging and Transport Properties 23

2.2.1.4 Physical Aging in Confined Systems 23

2.2.2 CO_2 Plasticization and Conditioning in Polymer Membranes 25

2.2.2.1 Definition of Plasticization and Conditioning in Membranes 25

2.2.2.2 Plasticization of Polymer Membranes 26

2.2.2.3 Thin Film Plasticization 27

2.2.3 Crystallinity in Polymer Membranes 29

2.2.3.1 Crystallinity in Polymers 29
2.2.3.2 Impact of Crystallinity on Transport in Polymer Membranes 30
2.2.3.3 Impact of Crystallinity on Physical Aging.....30
2.3 Background on Materials Used in This Work 31
2.3.1 Aromatic Polyimides 31
2.3.2 "TR" Polymers.....31
2.3.3 Cellulose Acetate 32
2.4 Industrial Separations.....35
2.4.1 Ethanol Dehydration for Biofuel 35
2.4.2 Natural Gas Purification 36
2.5 References.....37
Chapter 3: Materials and Experimental Methods 44
3.1 Materials 44
3.1.1 HAB-6FDA and HAB-6FDA TR 44
3.1.2 HFA-MDA-6FDA.....45
3.1.3 Cellulose Acetate 46
3.2 Film Preparation.....47
3.2.1 Thick Film (>10 μm) Casting.....47
3.2.2 Thin Film (<1 μm) Casting.....48
3.2.3 Measuring Film Thickness.....50
3.3 Polymer Characterization.....51
3.3.1 Density.....51
3.3.2 Fractional Free Volume 51
3.3.3 Water Uptake 51
3.3.4 Gel Fraction 52
3.3.5 Fourier Transform Infrared Spectroscopy (FTIR) 52
3.3.6 Thermal Stability 53
3.3.7 Glass Transition 53
3.3.8 Crystallinity.....54

3.4 Pervaporation Experiments 54
3.4.1 Equipment 54
3.4.2 Procedure 55
3.4.3 Calculations 56
3.5 Gas Permeation Measurements 57
3.5.1 Equipment 57
3.5.2 Procedure 58
3.5.3 Physical Aging 59
3.5.4 Plasticization 60
3.6 Gas Sorption Measurements 61
3.6.1 Pressure Decay Gas Sorption Apparatus 61
3.6.2 Sorption Isotherm Measurements 61
3.7 References 62
Chapter 4: Ethanol Dehydration with Thermally Rearranged Polyimides 64
4.1 Overview 64
4.2 Experimental Details 64
4.2.1 Materials 64
4.2.2 Pervaporation Experiments 65
4.3 Results and Discussion 66
4.3.1 Effect of Temperature and Feed Composition on Water Transport 66
4.3.2 Effect of Temperature on Mixed-Feed Permeability 69
4.3.3 Comparison of HAB-6FDA to Materials in the Pervaporation Literature 70
4.3.4 Comparison of HAB-6FDA TR to Commercial Vapor Permeation Membrane 73
4.4 Conclusions 77
4.5 Note on Subsequent Work 77
4.6 References 78

Chapter 5: Gas Transport and Thermal Stability of HFA-Containing Aromatic Polyimide 79
5.1 Overview and Introduction 79
5.2 Experimental Details....80
5.2.1 Materials 80
5.2.2 Glass Transition Temperature....81
5.2.3 Thermal Stability 82
5.3 Results....83
5.3.1 HFA-MDA-6FDA Characterization 83
5.3.2 Hydrogen-Bonding in the HFA Group 85
5.3.3 Pure Gas Permeability for Non-Plasticizing Gases 86
5.3.4 CO_2 Plasticization in HFA-MDA-6FDA....87
5.3.5 Effect of HFA Group on Gas Solubility and Diffusivity....90
5.3.6 High Temperature Reaction in HFA-MDA-6FDA and HFA-MDA-BAF....94
5.3.6.1 TGA Results for HFA-MDA-6FDA....94
5.3.6.2 TGA Results for HFA-MDA-BAF and Evaluation of Solvent Removal....97
5.3.6.3 Changes in T_g of HFA-MDA-6FDA....100
5.3.6.4 Chemical Analysis by FT-IR 101
5.4 Conclusions....106
5.5 References....106
Chapter 6 Characterization, Physical Aging and Plasticization in Cellulose Triacetate 110
6.1 Overview....110
6.2 Experimental Details....110
6.2.1 Materials 110
6.2.2 Casting Details....110
6.2.3 Crystallinity Determination 111
6.3 Results....112
6.3.1 Initial Characterization and Comparison with Literature 112

6.3.1.1 Density 112
6.3.1.2 Thermal Stability 114
6.3.1.3. Wide Angle X-Ray Diffraction 115
6.3.1.4 Effect of Sample Form on Thermal Characteristics 118
6.3.1.5 Permeability of CTA at 10 atm Compared to Literature 119
6.3.1.6 Solubility 120
6.3.1.7 Plasticization of CTA Relative to Literature 122
6.3.1.8 Methane Plasticization 124
6.3.2 Determination of Proper Annealing Conditions for CTA 125
6.3.3 Effect of Annealing on Crystallinity and Thermal Behavior of CTA 128
6.3.4 Effect of Casting Procedure on Crystallinity and Thermal Behavior of CTA 130
6.3.5 Effect of Annealing Temperature on Permeability and Aging of CTA 133
6.3.6 Effect of Thickness on Permeability and Aging 134
6.3.7 Effect of Thickness on CO_2 Plasticization 145
6.4 Conclusions 147
6.5 References 148

Chapter 7: Conclusions and Recommendations 150
7.1 Conclusions 150
7.1.1 Ethanol Dehydration 150
7.1.2 Effect of Hexafluoroalcohol on Gas Transport 151
7.1.3 Physical Aging and Plasticization in Cellulose Triacetate 152
7.2 Recommendations for Future Work 153
7.2.1 Chemical Structure Optimization for Ethanol Dehydration with TR Polymers 153
7.2.2 Other High-Temperature, Chemically Aggressive Separations 155
7.2.3 HFA Moiety in Other Polymer Backbones 156
7.2.4 High Temperature Reaction Products of HFA-MDA-6FDA and HFA-MDA-BAF 157

7.2.5 Effect of Acetate Group Distribution on Transport Properties in Cellulose Acetates....158
7.2.6 Decouple Thickness and Crystallinity in Cellulose Acetates ...159
7.3 References....160
References....163
Vita 174

List of Tables

Table 2.1 Components and pressure ranges of interest for natural gas purification membranes. Data were provided by Rick Peters at Cameron International. 37

Table 5.1 Summary of basic characterization of HFA-MDA-6FDA and reported values for MDA-6FDA.[26,27] 83

Table 5.2 Permeability at 10 atm and 35°C for HFA-MDA-6FDA. Pure gas selectivity at 35°C and 10 atm for selected gas pairs. 87

Table 5.3 Permeability, diffusivity and solubility for HFA-MDA-6FDA and MDA-6FDA.[26,27] 92

Table 6.1 Thermal properties of CTA hollow fiber, thick film and powder. T_c is the temperature of the crystallization peak, ΔH_c is the enthalpy of crystallization, T_m is the temperature of melting and ΔH_m is the enthalpy of melting. 119

Table 6.2 Permeability of several gases in Cameron CTA and Eastman samples[3]120

Table 6.3 Casting conditions where R stands for spinning speed in RPM, A is acceleration on a Laurell Technologies Spin Coater and T is spinning time in minutes. The 310nm sample used the listed spinning conditions sequentially three times. ℓ_0 is the thickness measured prior to annealing and ℓ_a is the adjusted film thickness.....135

List of Figures

Figure 2.1 Schematic of gas separation membrane where p is the pressure of the reservoir, C is the concentration of gas in the membrane face 8

Figure 2.2 Schematics of a) pervaporation and b) vapor permeation systems 10

Figure 2.3 CO_2/CH_4 upper bound plot. Dots represent individual samples, the lines are the empirical front.[9,10] 14

Figure 2.4 Selectivity versus permeate composition as a function of pressure ratio calculated from Equation 2.15 with a feed concentration of 60%$_{wt}$ ethanol and pressure ratios of 10, 20, 50 and 152.....16

Figure 2.5 Schematic of specific volume or specific enthalpy of a polymer above and below T_g.....21

Figure 2.6 Physical aging of thin polysulfone films tracked by permeability decay[67] 25

Figure 2.7 Permeability response of a cellulose acetate membrane in a plasticizing (CO_2) and non-plasticizing (CH_4) feed.[94] 27

Figure 2.8 Plasticization pressure curves of thick (20 μm) and thin (182 nm) Matrimid® films.[93] 28

Figure 2.9 Long CO_2 exposure times in Matrimid® thin (220nm) and thick (20 μm) films.[93].....29

Figure 2.10 Schematic showing the conversion of an ortho-hydroximide to polybenzoxazole TR polymer. 32

Figure 2.11 Chemical structures of cellulose and cellulose triacetate (DS = 3). ...33

Figure 2.12 Carigali Hess natural gas purification membrane operating data from 2008-2009. Plot generously provided by Rick Peters at Cameron International. 35
Figure 3.1 Chemical structure of HAB-6FDA and HAB-6FDA TR 45
Figure 3.2: Chemical structure of HFA-MDA-6FDA 46
Figure 3.3 Chemical structure of cellulose triacetate....47
Figure 3.4: Schematic of the pervaporation apparatus....55
Figure 3.5: Construction of a permeation sample....55
Figure 3.6: Schematic of the gas permeability system 57
Figure 3.7: Schematic of the pressure decay system 61
Figure 4.1: Chemical structure of HAB-6FDA and the resulting HAB-6FDA TR65
Figure 4.2: Water permeability of HAB-6FDA TR in a pure water feed and a 60:40%$_{wt}$ ethanol:water feed. 67
Figure 4.3: HAB-6FDA TR pure water flux and water and ethanol flux in a 60:40%$_{wt}$ feed....68
Figure 4.4: HAB-6FDA TR water and ethanol permeability in 60:40%$_{wt}$ feed 69
Figure 4.5: HAB-6FDA TR water/ethanol selectivity in 60:40%$_{wt}$ ethanol:water feed 70
Figure 4.6: Effect of temperature on water permeability vs. water/ethanol selectivity trade-off....72
Figure 4.7: Effect of polymer structure on water permeability vs. water/ethanol selectivity 72
Figure 4.8: Water permeance reported for UBE hollow fiber[7] and HAB-6FDA TR as measured and estimated for 0.1 μm film. 74

Figure 4.9: Ethanol permeance reported for UBE hollow fiber[7] and HAB-6FDA TR as measured and estimated for 0.1 micron film. 75

Figure 4.10 Water/ethanol selectivity for HAB-6FDA TR and UBE hollow fiber.[7]76

Figure 5.11 Effect of water/ethanol selectivity on permeate ethanol concentration with a 60%$_{wt}$ ethanol feed. Pressure ratios of 10, 20, 50 and 152 were used to generate these results. 77

Figure 5.1 Chemical structures of polymers used in this study, HFA-MDA-6FDA and HFA-MDA-BAF, and the reference material, MDA-6FDA. 81

Figure 5.2 Thermogravimetric analysis for HFA-MDA-6FDA. Heating rate was 5°C/min with N_2 atmosphere. 84

Figure 5.3 Transmission FT-IR spectrum of HFA-MDA-6FDA.....85

Figure 5.4 Permeability of He, O_2, N_2 and CH_4 in HFA-MDA-6FDA at 35°C as a function of upstream pressure. 86

Figure 5.5 a. Upstream CO_2 pressure during the plasticization experiment. b. CO_2 permeability at 35°C in HFA-MDA-6FDA. Red (filled) symbols are the first pressure cycle. Blue (open) symbols are the second pressure cycle. Arrows pointing up indicate a pressurization step; circles indicate high pressure hold; arrows pointing down indicate a depressurization step.88

Figure 5.6 a. Permeability of O_2 and CH_4 as a function of time after CO_2 exposure. b. Permeability of O_2 and CH_4 normalized by pre-exposure permeability as a function of time post-CO_2 exposure.....90

Figure 5.7 Sorption isotherms for N_2, O_2, CH_4 and CO_2 at 35°C for HFA-MDA-6FDA.....91

Figure 5.8 Upper bound plots for a. CO_2/CH_4, b. CO_2/N_2 and c. O_2/N_2. HFA-MDA-6FDA is a red, filled circle. MDA-6FDA data are open circles.[26,27] Grey symbols indicate data from the original upper bound plots.[37] .94

Figure 5.9 Chemical structures of HFA-MDA-6FDA and the proposed product, HFA-MDA-6FDA T. 95

Figure 5.10 Isothermal TFA results for HFA-MDA-6FDA. Samples were first held at 150°C for 30 minutes (not shown). Time zero was set to the beginning of the 5°C/minute ramp to the listed temperature. 97

Figure 5.11 TGA of HFA-MDA-BAF using a 5°C/minute heating rate under a N_2 purge 97

Figure 5.12 Chemical structures of HFA-MDA-BAF and proposed product, HFA-MDA-BAF T.....98

Figure 5.13 High resolution TGA results for HFA-MDA-BAF and the derivative of the mass loss curve.....99

Figure 5.14 3 sequential DSC scan results for HFA-MDA-6FDA. Sample dried in DSC at 150°C for 30 minutes (not shown). Heats performed at 10°C/minute with quench cools at 30°C/minute (not shown) between heats. 101

Figure 5.15 FT-IR spectra for HFA-MDA-6FDA and HFA-MDA-BAF.....103

Figure 5.16 FT-IR spectra for HFA-MDA-6FDA and the thermal treated sample, HFA-MDA-6FDA-T.....104

Figure 5.17 FT-IR spectra of HFA-MDA-BAF and the thermally treated sample, HFA-MDA-BAF-T. 105

Figure 6.1 Magnetic Suspension Balance sample mass versus surrounding Helium density. Sample mass taken from intercept (i.e., under vacuum) and sample volume taken from the slope of the best fit line. 113
Figure 6.2 Density of Cameron CTA (DS 2.99), Eastman samples of varying DS[3] and other literature values[5] 114
Figure 6.3 Thermal stability of CTA measured by TGA using a 5°C/minute and a 10°C/minute heating rate. 115
Figure 6.4 WAXD of CTA a. powder and b. 20 μm film sample. Tests were performed by Dr. Steven Swinnea at the Texas Materials Institute.117
Figure 6.5 CH_4 sorption isotherms Eastman[3] and Cameron cellulose acetate thick film samples. Sorption isotherms have been calculated on the basis of a. total polymer volume and b. mass of amorphous polymer (Equation 6.2).121
Figure 6.6 CO_2 sorption isotherms in Eastman[3] and Cameron cellulose acetate thick film samples. Sorption isotherms have been calculated on the basis of a. total polymer volume and b. mass of amorphous polymer (Equation 6.2). 122
Figure 6.7 Plasticization pressure curves for Cameron CTA and Eastman DS 2.84[3] 123
Figure 6.8 CO_2 plasticization pressure curves normalized by initial permeability at 1 atm for Eastman cellulose acetates[3] and Cameron CTA. 123
Figure 6.9 CH_4 plasticization pressure curve in CTA. 124
Figure 6.10 DSC results for the first and second heat of CTA. 126
Figure 6.11 Storage and tan δ results for CTA using testing conditions described in Chapter 3. 127

Figure 6.12 CTA mass loss during isothermal hold at 250°C for a. 15 hours and b. 15 minutes. 128
Figure 6.13 DSC results demonstrating the effect of different annealing conditions on thick film thermal behavior and crystallinity. 129
Figure 6.14 DSC results demonstrating the effect of different annealing conditions on thin film thermal behavior and crystallinity. 130
Figure 6.15 DSC results demonstrating the effect of thickness on the thermal behavior and crystallinity of unannealed films. The thicknesses of the thick and thin films were 60 μm and 200 nm respectively. 132
Figure 6.16 DSC results demonstrating the effect of thickness on the thermal behavior and crystallinity of annealed films. The thicknesses of the thick and thin films were 60 μm and 200 nm respectively. 133
Figure 6.17 O_2 permeability as a function of time in CTA thin films annealed at 185°C and 250°C. Black lines are drawn to guide the eye and have the same slope. 134
Figure 6.18 O_2 permeability in thick and thin CTA films as a function of time. 136
Figure 6.19 N_2 data as a function of thickness and aging time. 137
Figure 6.20 CH_4 permeability in CTA as a function of thickness and aging time 137
Figure 6.21 O_2 permeability in CTA normalized by initial permeability as a function of aging time and film thickness 139
Figure 6.22 N_2 permeability in CTA normalized by the initial permeability as a function of film thickness and aging time. 140
Figure 6.23 CH_4 permeability of CTA normalized by the initial permeability as a function of aging time and film thickness. 141

Figure 6.24 O_2 permeability normalized by initial permeability for CTA films and bulk PSF,[11] PPO[11] and Matrimid[11] as a function of aging time.....141
Figure 6.25 Relative O_2 permeability at 500 hours as a function of 1/thickness in CTA and polymers reported by Huang et al.[11] and Rowe et al.[12].....142
Figure 6.26 Relative O_2 permeability at 500 hours as a function of 1/thickness in CTA and polymers reported by Huang et al.[11] and Rowe et al.[12].....143
Figure 6.27 Plasticization pressure curve for 280 nm and 10 μm CTA films annealed at 185°C and aged for 100 hours prior to experiment.....145
Figure 6.28 CO_2 permeability in CTA and Matrimid[15] with 2 hour holds at each pressure. 146
Figure 6.29 Plasticization behavior of CTA and report polymer thin films[15] during a 2 hour pressure step experiment. 147

Chapter 1 Introduction

1.1 INTRODUCTION

A membrane's ability to selectively permeate one penetrant over another was first reported by Abbé Nollet in the 1700's.[1] Since that time, research in membrane science has driven the development of both a deeper fundamental understanding of small molecule transport through membranes and the development of commercial separation membranes.[2] The market for membrane-based separations is expected to continue growing,[3] driven by the contributions of numerous researchers in areas including materials science and process engineering.[2,4–17] Current industrial applications for membranes include: removal of CO_2 and other contaminants from natural gas, recovery of N_2 from air, and recovery of H_2 from refineries and ammonia plants.[2] Relative to conventional separation technologies (e.g., distillation and amine sorption), membrane units typically have lower capital and operating costs, smaller footprints, and require less maintenance, and also do not require toxic chemicals.[18] Current membrane research targets include new membrane materials and processes for separations such as: organic solvent dehydration (e.g., ethanol/water), carbon capture from flue gas, and olefin/paraffin separations (e.g., ethylene/ethane).[2]

Acid gas (e.g., CO_2 and H_2S) removal from natural gas provides a large market for membrane separations.[2,3] Worldwide usage of natural gas is over 95 trillion scf/yr.[18] Raw natural gas is primarily composed of CH_4, but it is frequently contaminated by water, carbon dioxide and higher hydrocarbons.[19] Such contaminants must be removed from natural gas to meet pipeline specifications, maintain heating value, recover the higher hydrocarbons[19] and re-inject the CO_2 for enhanced oil recovery.[18,19] In 2008, the demand for natural gas drove a $5 billion/year market for new gas separation

equipment.[18] Membrane units are utilized primarily for wells with high CO_2 contents, but the majority of the natural gas purification market is dominated by amine sorption.[18] To compete more effectively with amine sorption units, new membrane materials with better transport properties and a better fundamental understanding of membrane performance stability need to be developed.

The market for fuel-grade ethanol is a rapidly growing field.[20] The current biofermentation processes used to generate ethanol result in 3-15%$_{wt}$ ethanol in water.[21] To be used as fuel, this mixture must be dehydrated to greater than 99%$_{wt}$ ethanol.[22] Fuel-grade ethanol production is complicated by the water-ethanol azeotrope that exists at approximately 96%$_{wt}$ ethanol.[23] The current industrial process for producing fuel-grade ethanol uses two distillation columns to concentrate the ethanol to approximately 93%$_{wt}$ and then uses molecular sieve columns to create the final product.[24] This process has large heating requirements and, depending on the inlet ethanol concentration, the energy required to perform the separation can exceed the heating value of the ethanol produced.[21] The current limiting factor for ethanol dehydration membrane development is a lack of materials that are sufficiently stable in the high temperature water and ethanol feeds.[9,16] Novel materials with excellent transport abilities and high thermal and chemical stability are needed to develop this market opportunity.

1.2 Goals and Organization of this Thesis

This dissertation covers topics in two areas of membrane science, the development of new membrane materials with targeted properties and the study of the transport stability in a current material. The overarching goal of this work is to contribute to the development of new membrane applications both by contributing novel materials

and by improving the understanding of the fundamental material science that governs membrane behavior.

This dissertation is divided into seven chapters, including this introduction, which introduces and motivates the work. The second chapter provides background on several topics important to this dissertation. The chapter opens with a brief review of small molecule transport through non-porous membranes. Background on physical aging, plasticization and crystallinity in polymers is presented next. Finally, a brief introduction to the families of materials studied in this work and details of the relevant commercial separations are provided.

Chapter 3: Materials and Experimental Methods identifies the specific materials used in this work and details the processing of those materials. Also, experimental procedures used in sample preparation and measurements of the properties reported in later chapters are detailed.

Chapter 4: Ethanol Dehydration with Thermally Rearranged Polyimides details the evaluation of the so-called "TR" polymers[25] for their ethanol dehydration potential. Experimental results for a representative material are presented and then compared to both state-of-the-art materials in the literature[16] and a commercial membrane.[26] The TR polymer was found to have excellent transport properties and, when combined with the high thermal and chemical stability characteristic of these materials,[27–29] is a promising material for ethanol dehydration.

Chapter 5: Gas Transport and Thermal Stability of HFA Containing Polyimide evaluates the influence of the hexafluoroalcohol (HFA) moiety on the gas transport in an aromatic polyimide. Although this moiety has received attention in other fields for its ability to create strong intermolecular interactions,[30–39] its effect on gas transport has never been evaluated. Inclusion of the hexafluoroalcohol group improved the

permeability of all gases through the film. Furthermore, the hexafluoroalcohol-containing polyimide showed resistance to high pressure CO_2.

Chapter 6: Characterization, Physical Aging and Plasticization in Cellulose Triacetate reports the gas transport stability in commercial cellulose triacetate (CTA) films. Specifically, the physical aging and plasticization of thick (>10 μm) and thin (<1 μm) CTA films is reported. Unlike previously reported materials, [40–42] cellulose triacetate does not show accelerated physical aging or enhanced plasticization in thin films. Efforts to understand this departure from the expected behavior are founded on material and morphology characterization which indicate that the morphology of the CTA films may be the origin of the unusual behavior.

Finally, Chapter 7: Conclusions and Recommendations presents the major conclusions of this work along with recommendations for future studies to further enhance the field of membrane science.

1.3 REFERENCES

(1) Nollet, J. A. *J. Memb. Sci.* **1995**, *100*, 1–3.

(2) Sanders, D. F.; Smith, Z. P.; Guo, R.; Robeson, L. M.; McGrath, J. E.; Paul, D. R.; Freeman, B. D. *Polymer* **2013**, *54*, 4729–4761.

(3) Baker, R. W. *Ind. Eng. Chem. Res.* **2002**, *41*, 1393–1411.

(4) Yampolskii, Y. P. *Macromolecules* **2012**, *45*, 3298–3311.

(5) Wijmans, J.; Baker, R. W. *J. Memb. Sci.* **1995**, *107*, 1–21.

(6) White, L. S. In *Membrane Gas Separation*; Yampolskii, Y.; Freeman, B., Eds.; John Wiley & Sons, Ltd: Chichester, UK, 2010; pp. 313–332.

(7) Stannett, V. T.; Koros, W. J.; Paul, D. R.; Lonsdale, H. L.; Baker, R. W. In *Advances in Polymer Science*; Advances in Polymer Science; Springer Berlin Heidelberg: Berlin, Heidelberg, 1979; Vol. 32, pp. 69–121.

(8) Sridhar, S.; Smitha, B.; Aminabhavi, T. M. *Sep. Purif. Rev.* **2007**, *36*, 113–174.

(9) Shao, P.; Huang, R. Y. M. *J. Memb. Sci.* **2007**, *287*, 162–179.

(10) Paul, D. R. In *Comprehensive Membrane Science and Engineering, Volume 1*; Drioli, E.; Giorno, L., Eds.; Elsevier B.V., 2010; Vol. 1, pp. 75–90.

(11) Mondal, M. K.; Balsora, H. K.; Varshney, P. *Energy* **2012**, *46*, 431–441.

(12) Koros, W. J.; Paul, D. R. In *Proceedings 6th Annual Industrial Energy Conservation Technology Conference*; 1984; p. 525.

(13) Koros, W. J.; Paul, D. R. In *Synthetic Membranes*; Chenoweth, M. B., Ed.; MMI Press, 1986; pp. 155–189.

(14) Klopffer, M. H.; Flaconnèche, B. *Oil Gas Sci. Technol.* **2001**, *56*, 223–244.

(15) Ghosal, K.; Freeman, B. D. *Polym. Adv. Technol.* **1994**, *5*, 673–697.

(16) Chapman, P. D.; Oliveira, T.; Livingston, A. G.; Li, K. *J. Memb. Sci.* **2008**, *318*, 5–37.

(17) Bernardo, P.; Drioli, E.; Golemme, G. *Ind. Eng. Chem. Res.* **2009**, *48*, 4638–4663.

(18) Baker, R. W.; Lokhandwala, K. *Ind. Eng. Chem. Res.* **2008**, *47*, 2109–2121.

(19) Sanders, E. S. *Annu. Conv. Proc. - Gas Process. Assoc.* **2004**, *83*, 270–312.

(20) Sissine, F. *Energy Independence and Security Act of 2007: a summary of major provisions*; Library of Congress: Washington, 2007.

(21) Côté, P.; Noël, G.; Moore, S. *Desalination* **2010**, *250*, 1060–1066.

(22) Huang, Y.; Ly, J.; Nguyen, D.; Baker, R. W. *Ind. Eng. Chem. Res.* **2010**.

(23) *Azeotropic Data - III*; Horsley, L. H., Ed.; American Chemical Society, 1973.

(24) Vane, L. M.; Alvarez, F. R.; Huang, Y.; Baker, R. W. *J. Chem. Technol. Biotechnol.* **2009**, *85*, 502–511.

(25) Park, H. B.; Jung, C. H.; Lee, Y. M.; Hill, A. J.; Pas, S. J.; Mudie, S. T.; Van Wagner, E.; Freeman, B. D.; Cookson, D. J. *Science* **2007**, *318*, 254–258.

(26) Nakagawa, K.; Kusuki, Y.; Ninomiya, K. *Proc. Fourth Int. Congr. Pervaporation Process. Chem. Ind.* **1989**, 250–260.

(27) Evers, R. C.; Arnold, F. E.; Helminiak, T. E. *Macromolecules* **1981**, *14*, 925–930.

(28) Kubota, T.; Nakanishi, R. *Polym. Lett.* **1964**, *2*, 655–659.

(29) Tullos, G.; Mathias, L. *Polymer* **1999**, *40*, 3463–3468.

(30) Hall, D. S.; Osborn, B.; Patterson, K.; Burns, S. D.; Willson, C. G. In *Advances in Resist Technology and Processing XVIII*; Houlihan, F. M., Ed.; 2001; Vol. 4345, pp. 1066–1072.

(31) Kishimura, S.; Endo, M.; Sasago, M. *J. Photopolym. Sci. Technol.* **2002**, *15*, 625–628.

(32) Fender, N.; Brock, P. J.; Chau, W.; Bangsaruntip, S.; Mahorowala, A. P.; Wallraff, G. M.; Hinsberg, W. D.; Larson, C. E.; Ito, H.; Breyta, G.; Burnham, K.; Truong, H. D.; Lawson, P.; Allen, R. D. In *Advances in Resist Technology and Processing XVIII*; Houlihan, F. M., Ed.; 2001; Vol. 4345, pp. 417–427.

(33) Lee, S. H.; Kim, J. W.; Kim, J. W.; Oh, S. K.; Park, C. S.; Lee, J. Y.; Kim, S. S.; Lee, J. W.; Kim, D.; Kim, J.; Ban, K. Do; Bok, C. K.; Moon, S. C. In *Advances in Resist Materials and Processing Technology XXIV*; Lin, Q., Ed.; 2007; Vol. 6519, pp. 1–9.

(34) Allen, A. D.; Breyta, G.; Brock, P.; DiPietro, R.; Sanders, D.; Sooriyakumaran, R.; Sundberg, L. K. *J. Photopolym. Sci. Technol.* **2006**, *19*, 569–572.

(35) Snow, A. W.; Sprague, L. G.; Soulen, R. L.; Grate, J. W.; Wohltjen, H. *J. Appl. Polym. Sci.* **1991**, *43*, 1659–1671.

(36) Grate, J. W.; Kaganove, S. N.; Patrash, S. J.; Craig, R.; Bliss, M. *Chem. Mater.* **1997**, *9*, 1201–1207.

(37) Grate, J. W. *Chem. Rev.* **2008**, *108*, 726–745.

(38) Masser, K. A.; Runt, J. *Macromolecules* **2010**, *43*, 6414–6421.

(39) Yang, X.; Painter, P. C.; Coleman, M. M.; Pearce, E. M.; Kwei, T. K. *Macromolecules* **1992**, *25*, 2156–2165.

(40) Huang, Y.; Paul, D. R. *Polymer* **2004**, *45*, 8377–8393.

(41) Rowe, B. W.; Freeman, B. D.; Paul, D. R. *Polymer* **2009**, *50*, 5565–5575.

(42) Horn, N. R.; Paul, D. R. *Polymer* **2011**, *52*, 1619–1627.

Chapter 2 Background

2.1 Membrane Separations

2.1.1 Gas Separations

In the early 1800's, both Graham[1] and Mitchell[2] demonstrated that gas molecules can pass through non-porous rubber films. Furthermore, due to the lack of a monotonic correlation between the transport rate through the films and the known gas phase diffusion coefficients of the penetrants, Graham noted that transport through a polymer film must be based on both a chemical interaction parameter as well as the diffusion rate.[1] From these observations arose the solution-diffusion model, wherein a penetrant molecule first dissolves into the upstream face of a film, diffuses through the film, and then evaporates off the downstream surface. [3] Von Wroblewski used empirical observations of the effect of film thickness and gas pressure on the transport rate to define the permeation rate, or flux, as follows:[4]

$$N = P\frac{\Delta p}{l} \tag{2.1}$$

where N is penetrant flux, P is the permeability, Δp is the pressure difference across the membrane and l is the membrane thickness.

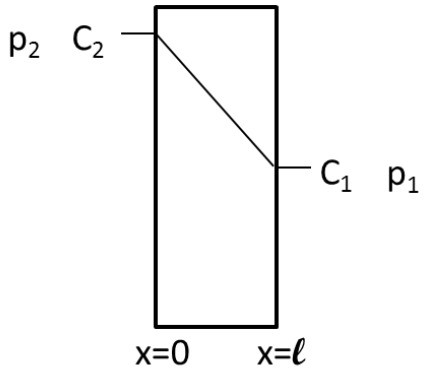

Figure 2.1 Schematic of gas separation membrane where p is the pressure of the reservoir, C is the concentration of gas in the membrane face

The system may also be considered from a fundamental transport perspective. A typical membrane process can be depicted as shown in Figure 2.1, where the membrane exists between two gas reservoirs and the pressure of the upstream is higher than the downstream. The gas flux, N, from the upstream to the downstream is defined by Fick's first law[5] (Equation 2.2).

$$N = \left(\frac{-D_{loc}}{1-w}\right)\frac{dC}{dx} \tag{2.2}$$

where N is the penetrant flu, D_{loc} is the binary mutual diffusion coefficient of the gas in the polymer, w is the gas mass fraction in the polymer, x is the distance across the film and C is the gas concentration in the film.

When Equation 2.2 is solved with the appropriate boundary conditions and combined with the empirical observations of von Wroblewski (Equation 2.1), the steady state permeability of a gas in a membrane may be written[4]:

$$P = \left(\frac{C_2 - C_1}{p_2 - p_1}\right)D \tag{2.3}$$

where P is permeability, C is the gas concentration in the membrane, p is the pressure, the subscript 1 represents the downstream side of the membrane, while the subscript 2 represents the upstream side and D is the average effective diffusion coefficient.

Finally, the typical form of the solution-diffusion model equation utilizes the assumption that the downstream reservoir is at sufficiently low pressures that both C_1 and p_1 are negligible relative to C_2 and p_2.[4] Since the concentration in the face of the membrane divided by the external pressure to that face is defined as the solubility coefficient, S,[5] the solution-diffusion model is generally written as follows:

$$P = S * D \tag{2.4}$$

where P is permeability, S the solubility coefficient and D the average diffusion coefficient.

Permeability, as defined above, is a material property of a membrane-gas pair and is a measure of gas throughput through the membrane. Permeability is a function of a thermodynamic equilibrium term, S, and a kinetic diffusion coefficient, D. The solubility of gases in a polymer generally scales with a measure of penetrant condensability, such as critical temperature, although penetrant-matrix interactions also play a role.[4] The gas diffusivity is primarily dependent on penetrant size because a diffusional step occurs only when a large enough transient gap opens between the polymer chains.[4]

The final parameter typically used to characterize gas transport in a polymer is the polymer's ability to selectively permeate one gas relative to another. The pure gas selectivity, α, is typically defined as the ratio of the permeability of the more permeable component, P_A, to that of the less permeable component, P_B (Equation 2.5).[5]

$$\alpha = \frac{P_A}{P_B} = \frac{S_A}{S_B} * \frac{D_A}{D_B} \tag{2.5}$$

2.1.2 Pervaporation and Vapor Permeation

Pervaporation and vapor permeation are two related membrane techniques for separating vapors. Pervaporation (Figure 2.2a) has a liquid feed that contacts the membrane. A portion of the feed dissolves into the membrane, diffuses across and evaporates on the low pressure, downstream side. Vapor permeation (Figure 2.2b) is similar, except that the feed is in the vapor phase. Although these membrane processes follow the solution-diffusion model described in the previous section, thermodynamic modeling is used to account for the increased non-idealities that are common in pervaporation and vapor permeation separations as well as the fact that pervaporation and vapor permeation measurements are typically done using mixed feeds. A summary of the derivation of the appropriate equations follows, though a detailed derivation may be found elsewhere.[6]

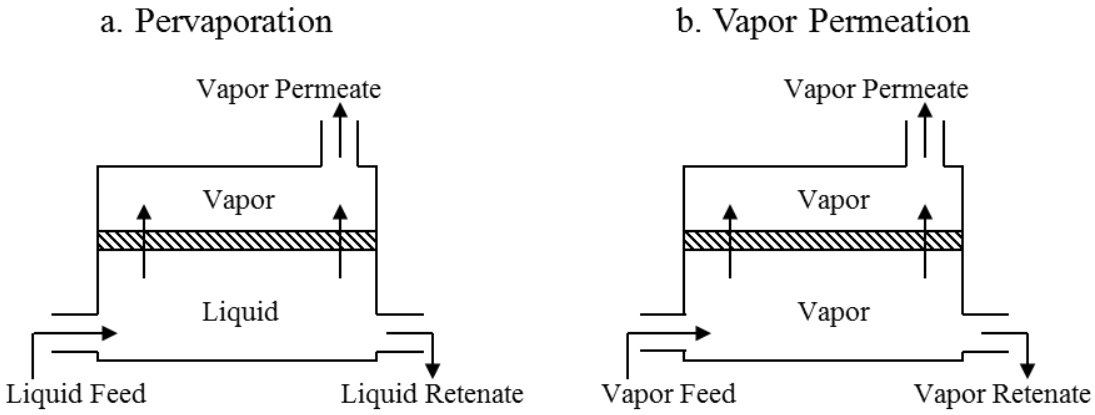

Figure 2.2 Schematics of a) pervaporation and b) vapor permeation systems

The fundamental driving force for all membrane processes is a difference in chemical potential across the membrane.[6] Thus the steady state flux across the membrane, N_i, can be written in terms of a phenomenological constant, L_i, and the change in chemical potential across the membrane, $d\mu_i/dx$, (Equation 2.6). [6]

$$N_i = -L_i \frac{d\mu_i}{dx} \tag{2.6}$$

By assuming an isothermal process, a linear fugacity coefficient profile across the membrane, negligible concentration polarization and utilizing the equivalence of fugacity between the membrane face and the external solution, the flux equation can be rewritten[6]:

$$N_i = \frac{\Lambda_i}{l}\left(\hat{f}_i^F - \hat{f}_i^P\right) \tag{2.7}$$

where Λ_i is the permeability of i, $\widehat{f_i}$ is the fugacity of i in either the feed, ^{F}, or the permeate, ^{P}.

The fundamental difference between Equation 2.7 and Equation 2.1 is that the non-idealities are separated from the material parameter, Λ_i. This equation is equally valid for both pervaporation and vapor permeation, however, the method of expressing the fugacity of the feed, $\hat{f}_i^F$, depends on the state of the feed.[6]

$$Liquid: \hat{f}_i = \gamma_i x_i \hat{\phi}_i^{sat} p_i^{sat} \exp\left(\frac{\int_{p_i^{sat}}^{p} V_i dp}{RT}\right) \tag{2.8}$$

$$Vapor: \hat{f}_i = \phi_i x_i p \tag{2.9}$$

where γ_i is the activity coefficient of species i in solution, x_i is the mole fraction of i in the feed, $\hat{\phi}_i^{sat}$ is the fugacity coefficient of saturated liquid, p_i^{sat} is the vapor pressure at the feed temperature, V_i is the liquid molar volume of i, R is the gas constant, T is temperature, and ϕ_i is the fugacity coefficient of i in solution.

By inserting the appropriate definitions of fugacity into Equation 2.7, the permeability, Λ_i, can be calculated from flux data. In most pervaporation and vapor permeation systems, several additional simplifications can be made. First, the variation

in the liquid phase molar volume with pressure may typically be neglected,[6] and the resulting exponential term, the Poynting factor, may be assumed to be unity in essentially all pervaporation and vapor permeation measurements.[6] Additionally, since the pressures, even on the feed side, are low enough that the ideal gas law is a good approximation, the fugacity coefficients may be assumed to be 1.[6] Finally, since the permeate side is maintained at near vacuum in the experimental set up, the permeate pressure, p^p, may be assumed to be 0.[6] Thus the simplified equations for permeability that will be used in this text are:

$$Pervaporation: \Lambda_i = \frac{N_i^{PV} * l}{\gamma_i^F x_i^F p_i^{sat}} \tag{2.10}$$

$$Vapor\ Permeation: \Lambda_i = \frac{N_i^{VP} * l}{x_i^F p^F} \tag{2.11}$$

Once the permeability has been calculated by the appropriate equation, the selectivity, α, may be defined analogously to Equation 2.5 (Equation 2.12). However, because much of the pervaporation and vapor permeation literature reports fluxes instead of permeabilities, a term called the separation factor, α_{SF}, is more frequently used (Equation 2.13). Both the flux and the separation factor are dependent on process conditions. [7]

$$\alpha_{ideal} = \frac{\Lambda_A}{\Lambda_B} \tag{2.12}$$

$$\alpha_{SF} = \frac{x_A^F / x_B^F}{x_A^P / x_B^P} \tag{2.13}$$

where x_i is the fraction of component i in either the feed, F, or the permeate, P.

To derive the permeability equations given in Equations 2.10 and 2.11, it was necessary to assume that concentration polarization was negligible.[6] Concentration polarization occurs when one component in a mixture permeates enough faster than the

other component that the feed on the upstream membrane face becomes depleted in the faster permeating component.[8] This lowers the driving force for the depleted component and thus lowers its apparent permeability. [8] Concentration polarization can be minimized by appropriate experimental design, i.e., introducing mixing on the upstream reservoir or by using a sufficient feed rate for a flowing system. [8]

2.1.3 General Membrane Design Considerations

An ideal membrane material would have both high permeability and selectivity. However, in 1991, Robeson found an empirical front in the performance of known polymers when the membrane selectivity was plotted against the permeability of the more permeable component on a log-log plot.[9,10] An example of this relationship is shown in Figure 2.3. This empirical front was termed the "upper bound", which was described by the following equation.

$$\alpha_{A/B} = \frac{\beta_{A/B}}{P_A^{\lambda_{A/B}}} \tag{2.14}$$

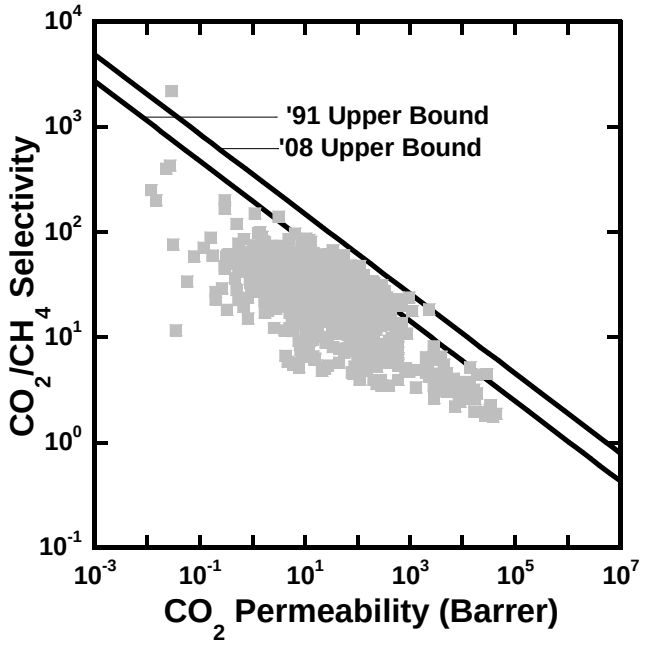

Figure 2.3 CO_2/CH_4 upper bound plot. Dots represent individual samples, the lines are the empirical front.[9,10]

A theoretical understanding of the upper bound was advanced by Freeman in 1999, where the slope of a given upper bound, $\lambda_{A/B}$, could be predicted with no adjustable parameters based on the difference in diameter of the gases being considered.[11] This implies that the slope of the upper bound arises from the strongly size sieving nature of the glassy materials that typically define the upper bound. The front factor, $\beta_{A/B}$, was found to depend on the free volume and the relative solubility of the penetrant gases, and could be estimated with only one adjustable parameter. [11] After the 1991 upper bound paper[9] was published, much of the literature focused on materials which approached or even surpassed the upper bound. In 2008, Robeson published an updated correlation which demonstrated the same trade-off relationship, although the limits had been pushed to higher performance.[10] Selecting a membrane for a particular separation is a matter of

choosing the best combination of selectivity and permeability for the economics of the separation.

Another consideration when selecting the targeted membrane transport properties are any inherent limitations due the overall process design. In a binary mixture, the concentration of the more permeable component in the permeate stream is a function of both the membrane selectivity and the pressure ratio (p^F/p^P) across the membrane (Equation 2.15).[8]

$$n_{i\ell} = \frac{\phi}{2}\left[n_{i0} + \frac{1}{\phi} + \frac{1}{1-\alpha} - \sqrt{\left(n_{i0} + \frac{1}{\phi} + \frac{1}{\alpha - 1}\right)^2 - \frac{4\alpha n_{i0}}{(\alpha - 1)\phi}}\right] \qquad 2.15$$

where n_i is the component i concentration on the upstream, subscript 0, or downstream, subscript l, side of the membrane, ϕ is the pressure ratio across the membrane (i.e., feed pressure/permeate pressure) and α is the membrane selectivity.

Equation 2.15 demonstrates that, for a given pressure ratio, as membrane selectivity increases, downstream purity will approach a limit based on the pressure ratio (Figure 2.4). Since an increase in membrane selectivity is tied to a decrease in permeability,[11] due to the trade-off described above, at a given pressure ratio, there exists an optimum selectivity which gives a reasonable product purity with maximum permeability.

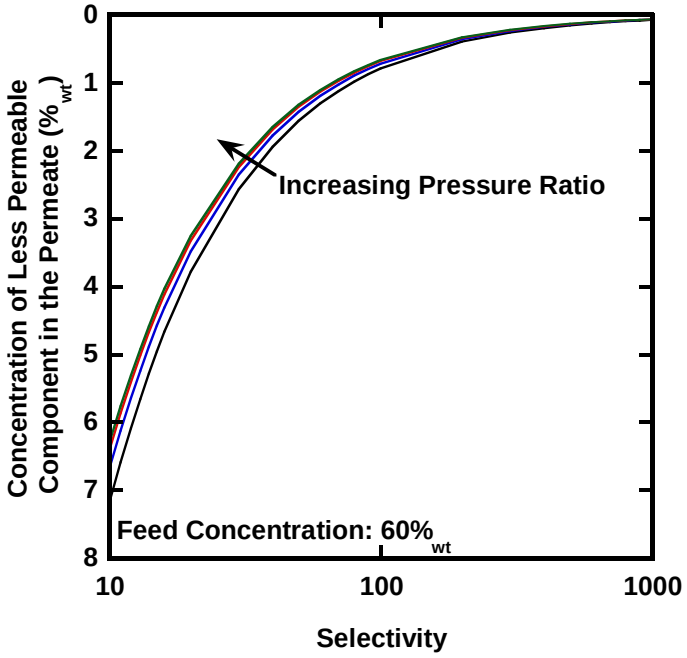

Figure 2.4 Selectivity versus permeate composition as a function of pressure ratio calculated from Equation 2.15 with a feed concentration of 60%$_{wt}$ ethanol and pressure ratios of 10, 20, 50 and 152.

In addition to sufficient transport properties, a membrane material must be stable over the module's lifetime. In the case of glassy gas separation membranes, the stability concerns arise primarily from physical aging and plasticization, which will be discussed in some detail in later sections (2.2.1 and 2.2.2 respectively). In an ethanol/water separation, there are additional concerns of thermal and chemical stability. Ethanol dehydration membranes will likely be run at temperatures over 100°C and pressures of a few bar.[12] At these conditions, many membranes could be chemically degraded by water or ethanol.[7] As the membrane degrades, it would be expected that the transport properties would also degrade.

A final consideration is that the material must be processable. Although the relevant material property for comparing permeation between materials is permeability, the relevant process parameter is flux. To minimize the membrane area required to treat a given feed stream, the membrane thickness should be minimized.[13] In practice, the solution is to use asymmetric membranes that have a very thin (i.e., ~100 nm) dense layer supported by a porous support that contributes little to mass transfer resistance.[8,13] These asymmetric membranes are produced by solution-based processing into either hollow fibers or spiral wound modules.[8] Thus, for a material to be of commercial interest for a membrane separation, it must be solution processable and form stable, asymmetric membranes.

2.1.4 Effect of Chemical Structure on Transport Properties

The influence of chemical structure on transport properties has been, and continues to be, a very active field of research.[14–18] In the search for high performance materials, a thorough understanding of the structure/property relationships allows for smarter material design. The following section is a brief overview of some of the more relevant effects of chemical structure on transport properties.

2.1.4.1 Glass Transition Temperature

Whether the membrane is above or below its glass transition temperature at use conditions is one of the primary properties that control transport properties. Rubbery polymers have higher molecular mobility than glassy polymers and so the activation energy of diffusion is correspondingly lower.[4] A lower activation energy of diffusion reduces the polymer's ability to differentiate between molecules based on size.[4] Thus, if it is desirable for a large molecule to permeate faster than a smaller molecule, a rubbery polymer, which separates primarily based on solubility differences, would be more

effective.[4] However, in many separations, such as natural gas purification, it is desirable to permeate the smaller molecule, which makes rigid, glassy structures more attractive.[4] Furthermore, as described above, glassy polymers frequently have a better combination of permeability and selectivity and define the upper bound.[10] The following discussion will focus on the chemical moieties for high productivity glassy membranes, which are the focus of this dissertation.

2.1.4.2 Backbone Structure

The permeability of a polymer scales with the fractional free volume in the polymer such that increasing the polymer's free volume will typically increase its permeability to all gases. Fractional free volume (FFV), defined below (Equation 2.16)[19,20], is a measure of the void space inside the polymer

$$FFV = \frac{V - V_o}{V} \text{ where } V_0 = 1.3 \sum V_w \tag{2.16}$$

where V is the sample's specific volume, V_0 is the occupied volume calculated as shown and V_w is the van der Waal's volume as calculated from group contribution methods.[19–21]

However, as mentioned above, chain rigidity is one of the factors influencing the ability of a polymer to discriminate between penetrants based on size, and, as the polymer's free volume increases, the barriers to chain rotation often decrease. Thus, to develop a structure with a good combination of permeability and selectivity, it is desirable to include groups that increase the free volume, but hinder chain motion.[22]

Many glassy polymers of interest to the gas separation literature have largely aromatic backbones. The aromatic groups are stable, rigid structures that provide a good basis for separation membranes. In addition, it is typically desirable to have the backbone connections para substituted.[23,24] It has been shown in numerous systems, including polysulfones, polyimides and polyesters, that meta-substituted rings have lower

chain mobility and higher chain packing.[23,25] Although the reduction in chain mobility might be advantageous for certain separations, meta-substituted rings show consistently lower permeability, solubility and diffusivity.[4,23–26] The lower packing density of the para-substituted structures is typically attributed to the availability of an aromatic ring rotation which could carve out additional free volume in the structure.[4] The experimental results are supported by recent modeling results.[26]

Additionally, increasing the barriers to rotation between the aromatic rings tends to improve membrane performance.[4] For example, changing from an ether (-O-) or methylene (-CH_2-) connection between aromatic rings to a isopropylidene (-$C(CH_3)_2$-) hinders the rotation around the connecting bonds.[27,28] Hindering chain rotation will typically reduce packing efficiency and improve permeability.[4] Going from the hydrocarbon isopropylidene (-$C(CH_3)_2$-) to a hexafluoroisopropylidene (-$C(CF_3)_2$-) further opens the structure, often with little loss in selectivity as the large trifluoromethyl groups strongly hinder chain mobility. [27,28] Hexafluoroisopropylidene moieties are frequently included in high performing membranes.[10]

2.1.4.3 Side Chain and Backbone Substitution

As with designing a glassy membrane backbone, promising side chains and backbone substitutions are typically bulky groups which increase the fractional free volume and/or increase the chain rigidity.[4] Typically the same group will cause both effects to some degree and so the exact performance result can be difficult to predict.[4] For example, methyl groups substituted onto the aromatic rings will tend to both open up additional free volume and hinder aromatic rotation.[25,29,30] Trifluoromethyl and larger fluorinated hydrocarbon chains have shown the unusual result of not only increasing the free volume, but also dramatically increasing the solubility coefficients.[30]

Trimethylsilane groups are another bulky substiuent that has been shown to increase solubility and diffusion coefficients, and thus, permeability, due to large increases in free volume.[4,31–33] Conversely, polar or hydrogen bonding groups have a tendency to reduce the free volume and hinder chain mobility by creating strong intermolecular interactions.[4,34] Finally, in aromatic polymers, symmetric substitution on the aromatic ring leads to higher permeability, while asymmetric substitution tends to reduce permeability.[4,30,35]

2.2 Polymer Properties and Phenomena

2.2.1 The Glassy State and Physical Aging

2.2.1.1 Definition of the Glass Transition Temperature and the Glassy State

One of the most important characteristics of a polymer is the glass transition, T_g, where the amorphous region of the polymer takes on the characteristics of the glassy state, i.e., rigidity, stiffness and sometimes brittleness.[36] As a polymer melt cools, eventually a temperature, T_g, is reached where there is too little energy for long-range, or segmental, motion and the polymer chains are frozen in place.[36] The glass transition is similar to a second order transition, appearing as a change in slope in a temperature vs. specific volume graph (Figure 2.5).[36] The glass transition has been shown to be a kinetic phenomenon, where the value of T_g found depends on the timescale of the measurement (i.e., a faster cooling rate results in a higher apparent T_g). Polymers are not the only materials that form glasses. However, due to their high molecular weights, they form glasses at relatively high temperatures.[37]

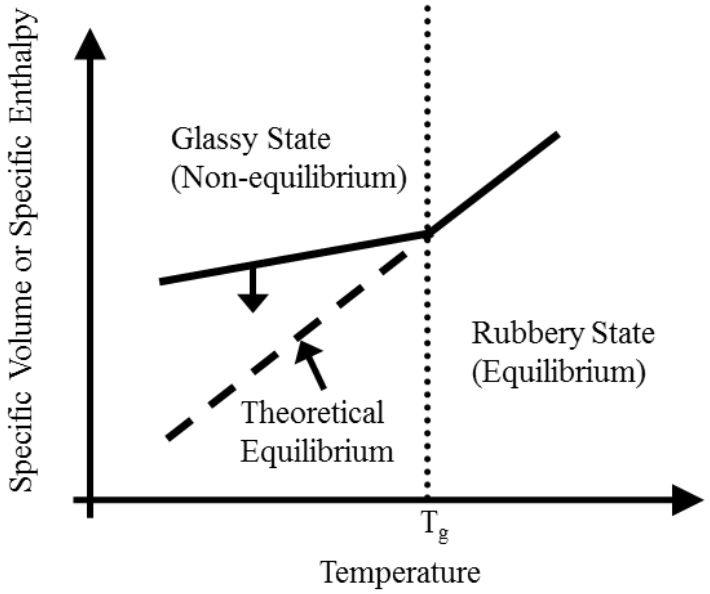

Figure 2.5 Schematic of specific volume or specific enthalpy of a polymer above and below T_g

2.2.1.2 Introduction to Physical Aging

Physical aging is the term used to describe the physical change in some property of a glassy material as a function of storage time below T_g in the absence of external influences.[38] Properties used to monitor aging include both macroscopic, or bulk, properties (e.g., specific volume,[39,40] enthalpy,[41,42] and mechanical properties[43–49]) and microscopic properties monitored by scattering or spectroscopic techniques.[39,50–52] The term physical is used to differentiate from chemical or biological aging. Chemical and biological aging both cause irreversible changes to the material, whereas physical aging is fully reversible with the appropriate heat treatment. [53]

As a material, such as a polymer, is cooled through its glass transition and long range motion becomes impossible, the polymer is no longer able to rearrange to its

equilibrium packing. [37] This causes the material to have various excess properties including specific volume and enthalpy.[37,54–60] Due to the thermodynamic requirement to move towards equilibrium, these excess properties tend to decay over time. [37]

The aging rate, or the rate of change in an excess property such as volume, has been modeled as shown below: [37]

$$Aging\ Rate = \frac{dv_{sp}}{dt} = \frac{v_{sp} - v_{\infty}}{\tau(v_{sp}, T)} \tag{2.17}$$

where v_{sp} is the polymer specific volume, t is time, v_{∞} is the equilibrium specific volume and τ is the timescale for molecular rearrangement, which is dependent on v_{sp} and temperature, T.

The driving force for physical aging is the excess property (e.g., v_{sp}-v_{∞}). The physical aging is slowed by the lack of large scale molecular motion, which is represented by timescale for molecular rearrangement, τ. τ is a function of both the specific volume, i.e., as the specific volume decreases, the timescale for molecular motion increases and temperature, i.e., when temperature decreases, tau increases. Over the course of physical aging, both the driving force for further aging and the polymer's ability to age are decreased. These factors cause the aging rate to decreases over time or, equivalently, physical aging is self-retarding. [37]

Both the limited motion available to the polymer chains and physical aging's self-retarding nature combine to cause physical aging to persist for very long times. Typically, the timescale for equilibration of a glassy material renders the equilibrated glass inaccessible except at temperatures very close to T_g (i.e., $T_g - T_{experiment} < \sim 15°C$). [37] Near T_g, the material is closer to equilibrium (cf., Figure 2.5) and the timescale for molecular rearrangement is sufficiently short that, with sufficient aging times, the equilibrium glass can be reached. [37] However, for most traditional glassy polymers, the

use temperature is far enough below T_g that the polymers will experience physical aging over their entire product lives. [37]

As described above, physical aging arises from the decay of excess thermodynamic properties such as specific volume and enthalpy towards equilibrium. The decay in these thermodynamic properties cause changes in any polymer properties that depend on them. [37] A typical physical aging experiment consists of measuring the evolution of one or more of these properties (e.g., enthalpy overshoot, permeability) over time at some temperature below T_g. [37]

2.2.1.3 Physical Aging and Transport Properties

A membrane's permeability is acutely sensitive to its free volume, and numerous reports show that permeability of glassy films declines over time.[40,61–75] This permeability decay has been demonstrated to be thermo-reversible[66] and is attributed to physical aging of the polymer matrix. Coupled with this decrease in permeability is a rise in selectivity for gas pairs that are separated by size (e.g., O_2/N_2)[67] because the larger gas molecules are more sensitive to the loss of free volume than the smaller ones.[67] Because most upper bound materials are deep in the glassy state and time to equilibrium for these materials is much longer than the lifetime of the membrane, these materials may be expected to age over their entire lifespan.

2.2.1.4 Physical Aging in Confined Systems

Many modern technologies make use of polymer glasses in geometries that are confined at the nanometer scale (e.g nanocomposites and gas separation membranes).[76] Physical aging in nanoconfined systems is known to differ significantly from bulk, but the phenomenon is not well understood.[76]

Because the aging rate is closely tied to how far below the T_g the polymer is aged, the effect of confinement on the T_g has been studied. [50,77] As the confining thickness (e.g., film thickness in a membrane) is decreased below a critical value, the glass transition temperature begins to deviate from bulk. [50] The nature of the deviations seems to be dependent on the type of interactions between the glass and non-glass interface. [50] When the substrate and polymer have attractive interactions, T_g is typically raised as the confinement increases.[76] Conversely, when the substrate-polymer interactions are repulsive or free/soft interface, T_g tends to decrease with increasing confinement.[76]

As with the T_g, physical aging experiments have been done in various configurations.[76,78–81] The response of a supported film, like the T_g, is complicated by the potential interactions with the substrate.[79] For example, one study used florescence measurements to compare the aging responses of polystyrene and PMMA on silica.[79] On polymer samples annealed 20°C below T_g, a 20 nm polystyrene sample showed no aging response, while a similar PMMA film showed aging was occurring even slightly above the bulk T_g.

Experiments with variable energy positron annihilation spectroscopy (PALS) have examined the spacial distribution of free volume and physical aging.[82] The PALS results showed that physical aging of 450nm polysulfone films occurred predominately by free volume element shrinkage rather than free volume element diffusion to the surface. Using variable energy measurements, free volume element size at different implantation depths were tracked over time. The results showed that physical aging was proceeding similarly across the thickness of the film. However, the near surface region of the film had, on average, smaller free volume elements, [82] which was attributed to rapid aging that occurred prior to the measurement. [82]

Permeability and optical aging studies on thin films of interest for gas separations (e.g., Matrimid, polysulfone and poly(phenylene oxide)) have routinely shown consistent results.[39,40,66–68,70,72,73,83–85] In these polymers, as the film thickness decreases below 1 μm, the aging rate increases (Figure 2.6). The aging rate increase appears as a more rapid decrease in the permeability over time in thinner flims. Additionally, good agreement has been found between the permeability decrease over time and the density increase measured via ellipsometry.[39]

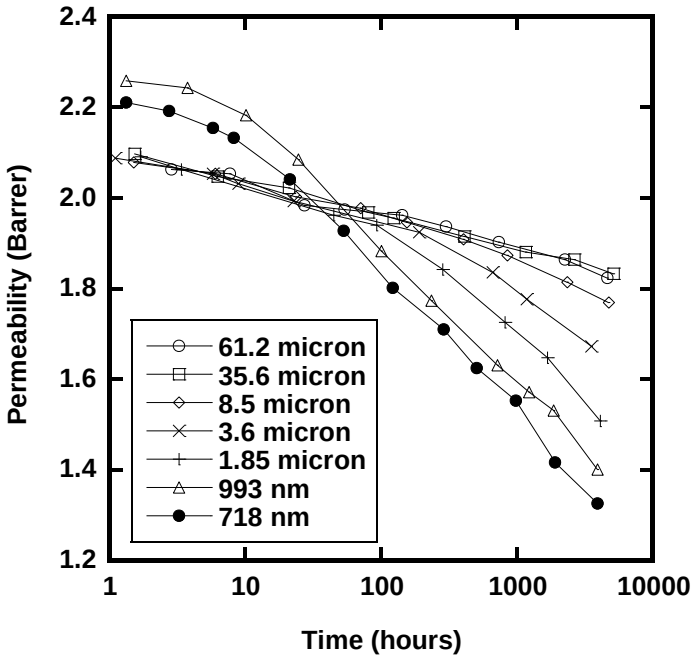

Figure 2.6 Physical aging of thin polysulfone films tracked by permeability decay[67]

2.2.2 CO_2 Plasticization and Conditioning in Polymer Membranes

2.2.2.1 Definition of Plasticization and Conditioning in Membranes

Polymer plasticization, as the term was originally used, is a phenomenon whereby a penetrant, called the plasticizer, sorbs into a polymer and causes the T_g of the matrix to decrease.[86] Membrane plasticization is the phenomenon where a highly-sorbing

penetrant sorbs into the polymer to such a degree that the polymer matrix begins to swell.[87–91] As the polymer swells, the membrane's permeability to all gases increases. [87–91] The permeability increase affects larger gas molecules more strongly, so the size-sieving ability of the polymer decreases, which commonly leads to a selectivity decrease.[87–91] The permeability increase has been linked with T_g suppression,[90,91] but this is not universally the case.[91] Most membrane plasticization studies do not attempt to measure the T_g of the swollen material. For the purposes of this work, the term plasticization is used to mean an increase in membrane permeability as the pressure is increased beyond a certain point, and the term plasticizer is used to mean a penetrant that causes the membrane to be plasticized. Due to limited mobility, a plasticized, glassy membrane cannot always revert to its original, unswollen state even after the plasticizer is completely removed.[92] This phenomenon has been referred to as conditioning and is typically tested by tracking the rate at which the polymer reverts to its initial permeability either with reduced plasticizer concentration or with a non-plasticizing penetrant.

2.2.2.2 Plasticization of Polymer Membranes

The extent of plasticization (i.e., the permeability increase relative to the pre-exposure permeability) is dependent on the plasticizer concentration and the exposure time. As feed concentration increases, the penetrant concentration in the polymer also increases, which increases the swelling and permeability. One common experiment to identify plasticization in a penetrant/polymer pair is the so-called plasticization pressure curve experiment.[93–95] In this experiment, the plasticizer feed pressure is increased step-wise with the permeability measured at each pressure. With increasing pressure in a non-plasticizing feed, a glassy polymer's permeability will either remain constant or decrease slightly due to dual-mode effects.[4] In a plasticizing feed, the permeability will typically

decrease at low concentrations, due to dual-mode effects,[4] and then rise with pressure. The resulting minimum in the permeability vs. pressure curve (Figure 2.7) is called the plasticization pressure[93] and is generally assumed to be where plasticization begins to be significant.[93] However, as stated previously, plasticization is also time-dependent. If a membrane is held at a constant pressure in a plasticizing atmosphere, the permeability will continue to rise.[93,94] In many samples, the permeability does not reach a steady value over experimentally accessible time-scales.[93]

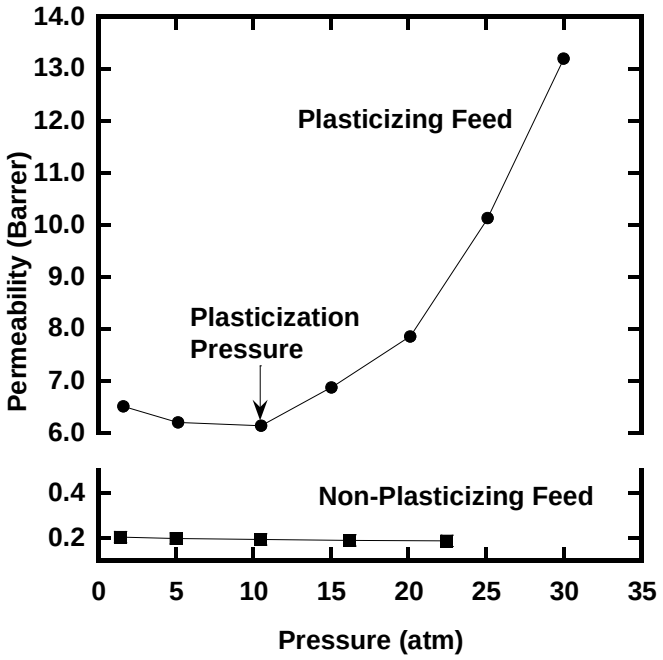

Figure 2.7 Permeability response of a cellulose acetate membrane in a plasticizing (CO_2) and non-plasticizing (CH_4) feed.[94]

2.2.2.3 Thin Film Plasticization

Similar to the physical aging studies, plasticization is generally more pronounced in thinner films.[93,96,97] As film thickness decreases below approximately 1 μm, both a

decrease in plasticization pressure and an increase in extent of plasticization have been observed (Figure 2.7).[93]

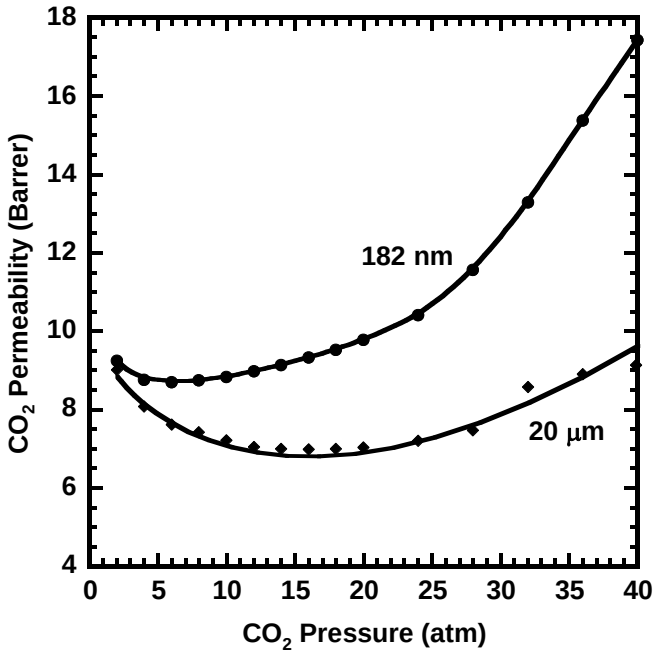

Figure 2.8 Plasticization pressure curves of thick (20 μm) and thin (182 nm) Matrimid® films.[93]

Although this phenomenon is not well understood, it has been attributed to the increased mobility of the thin films which allow polymer to swell more easily. It has not been determined if, given sufficient time, a thin and thick film would swell to the same degree due to the large difference in the timescales of these processes. Thick films have been shown to increase in permeability for periods exceeding 1000 hours.[93] However, at these time-scales, the thin films exhibit very different behavior (Figure 2.9).[93] The initial increase in thin film permeability has been attributed to plasticization, but at longer times, the permeability goes through a maximum and begins decreasing, which has been attributed to physical aging.[93] As discussed earlier, the physical aging of thin films is

faster than that of thick films, and at longer hold times, physical aging seems to dominate thin film permeability behavior.

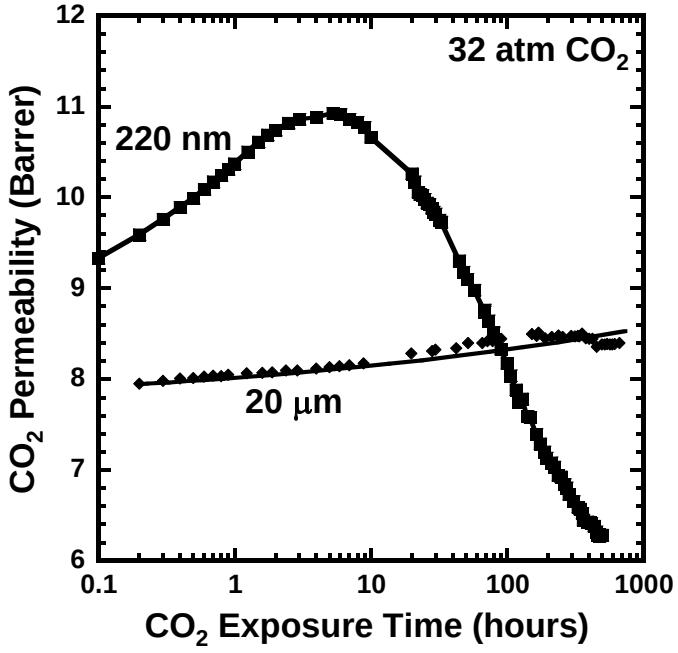

Figure 2.9 Long CO_2 exposure times in Matrimid® thin (220nm) and thick (20 μm) films.[93]

2.2.3 Crystallinity in Polymer Membranes

2.2.3.1 Crystallinity in Polymers

Polymers with sufficient structural regularity are capable of crystallizing.[36,86,98] Unlike small molecules, polymers generally cannot reach a 100% crystalline structure. [36,86,98] The size, shape and distribution of the crystalline domains are dependent on the chemical structure and regularity and several processing variables (e.g., solvent, thermal treatment, stress). [36,86,98]

2.2.3.2 Impact of Crystallinity on Transport in Polymer Membranes

Crystallinity also affects a polymer's transport properties. In general crystals do not absorb penetrants into their structure, which means that a fraction of the membrane material is unavailable for transport. The crystals thus reduce the measured uptake, or solubility, of a gas by the crystalline fraction.[94] Crystals can also influence penetrant diffusivity in the polymer by changing chain mobility, chain packing and diffusion path tortuosity.[99] It is more difficult to model the influence of crystallinity on diffusivity as the effects are strongly dependent on the shape and size of the crystallites, although models similar to those used for non-permeable nanocomposites can be used. [99] As both solubility and diffusivity are reduced by the presence of crystals, permeability must also decrease, though it can be hard to predict the extent of permeability suppression.

2.2.3.3 Impact of Crystallinity on Physical Aging

As crystals are equilibrium materials, they do not undergo physical aging. However, the presence of crystallites can influence the behavior of the amorphous phase. There is some evidence that the presence of crystal domains can restrict the mobility of the amorphous polymer near those domains, thus raising the T_g of that material while leaving the material farther from the crystals unchanged. [37,44,45,100,101] The bulk effect of the crystals is to broaden the glass transition of the polymer and complicate aging near T_g. When the aging temperature is far below T_g, the entire amorphous region should be deep in the glassy state, and the bulk aging should be similar to that of an amorphous glass. [37,44,45,100,101] As the temperature approaches the T_g of the material with the lowest T_g, the aging becomes more complicated and difficult to predict. Parts of the sample will begin to go through their glass transitions while others may still be aging. [37,44,45,100,101] Once the temperature surpasses the T_g of the material with the highest T_g, the sample will behave as a semi-crystalline rubber and physical aging will cease. [37,44,45,100,101]

In the systems and temperatures typically used in membrane aging studies (i.e., polymers more than 100°C below their glass transition), semi-crystalline polymers would be expected to age like purely amorphous glasses. Indeed, some work done comparing amorphous and semi-crystalline poly(phenylene oxide) showed a decrease in the absolute permeability of the semi-crystalline sample, but no change in the rate of permeability decay over time.[102]

2.3 Background on Materials Used in This Work

2.3.1 Aromatic Polyimides

Aromatic polyimides have been studied extensively for gas separations.[4,27,28,70,103–110] Broadly, they are a family of high-T_g materials with excellent size-sieving ability characterized by the presence of imide linkages in the polymer backbone. The relatively straightforward synthesis of these materials and widely available dianhydride and diamine monomers has allowed numerous structure-property studies to be performed.[27,28,103,104,107,109,111–113] Aromatic polyimides are frequently among the best performing separation materials.[10]

2.3.2 "TR" Polymers

Polybenzoxazoles (PBO), polybenzimidazoles (PBI) and polybenzthiozoles (PBT) are a family of polymers with high chemical and thermal stability.[114–116] Most of them are, however, insoluble in virtually all organic solvents, [114–116] which has limited their use in membrane applications as virtually all membranes are made by solution processing. In 2007, it was determined that PBOs synthesized by a high-temperature, solid state condensation from ortho-functional, aromatic polyimides and amides (Figure 2.10) had transport properties near or above the upper bound for numerous gas pairs.[117]

These materials have been termed "TR polymers" and have been widely studied as separation membranes since the original report.[118–127]

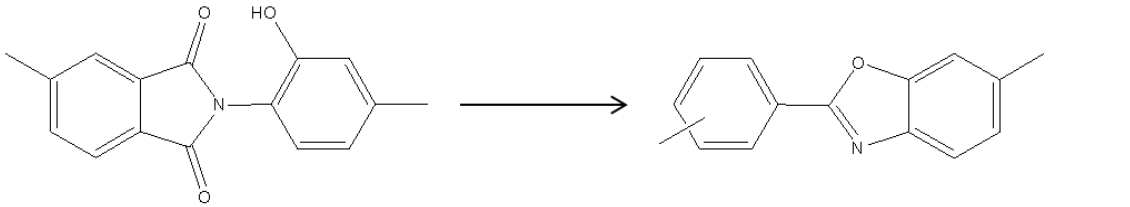

aromatic polyimide **TR polymer (polybenzoxazole)**

Figure 2.10 Schematic showing the conversion of an ortho-hydroximide to polybenzoxazole TR polymer.

2.3.3 Cellulose Acetate

Cellulose acetates (CA) are a family of materials synthesized by treating naturally occurring cellulose with sulfuric and acetic acids.[128] This process causes the acetylation of the cellulose hydroxyl groups (Figure 2.11). [129] The average number of acetylated hydroxyl groups per repeat unit is the degree of substitution (DS). Degree of substitution thus runs from 0 to 3. [129] Typical industrial production of cellulose acetate yields the triacetate (DS=3) product which may then be partially hydrolyzed back to the DS required.[128]

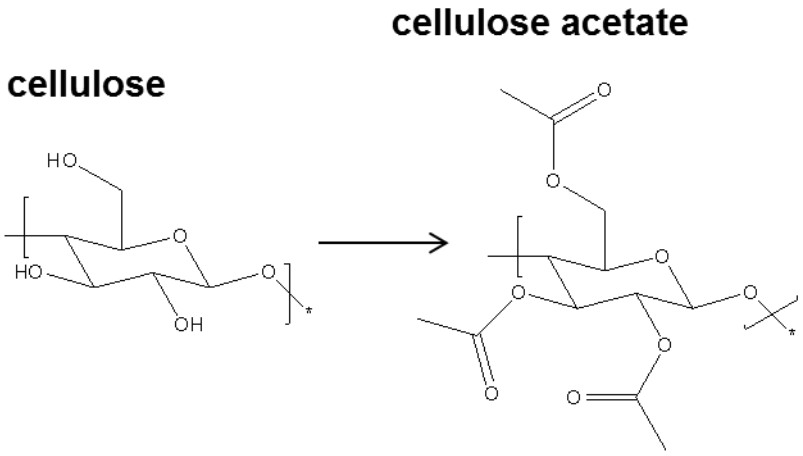

Figure 2.11 Chemical structures of cellulose and cellulose triacetate (DS = 3).

Many of CA's properties are dependent on the DS. For example, increasing DS reduces chain packing efficiency and hydrogen bonding between polymer chains, which decreases density[129] and glass transition temperature.[129] Furthermore, due to the differences in molecular structure and intermolecular interactions, cellulose acetate samples with different DS require different solvents.[94] Although unsubstituted cellulose is highly crystalline, the tri-substituted structure is the only acetylated repeat unit that can crystallize.[36,129] Thus, triacetate samples will typically be more crystalline than diacetates.

The degree of substitution also influences the transport properties of the cellulose acetate polymers. The more acetyl substitution on the cellulose chain, the higher the intrinsic gas sorption, i.e., gas sorption normalized by the polymer amorphous fraction.[94] The permeability also increases with DS due to the more open structure.[94] The reported permeability values for cellulose acetates show a wide variation likely due to different casting conditions (e.g., solvent), DS, crystallinity, and testing conditions (e.g., pure gas vs. mixed gas),[94,130–141] which are not rigorously reported in many papers.

Unlike the other polymers tested in this work, cellulose acetate is used for commercial gas separations. However, despite being in commercial use for acid gas removal from natural gas since the early to mid-1980s,[13] characterization of the physical aging of these materials, particularly thin-film aging, has never been studied. However, aging data does exist in the records of commercial membrane performance over time. Figure 2.12 (generously provided by Cameron International Corporation and used with permission) shows the performance of the Carigali Hess plant from March, 2008 to July, 2009. At the time, the Carigali Hess plant processed 700 MMScfd, reducing the CO_2 content of the natural gas streams from 37% to 15%. It has since been scaled up to over 1.28 Bscfd. Figure 2.12 shows capacity factor, which is a measure of membrane throughput and corresponds to permeability, and separation factor, which corresponds to selectivity. The Carigali Hess data show some initial increases in capacity factor, which have been attributed to initial membrane plasticization, but then the capacity stabilizes and remains constant for over a year. The selection factor is also constant for the entire duration plotted here. These results are surprising given that cellulose triacetate is known to be a glassy polymer that can be signficantly plasticized by CO_2.[94]

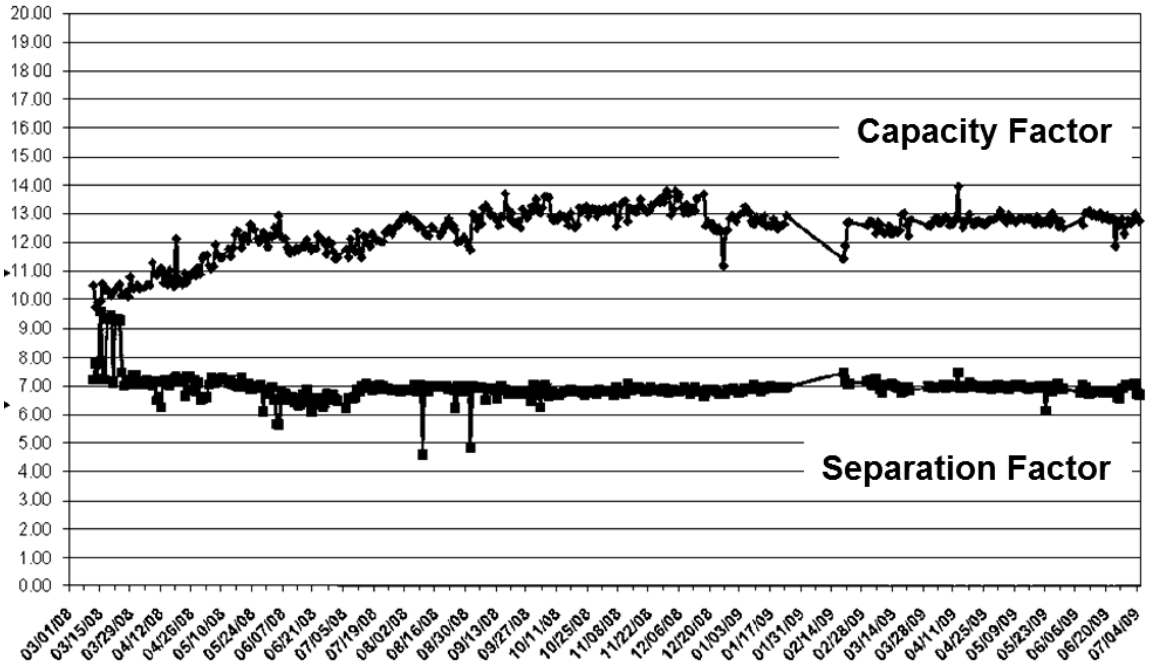

Figure 2.12 Carigali Hess natural gas purification membrane operating data from 2008-2009. Plot generously provided by Rick Peters at Cameron International.

2.4 INDUSTRIAL SEPARATIONS

2.4.1 Ethanol Dehydration for Biofuel

Current ethanol dehydration technology utilizes two distillation columns to decrease the water content from around 90%$_{wt}$ to around 10%$_{wt}$.[142] The distillation columns are followed by a molecular sieve column to take the ethanol through the azeotrope (~4%$_{wt}$ water)[143] to the final product specifications, water content <1%$_{wt}$. [142] This separation process consumes large amounts of energy and, depending on the ethanol feed concentration, the energy consumed by the separation can exceed the heating value of the produced ethanol.[144] Membranes have been proposed as replacements for one or more of these steps. Current plant designs have shown that if membranes were used to replace both the molecular sieve tower and the second distillation tower with membrane units, energy savings on the order of 50% could be achieved. [12] The parameters targeted

for this separation vary, but typical values are purification of a 50%$_{wt}$ ethanol stream to over 99%$_{wt}$ at an operating temperature over 120°C and pressure over 3 bar.[12,142,144–147]

2.4.2 Natural Gas Purification

As previously mentioned, membranes have been employed for industrial-scale acid gas removal from natural gas.[13] Due to the wide variation in the naturally occurring gas streams, each separation site must be individually evaluated and the membrane system modified for that site's particular requirements.[148] A membrane system will, typically, consist of a pretreatment system, the membrane units and the packaging of those components. [148] The pretreatment system removes stream contaminants that are known to be damaging to the membrane, including both naturally occurring contaminants (e.g., water, heavy hydrocarbons and aromatics) and those that are introduced to protect other parts of the gas production system (e.g., corrosion inhibitors, well additives and lube oil). [148] Different types of pretreatment systems have been used, but they all must reliably treat the feed stream to protect the membrane. The performance of the membrane module depends, not only on the separation properties of the membrane material, but also on the design of the module and the supporting equipment. [8,148] Both hollow fiber and spiral wound modules have been used commercially.[7] When studying membranes targeting these separations, colleagues at Cameron International have indicated to the author that the reasonable ranges of parameters include temperatures from 10-45°C and individual component pressures in the ranges listed in Table 2.1.

Gas	Pressure Range
CO_2	100-500 psi
CH_4	100-500 psi
C_2H_6	35-50 psi
C_3H_8	15-25 psi

Table 2.1 Components and pressure ranges of interest for natural gas purification membranes. Data were provided by Rick Peters at Cameron International.

2.5 REFERENCES

(1) Graham, T. *J. Memb. Sci.* **1995**, *100*, 27–31.

(2) Mitchell, J. K. *J. Memb. Sci.* **1995**, *100*, 11–16.

(3) Wijmans, J.; Baker, R. W. *J. Memb. Sci.* **1995**, *107*, 1–21.

(4) Matteucci, S.; Yampolskii, Y. P.; Freeman, B. D.; Pinnau, I. In *Materials Science of Membranes for Gas and Vapor Separations*; Yampolskii, Y.; Pinnau, I.; Freeman, B. D., Eds.; John Wiley & Sons, Ltd: Chichester, 2006; pp. 1–47.

(5) Ghosal, K.; Freeman, B. D. *Polym. Adv. Technol.* **1994**, *5*, 673–697.

(6) Ribeiro Jr., C. P.; Borges, C. P. *Brazilian J. Chem. Eng.* **2004**, *21*, 629 – 640.

(7) Chapman, P. D.; Oliveira, T.; Livingston, A. G.; Li, K. *J. Memb. Sci.* **2008**, *318*, 5–37.

(8) Baker, R. W. *Membrane Technology and Applications*; 2nd ed.; John Wiley & Sons, Ltd, 2004; pp. 1–538.

(9) Robeson, L. M. *J. Memb. Sci.* **1991**, *62*, 165–185.

(10) Robeson, L. M. *J. Memb. Sci.* **2008**, *320*, 390–400.

(11) Freeman, B. D. *Macromolecules* **1999**, *32*, 375–380.

(12) Huang, Y.; Baker, R. W.; Vane, L. M. *Ind. Eng. Chem. Res.* **2010**, *49*, 3760–3768.

(13) Sanders, D. F.; Smith, Z. P.; Guo, R.; Robeson, L. M.; McGrath, J. E.; Paul, D. R.; Freeman, B. D. *Polymer* **2013**, *54*, 4729–4761.

(14) Stern, S. A. *J. Memb. Sci.* **1994**, *94*, 1–65.

(15) Yampol'skii, Y. P.; Volkov, V. V. *J. Memb. Sci.* **1991**, *64*, 191–228.

(16) Nagai, K.; Masuda, T.; Nakagawa, T.; Freeman, B. D.; Pinnau, I. *Prog. Polym. Sci.* **2001**, *26*, 721–798.

(17) Koros, W. J.; Fleming, G. K. *J. Memb. Sci.* **1993**, *83*, 1–80.

(18) Ohya, H.; Kudryavtsev, V. V.; Semenova, S. I. *Polyimide Membranes: Applications, Fabrications, and Properties*; Kodansha LTD. and Gordon and Breach Science Publishers S. A.., 1996.

(19) Bondi, A. *Physical Properties of Molecular Crystals, Liquids, and Glasses*; John Wiley & Sons, Inc.: New York, 1968.

(20) Bondi, A. *J. Phys. Chem.* **1964**, *68*, 441–451.

(21) Van Krevelen, D. W. *Properties of Polymers: Their Correlation with Chemical Structure; Their Numerical Estimation and Prediction from Additive Group Contributions*; 3rd ed.; Elsevier: Amsterdam, 1990.

(22) Hellums, M. W.; Koros, W. J.; Husk, G. R.; Paul, D. R. *J. Memb. Sci.* **1989**, *46*, 93–112.

(23) Aitken, C. L.; Koros, W. J.; Paul, D. R. *Macromolecules* **1992**, *25*, 3651–3658.

(24) Aitken, C. L.; Koros, W. J.; Paul, D. R. *Macromolecules* **1992**, *25*, 3424–3434.

(25) Pixton, M. R.; Paul, D. R. In *Polymeric Gas Separation Membranes*; Paul, D. R.; Yampolskii, Y. P., Eds.; CRC Press: Boca Raton, Fl, 1994; pp. 83–153.

(26) Wang, X.-Y.; in't Veld, P. J.; Lu, Y.; Freeman, B. D.; Sanchez, I. C. *Polymer* **2005**, *46*, 9155–9161.

(27) Coleman, M. R.; Koros, W. J. *J. Memb. Sci.* **1990**, *50*, 285–297.

(28) Kim, T. H.; Koros, W. J.; Husk, G. R.; O'Brien, K. C. *J. Memb. Sci.* **1988**, *37*, 45–62.

(29) Muruganandam, N.; Koros, W. J.; Paul, D. R. *J. Polym. Sci. Part B Polym. Phys.* **1987**, *25*, 1999–2026.

(30) McHattie, J. S.; Koros, W. J.; Paul, D. R. *Polymer* **1991**, *32*, 840–850.

(31) Khotimskii, V. S.; Filippova, V. G.; Bryantseva, I. S.; Bondar, V. I.; Shantarovich, V. P.; Yampolskii, Y. P. *J. Appl. Polym. Sci.* **2000**, *78*, 1612–1620.

(32) Finkelshtein, E. S.; Gringolts, M. .; Ushakov, N. .; Lakhtin, V. .; Soloviev, S. .; Yampol'skii, Y. . *Polymer* **2003**, *44*, 2843–2851.

(33) Anwand, D.; Muller, F. W.; Strehmel, B.; Schiller, K. *Die Makromol. Chemie* **1991**, *192*, 1981–1991.

(34) Stannett, V.; Szwarc, M. *J. Polym. Sci.* **1955**, *16*, 89–91.

(35) Ghosal, K.; Freeman, B. D.; Chern, R.; Daly, W.; Negulescu, I. *Macromolecules* **1996**, *29*, 4360–4369.

(36) Odian, G. *Principles of Polymerization*; 4th ed.; John Wiley & Sons, Inc.: Hoboken, 2004.

(37) Struik, L. C. E. *Physical Aging in Amorphous Polymers and Other Materials*; Elsevier Scientific Publishing Company: Amsterdam, The Netherlands, 1978; Vol. 54.

(38) Hodge, I. M. *Science* **1995**, *267*, 1945–1947.

(39) Huang, Y.; Paul, D. R. *Macromolecules* **2006**, *39*, 1554–1559.

(40) Huang, Y.; Wang, X.; Paul, D. R. *J. Memb. Sci.* **2006**, *277*, 219–229.

(41) Hodge, I. M.; Berens, A. R. *Macromolecules* **1981**, *14*, 1598–1599.

(42) Nairn, K. M.; Walters, R. L.; Simon, G. P.; Hill, A. J. *Mater. Forum* **1992**, *16*, 167–172.

(43) Hedesiu, C.; Demco, D. E.; Kleppinger, R.; Poel, G. Vanden; Remerie, K.; Litvinov, V. M.; Blümich, B.; Steenbakkers, R. *Macromol. Mater. Eng.* **2008**, *293*, 847–857.

(44) Struik, L. C. E. *Polymer* **1989**, *30*, 799–814.

(45) Struik, L. C. E. *Polymer* **1989**, *30*, 815–830.

(46) Read, B. E.; Tomlins, P. E.; Dean, G. D. *Polymer* **1990**, *31*, 1204–1215.

(47) Beckmann, J.; McKenna, G. B.; Landes, B. G.; Bank, D. H.; Bubeck, R. A. *Polym. Eng. Sci.* **1997**, *37*, 1459–1468.

(48) Echeverria, I.; Su, P.-C.; Simon, S. L.; Plazek, D. J. *J. Polym. Sci. Part B Polym. Phys.* **1995**, *33*.

(49) Robertson, C. G.; Monat, J. E.; Wilkes, G. L. *J. Polym. Sci., Part B Polym. Phys.* **1999**, *37*, 1931–1946.

(50) Ellison, C. J.; Kim, S. D.; Hall, D. B.; Torkelson, J. M. *Eur. Phys. J. E. Soft Matter* **2002**, *8*, 155–166.

(51) Pye, J. E.; Roth, C. B. *Macromolecules* **2013**, *46*, 9455–9463.

(52) Baker, E. A.; Rittigstein, P.; Torkelson, J. M.; Roth, C. B. *J. Polym. Sci. Part B Polym. Phys.* **2009**, *47*, 2509–2519.

(53) Hutchinson, J. M. *Prog. Polym. Sci.* **1995**, *20*, 703–760.

(54) Berens, A. R.; Hodge, I. M. *Macromolecules* **1982**, *15*, 756–761.

(55) Hodge, I. M.; Berens, A. R. *Macromolecules* **1982**, *15*, 762–770.

(56) Hodge, I. M.; Huvard, G. S. *Macromolecules* **1983**, *16*, 371–375.

(57) Hodge, I. M. *Macromolecules* **1983**, *16*, 898–902.

(58) Hodge, I. M.; Berens, a. R. *Macromolecules* **1985**, *18*, 1980–1984.

(59) Hodge, I. M. *Macromolecules* **1987**, *20*, 2897–2908.

(60) Li, Q.; Simon, S. L. *Polymer* **2006**, *47*, 4781–4788.

(61) Chan, A. H.; Paul, D. R. *J. Appl. Polym. Sci.* **1980**, *25*, 971–974.

(62) Pfromm, P.; Koros, W. J. *Polymer*, 1995, *36*, 2379–2387.

(63) McCaig, M. S.; Paul, D. R. *Polymer* **1999**, *40*, 7209–7225.

(64) McCaig, M. S.; Paul, D. R. *Polymer* **2000**, *41*, 629–637.

(65) McCaig, M. .; Paul, D. R.; Barlow, J. . W. *Polymer* **2000**, *41*, 639–648.

(66) Huang, Y.; Paul, D. R. *J. Memb. Sci.* **2004**, *244*, 167–178.

(67) Huang, Y.; Paul, D. R. *Polymer* **2004**, *45*, 8377–8393.

(68) Priestley, R. D.; Broadbelt, L. J.; Torkelson, J. M. *Macromolecules* **2005**, *38*, 654–657.

(69) Huang, Y.; Paul, D. R. *Macromolecules* **2005**, *38*, 10148–10154.

(70) Kim, J. H.; Koros, W. J.; Paul, D. R. *Polymer* **2006**, *47*, 3094–3103.

(71) Kim, J.; Koros, W. J.; Paul, D. R. *J. Memb. Sci.* **2006**, *282*, 32–43.

(72) Huang, Y.; Paul, D. R. *Ind. Eng. Chem. Res.* **2007**, *46*, 2342–2347.

(73) Rowe, B. W.; Freeman, B. D.; Paul, D. R. *Polymer* **2009**, *50*, 5565–5575.

(74) Murphy, T. M.; Langhe, D. S.; Ponting, M.; Baer, E.; Freeman, B. D.; Paul, D. R. *Polymer* **2011**, *52*, 6117–6125.

(75) Huang, Y.; Paul, D. R. *J. Polym. Sci. Part B Polym. Phys.* **2007**, *45*, 1390–1398.

(76) Priestley, R. D. *Soft Matter* **2009**, *5*, 919.

(77) Roth, C. B.; Dutcher, J. R. *J. Electroanal. Chem.* **2005**, *584*, 13–22.

(78) Simon, S. L.; Park, J.-Y.; McKenna, G. B. *Eur. Phys. J. E. Soft Matter* **2002**, *8*, 209–216.

(79) Priestley, R. D.; Rittigstein, P.; Broadbelt, L. J.; Fukao, K.; Torkelson, J. M. *J. Phys. Condens. Matter* **2007**, *19*, 205120–205132.

(80) Nguyen, H. K.; Labardi, M.; Capaccioli, S.; Lucchesi, M.; Rolla, P.; Prevosto, D. *Macromolecules* **2012**, *45*, 2138–2144.

(81) Pye, J. E.; Rohald, K. A.; Baker, E. A.; Roth, C. B. *Macromolecules* **2010**, *43*, 8296–8303.

(82) Rowe, B. W.; Pas, S. J.; Hill, A. J.; Suzuki, R.; Freeman, B. D.; Paul, D. R. *Polymer* **2009**, *50*, 6149–6156.

(83) Dorkenoo, K. D.; Pfromm, P. H. *Macromolecules* **2000**, *33*, 3747–3751.

(84) Rowe, B. W.; Freeman, B. D.; Paul, D. R. *Polymer* **2010**, *51*, 3784–3792.

(85) Kim, J. H.; Koros, W. J.; Paul, D. R. *Polymer* **2006**, *47*, 3104–3111.

(86) McCrum, N. G.; Buckley, C. P.; Bucknall, C. B. *Principles of Polymer Engineering*; 2nd ed.; Oxford University Press: Oxford, 1997.

(87) Koros, W. J.; Paul, D. R. *Polym. Eng. Sci.* **1980**, *20*, 14–19.

(88) Bos, A.; Pünt, I. G. M.; Wessling, M.; Strathmann, H. *J. Memb. Sci.* **1999**, *155*, 67–78.

(89) Ismail, A. F.; Lorna, W. *Sep. Purif. Technol.* **2002**, *27*, 173–194.

(90) Chiou, J. S.; Barlow, J. W.; Paul, D. R. *J. App. Poly. Sci.* **1985**, *30*, 2633–2642.

(91) Sanders, E. S. *J. Memb. Sci.* **1988**, *37*, 63–80.

(92) Wonders, A.; Paul, D. R. *J. Memb. Sci.* **1979**, *5*, 63–75.

(93) Horn, N. R.; Paul, D. R. *Polymer* **2011**, *52*, 1619–1627.

(94) Puleo, A. C.; Paul, D. R.; Kelley, S. S. *J. Memb. Sci.* **1989**, *47*, 301–332.

(95) Chiou, J. S.; Paul, D. R. *J. Memb. Sci.* **1987**, *32*, 195–205.

(96) Horn, N. R.; Paul, D. R. *Macromolecules* **2012**, *45*, 2820–2834.

(97) Cui, L.; Qiu, W.; Paul, D. R.; Koros, W. J. *Polymer* **2011**, *52*, 5528–5537.

(98) Allcock, H. R.; Lampe, F. W.; Mark, J. E. *Contemporary Polymer Chemistry*; 3rd ed.; Pearson Education, Inc.: Upper Saddle River, 2003.

(99) Murphy, T. M.; Offord, G. T.; Paul, D. R. In *Membrane Operations*; Drioli, E.; Giorno, L., Eds.; Wiley-VCH Verlag GmbH & Co. KGaA: Weinheim, Germany, 2009; pp. 63–82.

(100) Struik, L. C. E. *Polymer* **1987**, *28*, 1521–1533.

(101) Struik, L. C. E. *Polymer* **1987**, *28*, 1534–1542.

(102) Huang, Y. Physical Aging of Thin Glassy Polymer Films, The University of Texas at Austin, 2005.

(103) Hirayama, Y.; Yoshinaga, T.; Kusuki, Y.; Ninomiya, K.; Sakakibara, T.; Tamari, T. *J. Memb. Sci.* **1996**, *111*, 169–182.

(104) Shimazu, A.; Miyazaki, T.; Matsushita, T.; Maeda, M.; Ikeda, K. *J. Polym. Sci. Part B Polym. Phys.* **1999**, *37*, 2941–2949.

(105) Wind, J. D.; Paul, D. R.; Koros, W. J. *J. Memb. Sci.* **2004**, *228*, 227–236.

(106) Shao, L.; Chung, T.; Goh, S.; Pramoda, K. *J. Memb. Sci.* **2005**, *256*, 46–56.

(107) Qiu, Z.; Wang, J.; Zhang, Q.; Zhang, S.; Ding, M.; Gao, L. *Polymer* **2006**, *47*, 8444–8452.

(108) Al-Juaied, M.; Koros, W. J. *J. Memb. Sci.* **2006**, *274*, 227–243.

(109) Xiao, S.; Feng, X.; Huang, R. Y. M. *Macromol. Chem. Phys.* **2007**, *208*, 2665–2676.

(110) Kraftschik, B.; Koros, W. J. *Macromolecules* **2013**, *46*, 6908–6921.

(111) C. O'Brien, K.; Koros, W. J.; Husk, G. R. *J. Memb. Sci.* **1988**, *35*, 217–230.

(112) Xu, W.; Paul, D. R.; Koros, W. J. *J. Memb. Sci.* **2003**, *219*, 89–102.

(113) Shindo, R.; Amanuma, S.; Kojima, K.; Sato, S.; Kanehashi, S.; Nagai, K. *Polym. Eng. Sci.* **2013**.

(114) Kubota, T.; Nakanishi, R. *Polym. Lett.* **1964**, *2*, 655–659.

(115) Evers, R. C.; Arnold, F. E.; Helminiak, T. E. *Macromolecules* **1981**, *14*, 925–930.

(116) Tullos, G.; Mathias, L. *Polymer* **1999**, *40*, 3463–3468.

(117) Park, H. B.; Jung, C. H.; Lee, Y. M.; Hill, A. J.; Pas, S. J.; Mudie, S. T.; Van Wagner, E.; Freeman, B. D.; Cookson, D. J. *Science* **2007**, *318*, 254–258.

(118) Choi, J. I.; Jung, C. H.; Han, S. H.; Park, H. B.; Lee, Y. M. *J. Memb. Sci.* **2010**, *349*, 358–368.

(119) Han, S. H.; Lee, J. E.; Lee, K.-J.; Park, H. B.; Lee, Y. M. *J. Memb. Sci.* **2010**, *357*, 143–151.

(120) Jung, C. H.; Lee, J. E.; Han, S. H.; Park, H. B.; Lee, Y. M. *J. Memb. Sci.* **2010**, *350*, 301–309.

(121) Park, H. B.; Han, S. H.; Jung, C. H.; Lee, Y. M.; Hill, A. J. *J. Memb. Sci.* **2010**, *359*, 11–24.

(122) Calle, M.; Chan, Y.; Jo, H. J.; Lee, Y. M. *Polymer* **2012**, *53*, 2783–2791.

(123) Calle, M.; Lozano, A. E.; Lee, Y. M. *Eur. Polym. J.* **2012**, *48*, 1313–1322.

(124) Sanders, D. F.; Smith, Z. P.; Ribeiro, C. P.; Guo, R.; McGrath, J. E.; Paul, D. R.; Freeman, B. D. *J. Memb. Sci.* **2012**, *409-410*, 232–241.

(125) Smith, Z. P.; Sanders, D. F.; Ribeiro, C. P.; Guo, R.; Freeman, B. D.; Paul, D. R.; McGrath, J. E.; Swinnea, S. *J. Memb. Sci.* **2012**, *415-416*, 558–567.

(126) Calle, M.; Doherty, C. M.; Hill, A. J.; Lee, Y. M. *Macromolecules* **2013**, *46*, 8179–8189.

(127) Kostina, J.; Rusakova, O.; Bondarenko, G.; Alentiev, A.; Meleshko, T.; Kukarkina, N.; Yakimanskii, A.; Yampolskii, Y. P. *Ind. Eng. Chem. Res.* **2013**, *52*, 10476–10483.

(128) Heinze, T.; Liebert, T. *Macromol. Symp.* **2004**, *208*, 167–238.

(129) Zugenmaier, P. *Macromol. Symp.* **2004**, *208*, 81–166.

(130) Choji, N.; Pusch, W.; Satoh, M.; Tak, T.; Tanioka, A. *Desalination* **1985**, *53*, 347–361.

(131) Haraya, K.; Obata, K.; Hakuta, T.; Yoshitome, H. *J. Chem. Eng. Japan* **1986**, *19*, 464–466.

(132) Haraya, K.; Obata, K.; Hakuta, T.; Yoshitome, H. *J. Chem. Eng. Japan* **1986**, *19*, 431–436.

(133) Kumazawa, H.; Sada, E.; Nakata, K.; Kawashima, N.; Kataoka, S.; Tada, K. *J. Appl. Polym. Sci.* **1994**, *53*, 113–119.

(134) Lee, a; Feldkirchner, H.; Stern, S.; Houde, A.; Gamez, J.; Meyer, H. *Gas Sep. Purif.* **1995**, *9*, 35–43.

(135) Pan, C. Y.; Jensen, C.; Bielech, C.; Habgood, H. *J. Appl. Polym. Sci.* **1978**, *22*, 2307–2323.

(136) Patel, V. M.; Patel, K. C.; Patel, R. D. *Die Makromol. Chemie* **1978**, *179*, 2531–2539.

(137) Sada, E.; Kumazawa, H.; Wang, J.-S.; Koizumi, M. *J. Appl. Polym. Sci.* **1992**, *45*, 2181–2186.

(138) Sada, E.; Kumazawa, H.; Xu, P.; Wang, S. T. *J. Polym. Sci. Part B Polym. Phys.* **1990**, *28*, 113–125.

(139) Sada, E.; Kumazawa, H.; Yoshio, Y.; Wang, S. T.; Xu, P. *J. Polym. Sci. Part B Polym. Phys.* **1988**, *26*, 1035–1048.

(140) Lee, S. Y. S.; Minhas, B. S.; Donohue, M. D. In *AIChE Symposium Series*; 1988; Vol. 84, pp. 93–101.

(141) Donohue, M.; Minhas, B.; Lee, S. *J. Memb. Sci.* **1989**, *42*, 197–214.

(142) Vane, L. M.; Alvarez, F. R.; Huang, Y.; Baker, R. W. *J. Chem. Technol. Biotechnol.* **2009**, *85*, 502–511.

(143) *Azeotropic Data - III*; Horsley, L. H., Ed.; American Chemical Society, 1973.

(144) Côté, P.; Noël, G.; Moore, S. *Desalination* **2010**, *250*, 1060–1066.

(145) Côté, P.; Roy, C.; Bernier, N. *Sep. Sci. Technol.* **2009**, *44*, 110–120.

(146) Huang, Y.; Baker, R. W.; Aldajani, T.; Ly, J. Dehydration Processes Using Membranes with Hydrophobic Coating. US 2009/0057224 A1, 2009.

(147) Osora, H.; Seiki, Y.; Yukumoto, A.; Yukio, T.; Ogino, S.; Hiroshima-Ken, M. Membrane system for the dehydration of solvents. EP 2 263 783 A1, 2010.

(148) Sanders, E. S. *Annu. Conv. Proc. - Gas Process. Assoc.* **2004**, *83*, 270–312.

Chapter 3: Materials and Experimental Methods

3.1 MATERIALS

3.1.1 HAB-6FDA and HAB-6FDA TR

The precursor to the material used in the ethanol dehydration study (Chapter 4) was an aromatic polyimide synthesized from 3,3'-hydroxy-4,4'-diaminobiphenyl (HAB) and 2,2'-bis-(3,4-dicarboxyphenyl) hexafluoropropane dianhydride (6FDA) (Figure 3.1) via thermal imidization in solution from the corresponding polyamic acid. To convert the sample to a partial polybenzoxazole (PBO) structure (Figure 3.1), the sample was placed in a ceramic dish in a Carbolite Three Zone Hinged Tube Furnace (Model HZS 12/-/600, Watertown, WI, USA) with a N_2 purge. The sample was heated at 5°C/minute to 300°C and held for 1 hour to ensure complete imidization. The sample was then heated at 5°C/minute to the rearrangement temperature, 350°C, and held for an additional hour. The furnace was then cooled to below 100°C at a cooling rate below 10°C/minute and removed from the furnace. The physical and gas transport properties of this polymer have been reported elsewhere.[1,2]

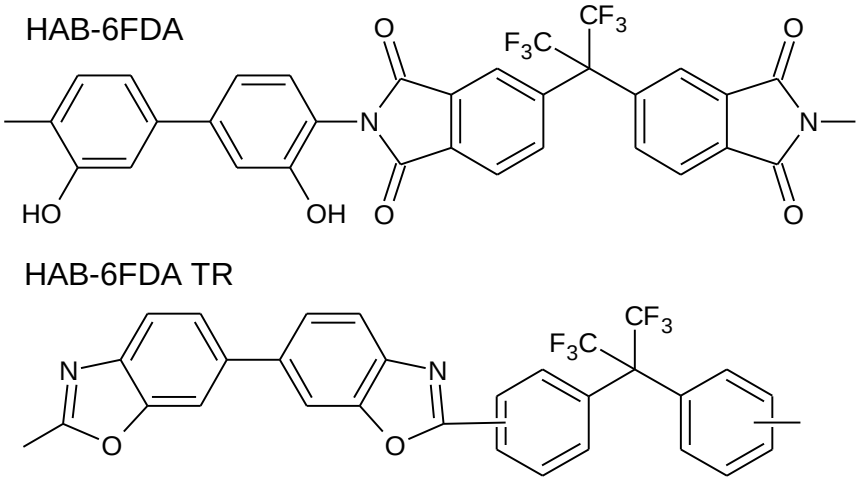

Figure 3.1 Chemical structure of HAB-6FDA and HAB-6FDA TR

3.1.2 HFA-MDA-6FDA

The polymer used in the study detailed in Chapter 5 was an aromatic polyimide synthesized from 4,4'-(hexafluoroisopropylidene)diphthalic anhydride (6FDA) and ortho-hexafluoroalcohol substituted-4,4'methylenedianiline (HFA-MDA). HFA-MDA-6FDA (Figure 3.2) was kindly supplied by Central Glass Co., Ltd as films ranging from 15-30 μm in thickness. The HFA-MDA-6FDA was synthesized by solid-state imidization from the polyamic acid. The films were additionally dried under vacuum at 120°C for at least 12 hours before use to remove any sorbed water.

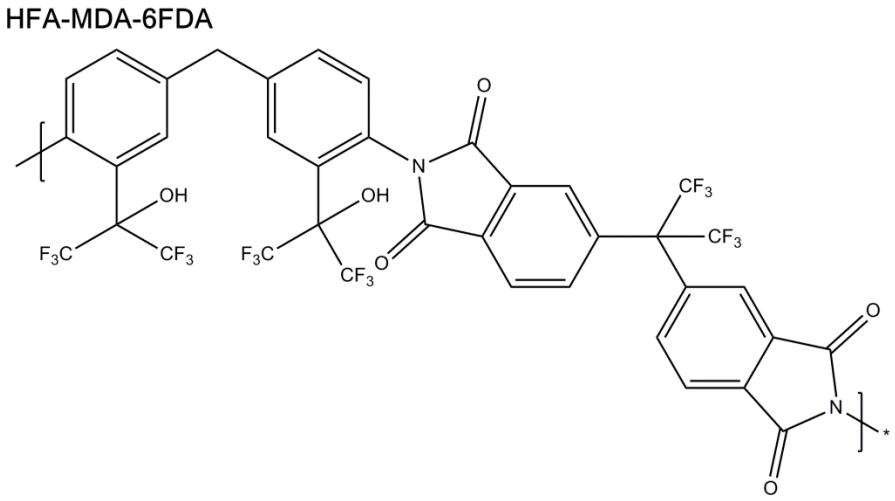

Figure 3.2: Chemical structure of HFA-MDA-6FDA

3.1.3 Cellulose Acetate

Two types of cellulose acetate were utilized in the study detailed in Chapter 6. The first, cellulose triacetate (CTA) (Figure 3.3), was provided by Cameron International Corporation as a powder. The degree of substitution was 2.99. The solvents used for CTA were either *n*-methyl-2-pyrrolidone as a low volatility solvent or a mixture of 9:1 (m:m) dichloromethane and ethanol as a high volatility solvent. The second cellulose acetate material (ECA1.75) was provided by Eastman Chemical Company with a degree of substitution of 1.75 which means that an average of 1.75 of the three cellulose hydroxyl groups are acetylated. 1-Methoxyethanol was the only solvent used for ECA1.75. Finally, the heat of melting for a 100% crystalline cellulose triacetate used in this work was 8.2 cal/g.[3]

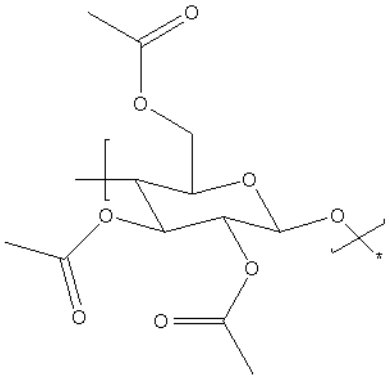

Figure 3.3 Chemical structure of cellulose triacetate

3.2 FILM PREPARATION

3.2.1 Thick Film (>10 μm) Casting

Thick films were prepared using solution casting techniques. The polymer was first dissolved in an appropriate solvent at concentrations ranging from 2-10%$_{wt}$. The solution was then filtered using a series of syringe filters with pore sizes as small as 0.1 μm. One of two types of casting plates was used. The first was a polished metal casting ring approximately 3 inches in diameter set on a silicon wafer on the surface. The second was a glass plate with a glass casting ring, 2-5 inches in diameter, which was glued to the plate using GE Premium Waterproof Silicone. After the casting plate was leveled, the polymer solution was poured into the casting ring and the solvent evaporated. The evaporation rate was controlled by adjusting the temperature and atmosphere above the casting solution. For solvents with high vapor pressures at room temperature, the casting ring was covered by a glass plate which was then lifted by a doubled over paper towel. This small gap allowed slow circulation of air and kept the concentration of solvent near the surface of the film high to slow solvent evaporation. If the solvent was hygroscopic, this could be performed in a N_2 purged glove bag or vacuum oven to reduce water content. If the solvent had a low vapor pressure at room temperature, the casting

proceeded in a vacuum oven. The temperature would be slowly raised over the course of several hours or days while the pressure was maintained at approximately -10 inHg. Whether cast at ambient or elevated temperatures, when a solid film was formed, the film was lifted off the casting surface and placed between two glass plates and placed into a vacuum oven at a temperature above the boiling point of the solvent and under maximum vacuum (-30 inHg) until no residual solvent could be detected by thermogravimetric analysis (TGA).

3.2.2 Thin Film (<1 μm) Casting

Thin films were prepared by spin-casting.[4] The solutions were prepared as described in section 3.2.1, except the solvent choice was further limited to having a boiling point over 100°C. After filtering, the solution was allowed to settle for at least 12 hours to remove any bubbles caused by the filtration process. The solution was then cast onto a silicon wafer by spin coating in a cleanroom. All films were prepared using a Laurell Technologies Spincoater. The spinning conditions used are reported in the subsequent chapters. The thickness of the film can be increased by using a more concentrated casting solution, decreasing the spin speed and acceleration or casting multiple layers on top of each other. The film could be subsequently heated for a few minutes to drive off residual solvent and then the thickness measured by ellipsometry. The film coupons were then lifted off the silicon wafer using a non-solvent, preferably distilled water. The coupons were then lifted onto thin wire frames. By only supporting the film on two opposing sides and using very thin copper wire, the films could easily relax when annealed above T_g. This process removes the additional chain orientation that is introduced by spin coating.

A major challenge to studying gas transport behavior of thin polymer films is the presence of microscopic defects that form with increasing frequency as film thickness decreases.[5] The convective flow through these defects is orders of magnitude faster than the solution/diffusion transport through the film. At an area fraction of 10^{-6}, these defects can dominate the permeation behavior and render the film non-selective.[6] The use of poly(dimethylsiloxane) (PDMS) as a coating layer effectively blocks these defects.[7] Since the transport through the PDMS is also based on the solution/diffusion mechanism, the change in measured permeability relative to a defect free film is proportional to the area fraction of the defects and, thus, the permeability change relative to a defect-free film is negligible. The permeation behavior of the film of interest may be recovered using a simple series resistance model, although typically the influence of the highly permeable PDMS is also negligible.

The PDMS system used in this study was Dehesive 944A with a proprietary crosslinker, V24, and catalyst, OL, from Wacker Silicones Corporation, Adrian, MI. The PDMS arrived as a $30\%_{wt}$ solution in naptha which was further diluted with cyclohexane to $12\%_{wt}$ silicon content. This solution was stored in a refrigerator and spun onto the thin film prior to lifting. The wafer was then heated to 110°C for 15 minutes to crosslink the PDMS and drive off residual solvent. The thickness of the PDMS was then measured using a Dektak 6M Stylus Profilometer and typically ranged from 3-7 μm. PDMS is more than 150°C above its T_g at ambient conditions, and so it does not age at the conditions used in these studies. PDMS has been previously shown to have no effect on the aging[7] behavior of thin, glassy films.

3.2.3 Measuring Film Thickness

Films with thicknesses greater than 10 μm were measured with a micrometer to the nearest 0.1 μm. These films will be termed "thick films" throughout this dissertation and were used for thermal studies, permeation studies and sorption studies.

Films with thicknesses ranging from 1 to 10 μm were measured using a Dektak 6M Stylus Profilometer. The only films in this range were the PDMS coatings on the thinner films. Thus, the profilmeter was used to measure the step change between the PDMS and a region of uncoated thin polymer film.

Films with thicknesses below 1 μm were measured using an M2000 Spectroscopic Ellipsometer from J.A. Woollam. Ellipsometry measures the change in polarization of light as it reflects or transmits through a material. These changes in polarization are captured by an amplitude ratio, ψ, and a phase difference, Δ. The change in polarization is dependent on both film thickness and optical properties; therefore, it is necessary to simultaneously evaluate both. There are two important optical parameters that make up the complex refractive index, the refractive index, or the phase velocity of light relative to the velocity in a vacuum, and the extinction coefficient, related the loss of wave energy to the material. In this work, the refractive index is modeled with the Cauchy dispersion relationship (Equation 3.1) which assumes the extinction coefficient is zero.[8]

$$n = A + \frac{B}{\lambda^2} + \frac{C}{\lambda^4} \tag{3.1}$$

where n is the refractive index, λ is the wavelength of incident light and A, B and C are empirical fitting parameters.

The measurement of the film thickness proceeds as follows: first, the sample is measured in the ellipsometer, and then a model is constructed using the known optical parameters of the silicon substrate and native oxide layer, which are provided by J.A.

Woollam, and a Cauchy layer to represent the film. The model is then used to calculate the predicted light response using Fresnel's equations.[8] The unknown parameters, thickness, A, B and C are then varied using software provided by J.A. Woollam (WVase 32 or CompleteEase) to minimize the mean square error between the predicted and experimental results.

3.3 POLYMER CHARACTERIZATION

3.3.1 Density

The film density was measured using a Mettler Toledo benchtop density kit (for AX/AT/AG balances, Mettler Toledo, Greifensee, Switzerland). *n*-Heptane was used as the reference fluid as the sorption of *n*-heptane in the polymer samples was minimal over the timescale of the measurement.

3.3.2 Fractional Free Volume

The density was used to estimate the free volume as follows: [9,10]

$$FFV=\frac{V-V_0}{V} \text{ where } V_0=1.3\sum V_w \qquad (3.2)$$

where FFV is the fractional free volume, V is the specific volume of the sample, V_0 is the occupied volume calculated as shown and V_w is the van der Waal's volume of the various units that make up the chemical structure of the polymer.[9–11]

3.3.3 Water Uptake

The water uptake samples were prepared by fully drying the films under vacuum for more than 12 hours. The samples were then weighed using an analytical balance and immersed in a jar of distilled water which was sealed and placed in a 35°C water bath. Water uptake was measured by removing the sample from the distilled water and quickly

and lightly wiping any excess liquid water off the film surface. The sample was then weighed on the same analytical balance before being returned to the distilled water. Measurements were repeated periodically over a week until a constant mass was obtained indicating that equilibrium uptake had been reached.

3.3.4 Gel Fraction

Gel fraction was characterized by measuring the dry mass of the polymer (Sartorius Cubis® Analytical Balance, Sartorius Weight Technology, GmbH, Goettinger, Germany) after fully drying the film in a vacuum oven. The sample was then placed in a Soxhlet extractor with the chosen solvent and refluxed for up to 12 hours. If the film did not dissolve, it was removed from the Soxhlet extractor and fully dried in a vacuum oven before being weighed. The gel fraction was calculated as follows:

$$gel\ fraction = \frac{m_{final}}{m_{initial}} \tag{3.3}$$

where m_{final} is the dry polymer mass after extraction and $m_{initial}$ is the dry polymer mass prior to extraction.

3.3.5 Fourier Transform Infrared Spectroscopy (FTIR)

FTIR was used to evaluate both chemical structure and hydrogen bonding interactions. FTIR samples were dried prior to measurement in a vacuum oven, and spectra were collected using a ThermoScientific Nicolet 6700 FTIR using either transmittance mode or attenuated total reflectance (ATR) mode using a diamond crystal. Transmittance mode is limited to thinner samples and probes the full thickness of the film while diamond crystal ATR probes approximately the first 2 microns of the film.[12]

3.3.6 Thermal Stability

Polymer thermal stability was evaluated by thermal gravimetric analysis (TGA) using a TA Instruments TGA Q500 with an N_2 atmosphere with flow rates of 40 mL/min to the balance and 60 mL/min to the sample. Samples from 2-12 mg were loaded into the sample pan and allowed to equilibrate in the furnace for at least 5 minutes at 25°C. The sample was then heated at 5°C/minute. The heating protocols are reported with the results in subsequent chapters.

3.3.7 Glass Transition

Glass transition temperatures (T_g) were determined using a Q100 differential scanning calorimeter (DSC) from T.A. Instruments using a dry N_2 purge. Polymer samples weighing 2-10 mg were loaded in aluminum pans and allowed to equilibrate in the instrument at 40°C for at least 15 minutes. Different heating rates and hold times were used depending on the polymer. These detailed experimental protocols will be reported with the results in subsequent chapters. The T_g is reported as the midpoint of the step change in heat capacity.

The T_g's of some samples were also evaluated using dynamic mechanical analysis (DMA) using a DMAQ800 from TA Instruments. Samples were measured using a film tension clamp with films that were approximately 10mm x 5mm x 0.08mm. Each sample was first equilibrated at -120°C for 15 minutes, and then the temperature was ramped at 3°C/minute to 300°C. A static preload force of 0.1 N was used to maintain the sample tension. The measurement was performed using an oscillating amplitude of 15 microns at a frequency of 1 Hz.

3.3.8 Crystallinity

Two techniques were used for determining the crystal content of the cellulose acetate polymers considered. The first, wide angle x-ray scattering (WAXD) was used on a limited number of samples; however, the results were inconclusive so differential scanning calorimetry (DSC) was used for the majority of this work. To determine the % crystallinity by DSC, a 2-10mg sample was loaded into an aluminum DSC pan. The sample was then held at 40°C for 15 minutes to equilibrate with the instrument. The sample was then heated, typically at 20°C/minute, through both the cold crystallization exotherm and the melting endotherm. The percent crystallinity was determined using the net melting endotherm, determined from the heat of melting (ΔH_m) and the heat of crystallization (ΔH_c), scaled by the heat of melting of a 100% crystalline sample (ΔH^0_m) (Equation 3.4).

$$\% \, crystallinity = \frac{\Delta H_m - \Delta H_c}{\Delta H_m^0} x100\% \tag{3.4}$$

3.4 PERVAPORATION EXPERIMENTS

3.4.1 Equipment

A schematic of the pervaporation apparatus is shown in Figure 3.4. The upstream feed was a 500 mL reservoir that rested on top of the film and was stirred with a suspended magnetic stir bar to reduce concentration polarization. The membrane sample was mounted in aluminum tape as pictured in Figure 3.5. The metal reservoir and sample holder was submerged in an oil bath for temperature control. The downstream face of the membrane connected to a glass manifold with removable glass sample collection vessels. The two sample collectors were alternated to allow sample collection to proceed continuously. The permeate samples were collected by condensing them with liquid N_2. The downstream pressure was maintained at less than 1 torr using a vacuum pump.

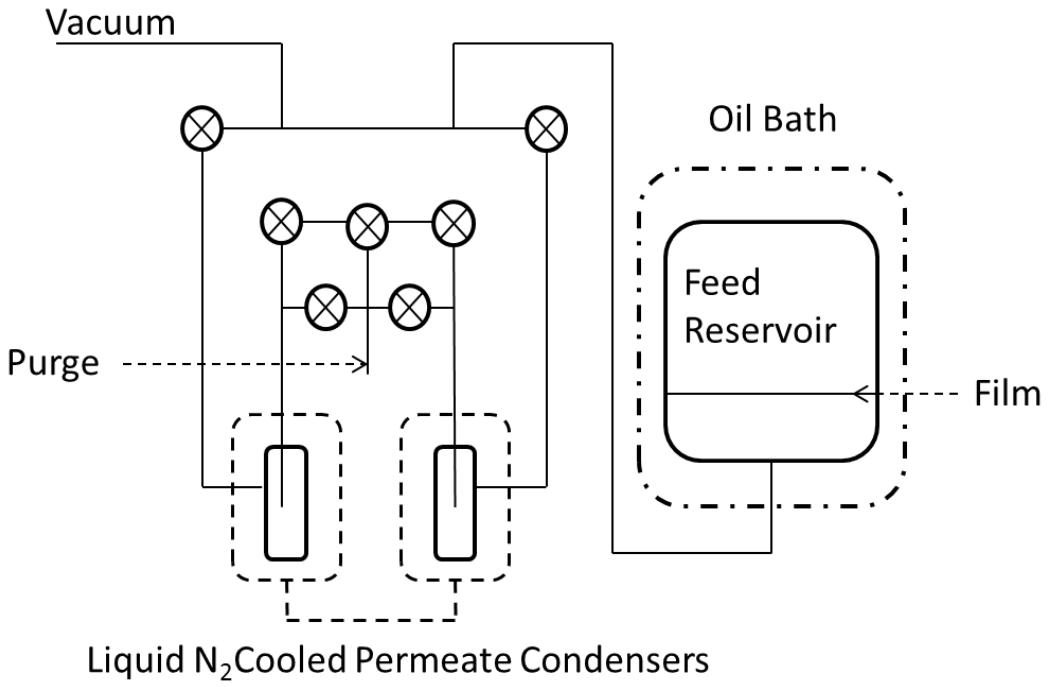

Figure 3.4: Schematic of the pervaporation apparatus

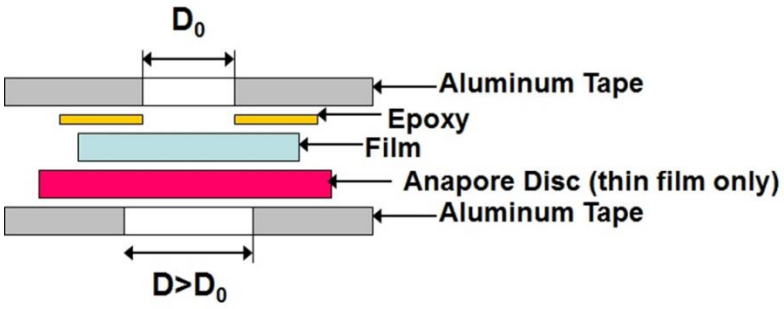

Figure 3.5: Construction of a permeation sample

3.4.2 Procedure

A pervaporation experiment was begun by mounting the film sample into the sample holder and then introducing either pure liquid water or a water/ethanol mixture into the reservoir. The sample chamber was then placed in the oil bath, and the downstream face of the membrane was exposed to vacuum. The system was then

allowed to rest overnight to come to thermal equilibrium before liquid N_2 was introduced to the sample condenser and samples collected.

The permeate samples were allowed to thaw in the sample condenser and would subsequently be weighed to determine the total amount of permeate. When a mixed water/ethanol feed was used, the sample would be further diluted with water before a Hewlett Packard 5890 Gas Chromatograph was used to determine the ethanol content of the permeate.

3.4.3 Calculations

Raw mass data was converted to total and component fluxes according to the following equations:

$$Total\ Flux: N_T = \frac{M_{S+SC} - M_{SC}}{Area * time} \tag{3.5}$$

$$Ethanol\ Flux: N_{EtOH} = C_{EtOH} * N_T \tag{3.6}$$

$$Water\ Flux: N_{H_2O} = N_T - N_{EtOH} \tag{3.7}$$

Where N_i is the mass flux of component i or total flux, T, M_{S+SC} is the mass of the sample and sample container, M_{SC} is the mass of the empty sample container, and C_{EtOH} is the mass concentration of ethanol in the permeate determined using a calibration curve and gas chromatography.

The component fluxes were then converted to permeability using Equation 2.10 in Chapter 2. The activity coefficients were calculated using the NRTL method[13] and the vapor pressure was calculated using Antoine's equation.[13]

3.5 GAS PERMEATION MEASUREMENTS

3.5.1 Equipment

All of the permeability measurements were made using a constant volume, variable pressure permeability apparatus (Figure 3.6). This apparatus consists of the upstream gas delivery system, a 47 mm Millipore filter holder for the sample and the downstream measurement system.

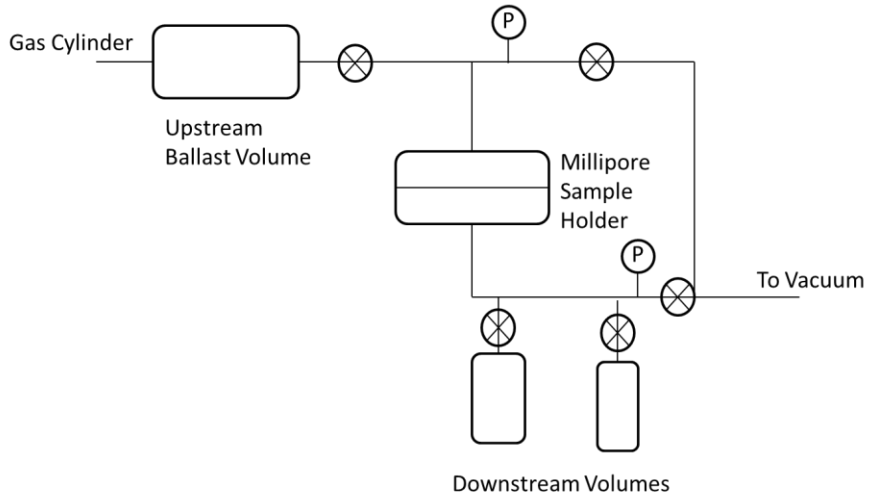

Figure 3.6: Schematic of the gas permeability system

The upstream gas delivery system consists of a connection to a high-pressure gas cylinder and an upstream ballast volume. Systems with two different designs were used. The first is designed to be open to the gas cylinder at all times, and the second is given a charge of gas at the beginning of the experiment but is then disconnected from the cylinder. The first design was used for the general gas permeability measurements on HFA-MDA-6FDA work (Chapter 5), while the second design was used for the plasticization of HFA-MDA-6FDA (Chapter 5) and all of the cellulose acetate

measurements (Chapter 6). The design of the upstream should not change the measured gas fluxes.

The downstream portion of the apparatus consists of a downstream volume, a 10 torr pressure transducer and a vacuum line. The downstream volume consists of both the necessary tubing and optional volumes which may be opened for higher flux samples.

3.5.2 Procedure

Gas permeation samples were mounted in the same manner as in the pervaporation experiment, although the exposed area was smaller (Figure 3.5). Devcon epoxy was used to seal the sample to the upstream aluminum tape because the adhesion between the films studied and the aluminum tape was not sufficient to provide a leak-free sample. In the case of thin films, the PDMS layer faced the downstream side of the system, thus allowing the film of interest to be in contact with the feed. The thin film was further mechanically supported by Anapore ceramic filters with a 0.02 micron pore size which provide negligible mass transfer resistance.

Permeability measurements were made by first mounting the sample and pulling vacuum until the maximum vacuum had been achieved. This process helps to remove sorbed gases in the sample or water which may have sorbed onto the downstream tubing. The time required to degas the sample varied depending on the sample thickness, but it was typically no longer than overnight.

After the sample was degassed, the upstream system was pressurized with the desired gas with the downstream still under vacuum. The sample was then allowed to come to steady state as indicated by the development of a constant downstream pressure while the sample was exposed to vacuum. When steady state was achieved, the flux of gas through the membrane was measured by isolating the downstream volume from the

vacuum pump and recording the downstream pressure rise with Labview software from National Instruments. The calculation of permeability from the raw pressure vs. time data was done according to Equation 3.8. Typically at least three measurements were made at each pressure to ensure that steady state had been reached. The pressure was then changed for the next measurement, or the sample was again degassed to prepare for measurement of a different gas.

$$P_A = \frac{V_d l}{p_2 ART}\left[\left(\frac{dp_1}{dt}\right)_{ss} - \left(\frac{dp_1}{dt}\right)_{leak}\right] \tag{3.8}$$

where P_A is the permeability of gas A, V_d is the downstream volume, l is the film thickness, p_2 is the upstream pressure, A is the exposed area of the film, R is the gas constant, T is temperature, dp_1/dt is the downstream rate of pressure rise at either steady state (SS) or due to leaks (leak).

3.5.3 Physical Aging

A physical aging experiment ideally began with the thermal annealing of the film sample. Annealing was done in the free standing state, prior to the sample being mounted with aluminum tape. The annealing temperature should be sufficiently above the T_g to erase any prior aging and set a known thermal history for the sample. The annealing time and temperature will be noted with the relevant results. After the annealing process, the sample was removed from the oven and quench cooled to room temperature before being prepared as described above (3.5.2). The time from oven to mounting in the cell to begin degassing was approximately 15 minutes.

Once the sample was degassed, the permeability measurements were performed as described above (3.5.2). Physical aging measurements consisted of measuring the O_2, N_2, and CH_4 permeability at 2 atm upstream pressure. The relatively mild upstream pressure reduces the chance of the film breaking prior to completion of the measurement.

3.5.4 Plasticization

Due to the exposure-time sensitive nature of CO_2 permeability, special care was taken when making CO_2 measurements. CO_2 permeability measurements require precise control of exposure time and pressure, and once the film has been exposed to a program of CO_2, it was not used for further testing. Three types of CO_2 experiments are described below.

A plasticization pressure curve (PPC) experiment was done by measuring the CO_2 permeability as the pressure was increased step-wise through a series of pressures. The number of pressure steps used depended on the film being tested and can influence the results. Unless otherwise noted, the pressure was held at each step for 10 minutes in the case of a thick film or 3 minutes for a thin film. This difference in holding times was necessary due to the increased time to achieve steady state permeation in thick films.

A hysteresis experiment is a PPC experiment with a longer hold at the highest pressure and then a step-wise depressurization that mirrors the pressurization cycle. This cycle of stepwise pressure increases, high pressure hold and stepwise pressure decreases made up a single hysteresis loop. Multiple loops were sometimes performed on the same sample to further investigate sample recovery.

A 2 hour exposure experiment is similar to a PPC except that it utilizes fewer pressures with two hour holds at each pressure. The stepwise increases in pressure were performed in the same manner, but the permeability was measured several times throughout the two hour holds to evaluate the time evolution of the plasticization response.

3.6 GAS SORPTION MEASUREMENTS

3.6.1 Pressure Decay Gas Sorption Apparatus

Gas sorption measurements were made using a dual volume, dual transducer gas sorption apparatus (Figure 3.7), which has also been described elsewhere.[14,15] The apparatus consisted of a pair of small chambers of known volume connected by a valve. Each chamber was connected to a pressure transducer.

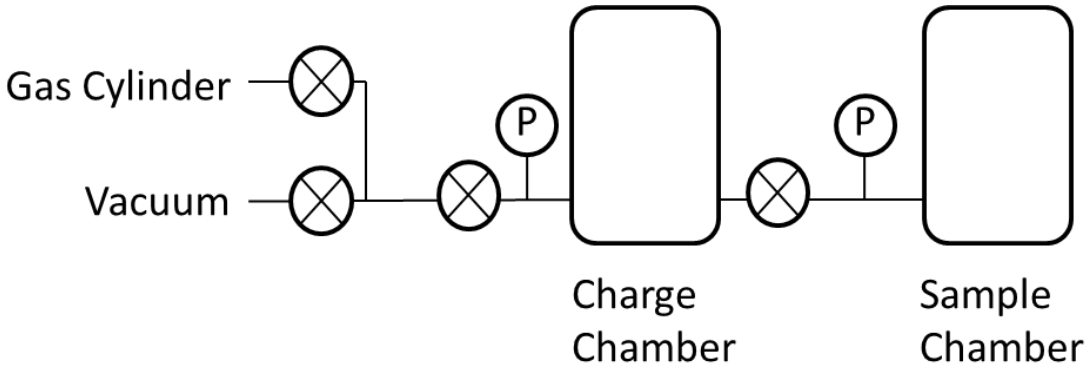

Figure 3.7: Schematic of the pressure decay system

3.6.2 Sorption Isotherm Measurements

Approximately one gram of polymer film was placed in the sample chamber and both chambers were evacuated for at least 12 hours. The charge chamber was then pressurized; and temperature and pressure were allowed to stabilize for 30 minutes to one hour. The valve between the two chambers was opened and then closed to introduce a known amount of gas into the sample chamber. The gas pressure in the sample chamber decreased over time until equilibrium was reached. The amount of gas sorbed into the polymer was calculated from the known volume and temperature and measured pressure reading using the Virial Equation of State.[16] Following equilibration at the first pressure, the pressure was increased to the next level without pulling vacuum in between. The

sample was fully evacuated prior to using another gas. As with permeability measurements, CO_2 sorption isotherms require special care. Due to CO_2 plasticization, the amount of CO_2 in the sample increases slowly over time. Thus, for CO_2 isotherms a set exposure time of 24 hours was used to minimize the effect of plasticization.

3.7 REFERENCES

(1) Smith, Z. P.; Sanders, D. F.; Ribeiro, C. P.; Guo, R.; Freeman, B. D.; Paul, D. R.; McGrath, J. E.; Swinnea, S. *J. Memb. Sci.* **2012**, *415-416*, 558–567.

(2) Sanders, D. F.; Smith, Z. P.; Ribeiro, C. P.; Guo, R.; McGrath, J. E.; Paul, D. R.; Freeman, B. D. *J. Memb. Sci.* **2012**, *409-410*, 232–241.

(3) Puleo, A. C.; Paul, D. R.; Kelley, S. S. *J. Memb. Sci.* **1989**, *47*, 301–332.

(4) Huang, Y.; Paul, D. R. *J. Memb. Sci.* **2004**, *244*, 167–178.

(5) Frank, C. W.; Rao, V.; Despotopoulou, M. M.; Pease, R. F. W.; Hinsberg, W. D.; Miller, R. D.; Rabolt, J. F. *Science* **1996**, *273*, 912–915.

(6) Henis, J. M. S.; Tripodi, M. K. *Science* **1983**, *220*, 11–17.

(7) Rowe, B. W.; Freeman, B. D.; Paul, D. R. *Polymer* **2009**, *50*, 5565–5575.

(8) Tompkins, H. G.; McGahan, W. A. *Spectroscopic Ellipsometry and Relectometry*; John Wiley & Sons, Inc.: New York, 1999.

(9) Bondi, A. *Physical Properties of Molecular Crystals, Liquids, and Glasses*; John Wiley & Sons, Inc.: New York, 1968.

(10) Bondi, A. *J. Phys. Chem.* **1964**, *68*, 441–451.

(11) Van Krevelen, D. W. *Properties of Polymers: Their Correlation with Chemical Structure; Their Numerical Estimation and Prediction from Additive Group Contributions*; 3rd ed.; Elsevier: Amsterdam, 1990.

(12) *Scientific Instruments Training Institute: Fundamentals of Analysis Manual*; ThermoScientific.

(13) Gmehling, J.; Onken, U.; Arlt, W. *Vapor-Liquid Equilibrium Data Collection*; Dechema: Frankfurt, 1977.

(14) Lin, H.; Freeman, B. D. In *Springer Handbook of Materials Measurement Methods*; Czichos, H.; Saito, T.; Smith, L., Eds.; Springer: New York, 2006; pp. 371–387.

(15) Koros, W. J.; Paul, D. R.; Rocha, A. A. *J. Polym. Sci. Polym. Phys. Ed.* **1976**, *14*, 687–702.

(16) Dymond, J. H.; Marsh, K. N.; Wilhoit, R. C.; Wong, K. C. *The Virial Coefficients of Pure Gases and Mixtures*; Frenkel, M.; Marsh, K. N., Eds.; Landolt-Bornstein: Darmstadt, 2001.

Chapter 4: Ethanol Dehydration with Thermally Rearranged Polyimides

4.1 Overview

The goal of this work was to evaluate the potential of thermally rearranged polyimides (TR polymers) for ethanol dehydration. The targeted separation is the high temperature (>100°C), high water content (>10%$_{wt}$) dehydration of ethanol vapor. Doing the separation at these conditions allows for greater energy integration over traditional lower temperature, low water content ethanol liquid dehydration for which membranes are typically developed. To evaluate the feasibility of this project, the pervaporation performance of a sample material was measured and evaluated against literature reports.

4.2 Experimental Details

4.2.1 Materials

The TR precursor material selected for this study was synthesized from 3,3'-hydroxy-4,4'-diaminobiphenyl (HAB) and 2,2'-bis-(3,4-dicarboxyphenyl) hexafluoropropane dianhydride (6FDA). The resulting polyimide, HAB-6FDA, (Figure 4.1), is a high molecular weight member of the soluble TR-precursor family. High molecular weight improves the mechanical stability of the material which is important in producing free standing films of sufficient size to measure the pervaporation properties. The precursor film was rearranged under a 900 mL/minute N_2 purge in a Carbolite Three Zone Hinged Tube Furnace (Model HZS 12/-/600, Watertown, WI, USA) using the following protocol: heat at 5°C/minute to 300°C, hold for 1 hour to insure complete imidization, heat at 5°C/minute to 350°C, hold for 1 hour for rearrangement, cool to room temperature at a maximum rate of 10°C/minute. The resulting chemical structure of the film is a mixture of the precursor, HAB-6FDA, and the TR analog, HAB-6FDA TR

(Figure 4.1). Although Figure 4.1 only shows a linear rearranged structure, it is likely that the material undergoes some crosslinking during TR reaction. The same film (92.6μm thick) was used for all experiments. The exposed area was controlled with aluminum tape and epoxy, as described in Chapter 3.

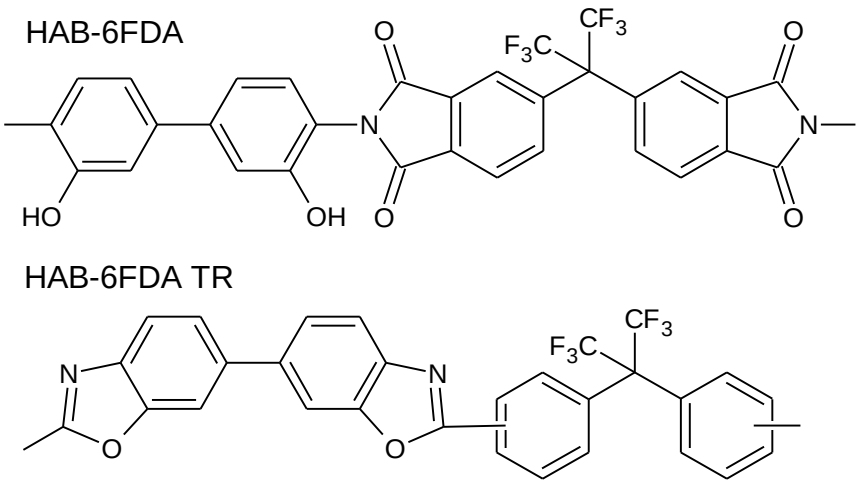

Figure 4.1: Chemical structure of HAB-6FDA and the resulting HAB-6FDA TR

4.2.2 Pervaporation Experiments

All pervaporation experiments were performed as described in Chapter 3. The permeability was first measured with a 53:47%$_{mole}$ (60:40%$_{wt}$) ethanol:water feed as the temperature was lowered from 76 to 66 to 56°C. The sample was maintained at each temperature overnight to ensure that thermal equilibrium was reached and then permeate samples were collected until a constant composition and flux were achieved. The membrane was at each temperature for roughly 24 hours. After the series of mixed feed experiments, the feed was removed, and the membrane was dried before the same membrane was remounted in the permeation cell for measurements with a pure water feed at 66 and 95°C.

4.3 Results and Discussion

4.3.1 Effect of Temperature and Feed Composition on Water Transport

The water permeability of HAB-6FDA TR depends on both temperature and feed composition (Figure 4.2). In a pure water feed, when temperature is raised from 66°C to 95°C, permeability decreases by almost a factor of two. The diffusivity of molecules through a polymer is expected to increase monotonically with temperature; therefore, for the permeability to decrease with temperature, the decrease in solubility of water with increasing temperature must be more than the increase in diffusivity. However, even as the permeability decreases as temperature increases, the water flux doubles as temperature increases from 66°C to 95°C (Figure 4.3). The rise in flux is due to the rapid increase in the vapor pressure of water, or driving force, as the temperature approaches the normal boiling point of water. This rapid increase in driving force with temperature is one of the motivations for performing this separation at high temperatures. Another reason is that the feed is likely to be the vapor from a distillation column where the temperature is that given by the vapor-liquid equilibrium at operating pressures.[1] Finally, better heat integration with the rest of the ethanol dehydration process can be achieved by operating at higher temperatures and pressures.[2]

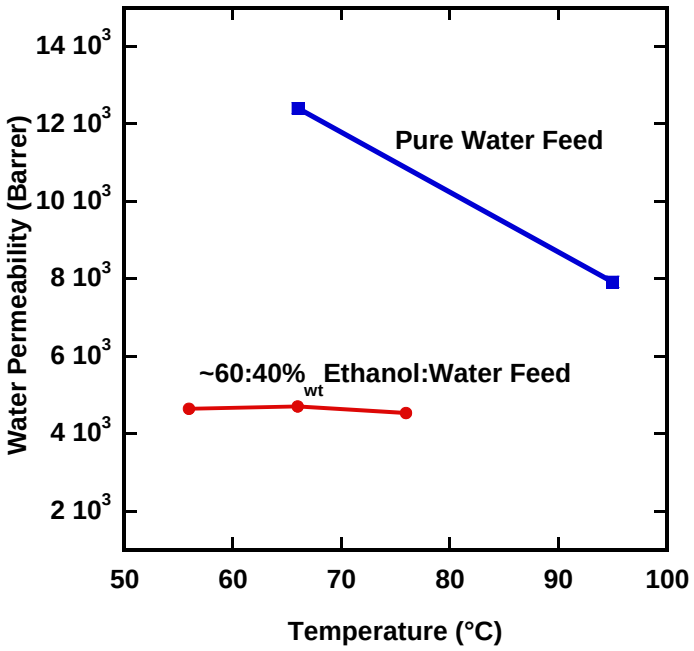

Figure 4.2: Water permeability of HAB-6FDA TR in a pure water feed and a 60:40%$_{wt}$ ethanol:water feed.

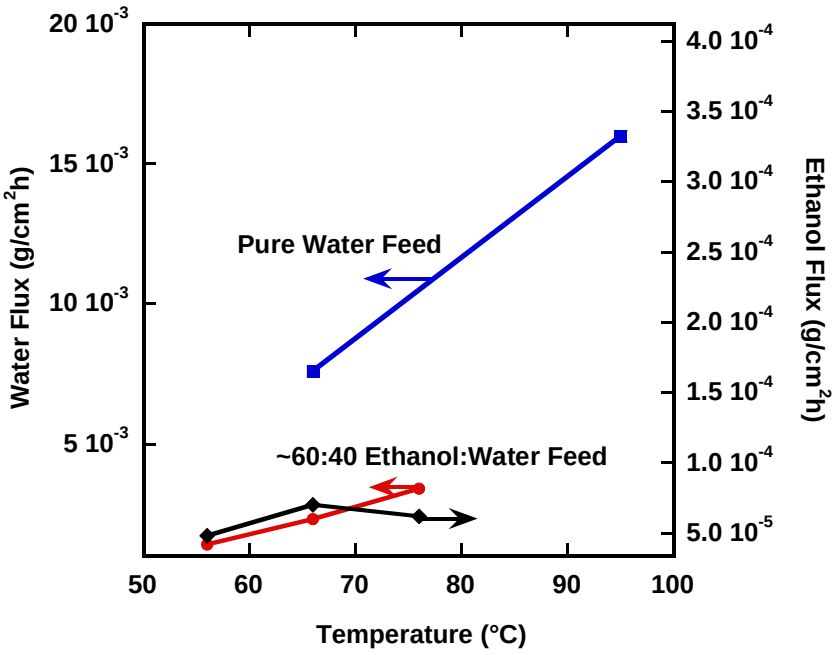

Figure 4.3: HAB-6FDA TR pure water flux and water and ethanol flux in a 60:40%$_{wt}$ feed

When the feed is only 40%$_{wt}$ water, the water permeability is far less sensitive to temperature. Furthermore, the permeability of water in the mixed feed is greatly suppressed relative to that in the pure feed. This result can possibly be explained, at least in part, by competitive sorption, where, due to the presence of two species competing for the same excess free volume elements, the sorption of each component is lower than their pure component sorption values. Beyond competitive sorption, permeability of a component can be lowered in a mixed feed if one of the components (or a combination of the components) plasticizes the membrane. As the feed concentration of the plasticizing component decreases, the swelling of the membrane due to plasticization decreases, which decreases the permeability of all species.

Although the permeability of water in the mixed feed is almost independent of temperature, water flux still rises with temperature (Figure 4.3). Again, this phenomenon

is due to the increase in driving force for water transport with increasing temperature. However, the driving force for the mixed feed is lower at a given temperature than that of the pure feed.

4.3.2 Effect of Temperature on Mixed-Feed Permeability

The water permeability of HAB-6FDA TR in the 53%$_{mole}$ ethanol feed is roughly two orders of magnitude higher than the ethanol permeability (Figure 4.4). Because water is both smaller and more condensable than ethanol, water diffusivity and solubility, and thus the water permeability, should be higher than those of ethanol.[3] In addition, the ethanol permeability is more dependent on temperature than the water permeability, showing more than a factor of two decrease in permeability as the temperature was raised from 56°C to 76°C. This difference in thermal response between the water and ethanol is the origin of the increase in water/ethanol selectivity with temperature (Figure 4.5).

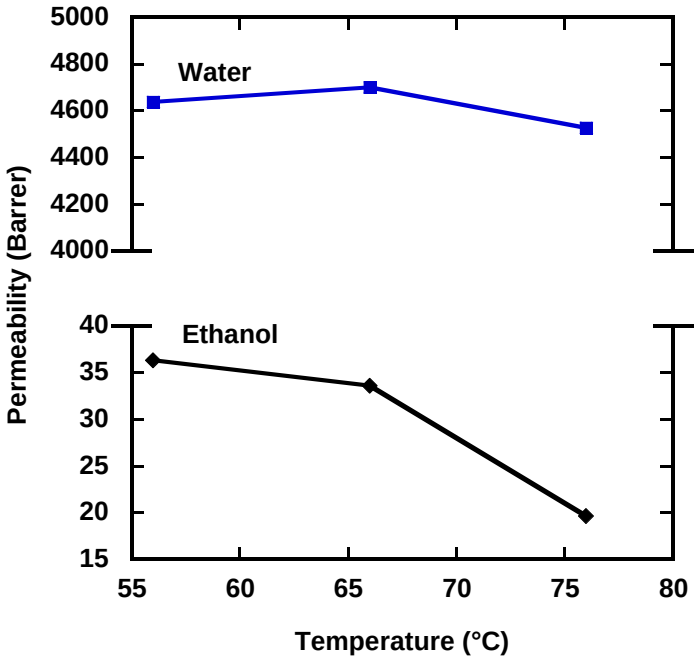

Figure 4.4: HAB-6FDA TR water and ethanol permeability in 60:40%$_{wt}$ feed

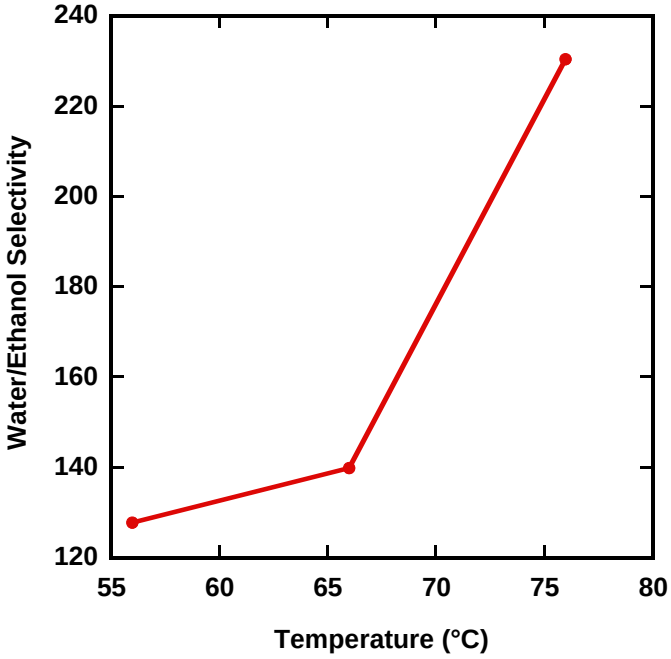

Figure 4.5: HAB-6FDA TR water/ethanol selectivity in 60:40%$_{wt}$ ethanol:water feed

Furthermore, because the same sample was used for the entire mixed feed temperature study, the stability of the water permeability over the course of the experiment indicates that, at these conditions, the membrane seems to be chemically and thermally stable, as expected. If wide scale degradation were occurring, the permeability of all species would be expected to rise and lead to a catastrophic decay of selectivity, which was not observed.

4.3.3 Comparison of HAB-6FDA to Materials in the Pervaporation Literature

There is no consensus in the ethanol/water pervaporation literature as to the best conditions to use to test the transport properties of various materials. Figure 4.6 presents a permeability/selectivity trade-off plot in the manner of a Robeson upper bound plot[4,5] using data from a recent review article.[6] Experiments represented in this plot range in temperature from 25°C to 75°C. Furthermore, the feed conditions range from 89-96%$_{wt}$ ethanol. Few experiments have been reported at feed conditions with water content

higher than approximately $10\%_{wt}$, frequently due to membrane stability problems. The HAB-6FDA TR sample (Figure 4.6) shows a combination of transport properties that put it below the majority of samples shown, although it is similar to many materials tested at the highest temperatures. These experiments are all subject to the same considerations discussed above; the decrease in water sorption with increasing temperature causes water permeability to decrease. Figure 4.7 shows the same trade-off plot, but this time highlights the families of materials instead of temperature. HAB-6FDA TR shows performance in the range of many of the aromatic polyimides, which have structures similar to that of the HAB-6FDA precursor. Although HAB-6FDA does not have a permeability/selectivity combination that puts it among the highest performing materials, it does have stable performance in high temperature water/ethanol mixtures and would be expected to withstand more aggressive feed conditions than most of the polymers shown here.

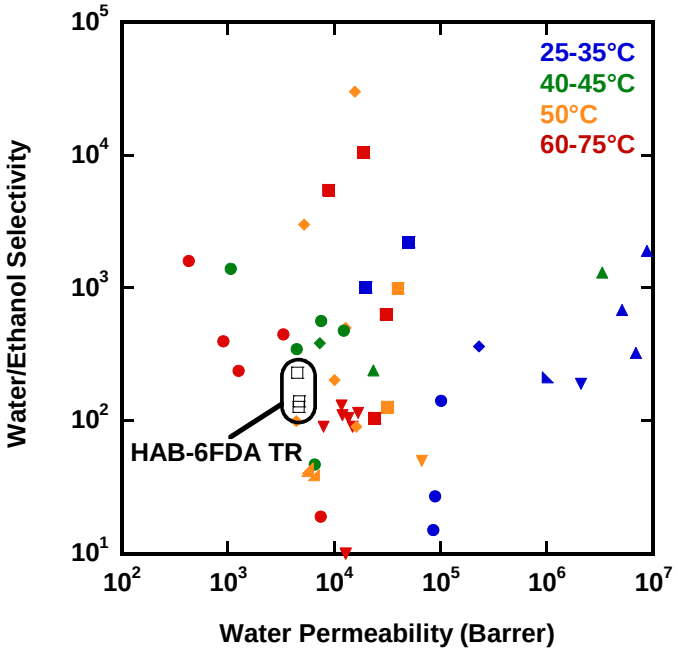

Figure 4.6: Effect of temperature on water permeability vs. water/ethanol selectivity trade-off

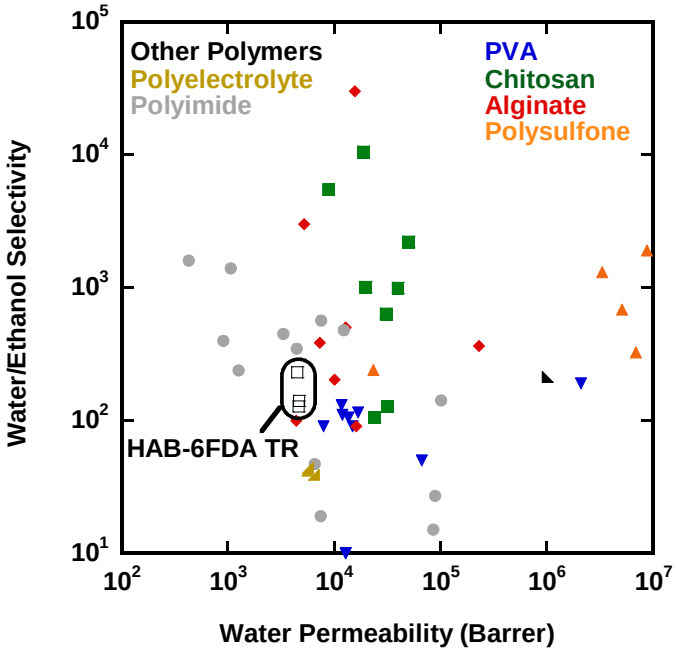

Figure 4.7: Effect of polymer structure on water permeability vs. water/ethanol selectivity

4.3.4 Comparison of HAB-6FDA TR to Commercial Vapor Permeation Membrane

Membranes have been commercialized for ethanol vapor dehydration purposes with limited temperature and pressure ranges. One such polymer is produced by UBE Industries, Ltd. who have published some of their results.[7] These membranes provide a realistic benchmark for evaluating the performance of the TR membrane. The exact structure of the UBE membrane is not reported, but it is an aromatic polyimide. The necessary calculations have been done to change the reported flux data into permeance, (i.e., permeability divided by thickness) but as the UBE material was tested as an asymmetric hollow fiber, the thickness of the selective layer is unknown.

Because the permeability of the UBE material cannot be calculated, it is necessary to evaluate the permeance of the TR material. Asymmetric hollow fibers typically have selective layers on the order of 0.1 μm thick, which is roughly four orders of magnitude thinner than the TR material tested. Figure 4.8 shows the water permeance of the UBE hollow fiber with two different feeds and the TR material as measured (thickness of 92.6 μm) and an estimated permeance for a 0.1 μm film. The estimation assumes that there is no change in permeability as thickness decreases, which, in the TR materials, also assumes that the conversion reaction is independent of thickness. On this basis, the permeance of the UBE hollow fiber is almost two orders of magnitude lower than the estimated permeance for a 0.1 μm HAB-6FDA TR film. The ethanol results (Figure 4.9) are similar in that the HAB-6FDA TR would have higher permeance if its thickness were closer to that of the UBE polyimide. Because the flux of the membrane determines the membrane area needed to purify a given stream, on a throughput basis, HAB-6FDA TR compares very well to the commercial UBE fiber.

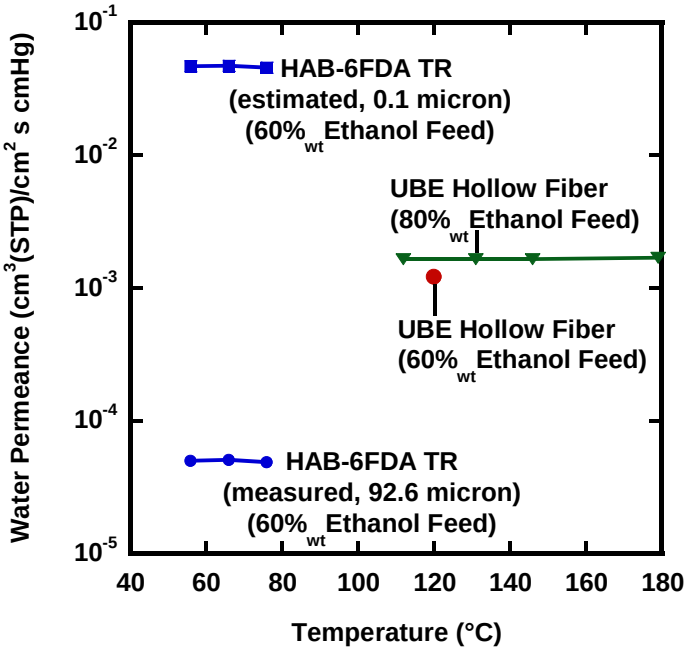

Figure 4.8: Water permeance reported for UBE hollow fiber[7] and HAB-6FDA TR as measured and estimated for 0.1 μm film.

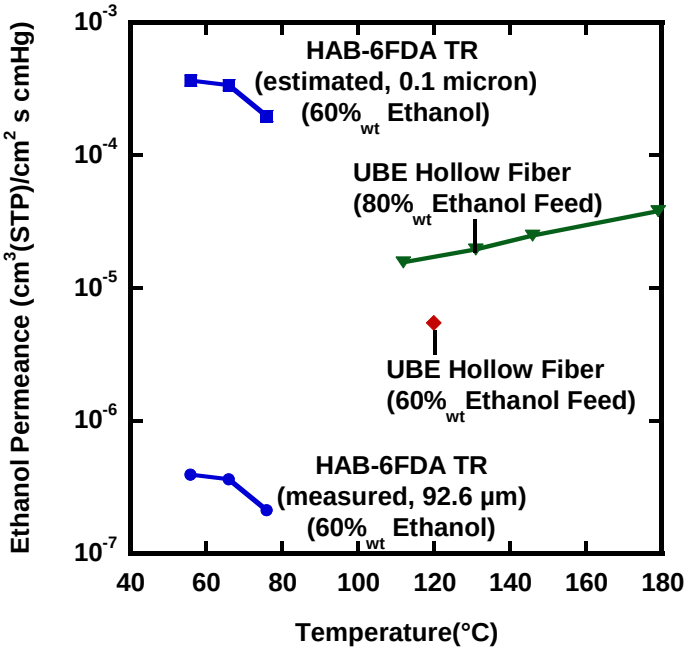

Figure 4.9: Ethanol permeance reported for UBE hollow fiber[7] and HAB-6FDA TR as measured and estimated for 0.1 micron film.

The selectivity of the membrane (Figure 4.10) is the second important transport parameter to consider. In terms of selectivity, the HAB-6FDA membrane is approximately the same as that of the UBE hollow fiber. The decrease in selectivity at higher ethanol feed content for the UBE fiber indicates that the membrane is plasticized by ethanol. The TR membrane has selectivity similar to that of the UBE material at similar feed concentrations.

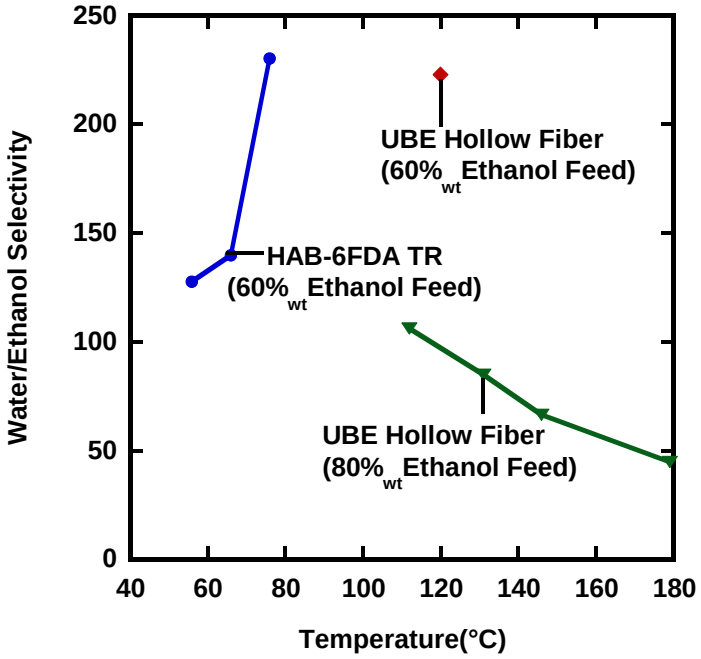

Figure 4.10 Water/ethanol selectivity for HAB-6FDA TR and UBE hollow fiber.[7]

Finally, it is important to evaluate the necessary selectivity for a practical separation. As described by Richard Baker, the content of ethanol in permeate (i.e., the amount of ethanol lost through the membrane) depends on both the membrane selectivity and the pressure ratio across the membrane (Equation 2.15).[8] Evaluation of the given equation for these feed conditions (Figure 4.11) demonstrates that at around a selectivity of 100, the purity of the permeate becomes less dependent on membrane selectivity, or equivalently, the separation moves into the pressure-ratio-limited regime. Because of the trade-off between permeability and selectivity, increases in selectivity are usually coupled with decreases in permeability. Thus, it is typically desirable to have a selectivity high enough to be in the pressure ratio limited region, but no higher. The TR polymers are close to this ideal level of selectivity, though perhaps some selectivity could be traded for permeability via changes in the chemical structure.

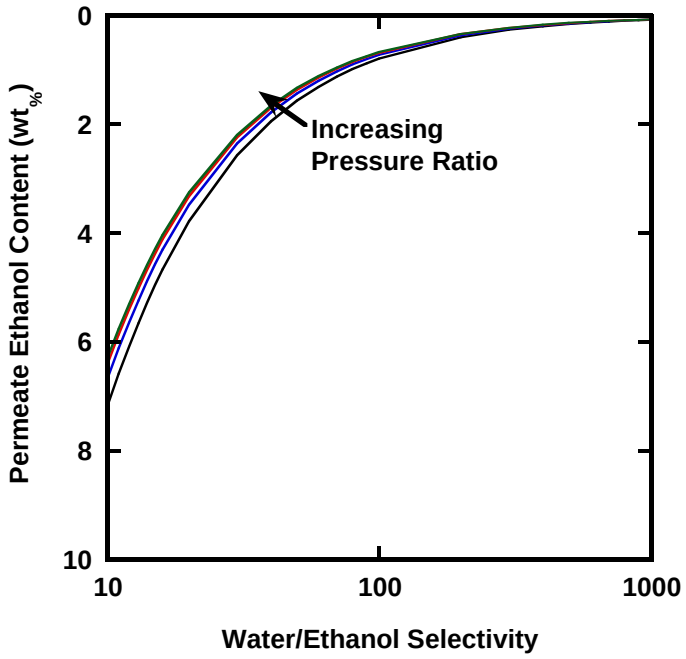

Figure 5.11 Effect of water/ethanol selectivity on permeate ethanol concentration with a 60%$_{wt}$ ethanol feed. Pressure ratios of 10, 20, 50 and 152 were used to generate these results.

4.4 CONCLUSIONS

HAB-6FDA TR has promise as an ethanol dehydration material. It has comparable permeability and selectivity to those of commercial membranes, and while not as high performing as some of the best materials the literature has to offer, TR polymers have higher thermal and chemical stability, which would allow the separation to be performed in the optimum temperature/pressure regime.

4.5 NOTE ON SUBSEQUENT WORK

Research on ethanol dehydration with TR polymers has been continued by other researchers, Dr. Kris Gleason, Dr. Wenfang Liu, and Dr. Chaoyi Ba.[9] Their work has focused on evaluating the stability of the precursors and TR materials, as well as the TR polymers' transport properties in realistic temperature and pressure ranges. The stability

studies were done using an exposure cell to hold samples at 120°C and 3 bar pressure under a 50%wt water/ethanol vapor. FTIR, TGA and pervaporatation testing demonstrate that sample with near 100% conversion to the TR structure are stable in these conditions, though precursors and samples with lower conversion are not. Additionally, the vapor permeation ethanol dehydration of 100% converted HAB-6FDA TR has been tested with both pure and mixed feeds using temperatures up to 170°C and pressures up to 6.4 atm. The results of the vapor permeation studies indicate that, as predicted by these results, TR materials have reasonable transport properties in the vapor phase. Both the stability testing and vapor permeation testing also demonstrate the high chemical and thermal stability of these polymers, although it is necessary to use samples that are more highly converted than the one used in this study.

4.6 REFERENCES

(1) Huang, Y.; Baker, R. W.; Vane, L. M. *Ind. Eng. Chem. Res.* **2010**, *49*, 3760–3768.

(2) Côté, P.; Roy, C.; Bernier, N. *Sep. Sci. Technol.* **2009**, *44*, 110–120.

(3) Matteucci, S.; Yampolskii, Y. P.; Freeman, B. D.; Pinnau, I. In *Materials Science of Membranes for Gas and Vapor Separations*; Yampolskii, Y.; Pinnau, I.; Freeman, B. D., Eds.; John Wiley & Sons, Ltd: Chichester, 2006; pp. 1–47.

(4) Robeson, L. M. *J. Memb. Sci.* **1991**, *62*, 165–185.

(5) Robeson, L. M. *J. Memb. Sci.* **2008**, *320*, 390–400.

(6) Chapman, P. D.; Oliveira, T.; Livingston, A. G.; Li, K. *J. Memb. Sci.* **2008**, *318*, 5–37.

(7) Nakagawa, K.; Kusuki, Y.; Ninomiya, K. *Proc. Fourth Int. Congr. Pervaporation Process. Chem. Ind.* **1989**, 250–260.

(8) Baker, R. W. *Membrane Technology and Applications*; 2nd ed.; John Wiley & Sons, Ltd, 2004; pp. 1–538.

(9) Gleason, K. L.; Paul, D. R.; Freeman, B. D. Vapor Permeation of Ethanol and Water in Thermally Rearranged (TR) Polymers, 2013.

Chapter 5: Gas Transport and Thermal Stability of HFA-Containing Aromatic Polyimide

5.1 Overview and Introduction

The purpose of this work was to evaluate the effect of the hexafluoroalcohol (HFA) moiety on the gas transport properties of an aromatic polyimide. Studies have found that inclusion of certain moieties, such as hexafluoroisopropylidene, can substantially improve the gas separation properties of numerous backbone structures.[1–6] Although the HFA group has been utilized to improve the chlorine resistance of reverse osmosis membranes,[7–9] this moiety's influence on gas separation properties has never been tested. Additionally, it was discovered that the HFA-polyimide undergoes an unusual reaction or degradation at high temperatures and some work has been done to characterize this reaction.

The HFA group's unique chemistry has been utilized in several different fields including: increasing the solubility of 157 and 193nm photoresists,[10–14] increasing organic-vapor sensor sensitivity[15–17] and increasing blend miscibility windows.[18,19] In each of these applications, the HFA group increases intermolecular interactions by being a strong hydrogen-bond donor. Although HFA's pKa (reported values range from 9-11[11,20,21]) is approximately equal to phenol, HFA is much more hydrogen-bond acidic than phenol.[17,22] Simultaneously, HFA is less hydrogen-bond basic than phenol,[17,22] which causes HFA to have limited self-association.[17,19] The combination of these factors allow HFA groups to interact very strongly with other molecules, particularly any that have hydrogen-bond acceptor groups.[23] Strong interactions between polymer chains can increase structural rigidity, which has increased the selectivity of multiple polymer structures.[24] Additionally, trifluoromethyl groups are very bulky which could decrease packing efficiency and raise permeability.[24] The combination of decreased packing

efficiency and increased chain stiffness from strong inter-chain interactions could cause the HFA group to improve the gas separation properties of the polyimide.

5.2 Experimental Details

5.2.1 Materials

The main polymer used in this study was an aromatic polyimide synthesized from 4,4'-(hexafluoroisopropylidene)diphthalic anhydride (6FDA) and ortho-hexafluoroalcohol substituted-4,4'methylenedianiline (HFA-MDA). HFA-MDA-6FDA (Figure 5.1) was kindly supplied by Central Glass Co., Ltd as films ranging from 15-30 μm in thickness. The HFA-MDA-6FDA was synthesized by solid-state imidization from the polyamic acid. The films were additionally dried under vacuum at 120°C for at least 12 hours before use to remove any sorbed water.

The second polymer was an HFA-containing aromatic polyamide synthesized from HFA-MDA and 4,4'-[2,2,2-trifluoro-1-(trifluoromethyl)ethylidene]bis-benzoyl chloride (BAF). HFA-MDA-BAF (Figure 5.1), which corresponds to the HFA-MDA-6FDA above, was supplied by Central Glass Co., Ltd. as large chunks. Films of HFA-MDA-BAF were cast from tetrahydrofuran (THF) using a silicon wafer and metal casting ring in a fume hood. Films that were approximately 30 μm thick were successfully cast, but thinner films cracked prior to lifting. THF was used as a solvent at the suggestion of our colleagues at Central Glass, but later analysis demonstrated that use of THF introduced potential complications due to the complexation chemistry available to fluoroalcohols (cf. 5.3.6.2).[25] No other suitable solvents were found. Due to suspected residual solvent, the gas transport properties of this polymer are not reported.

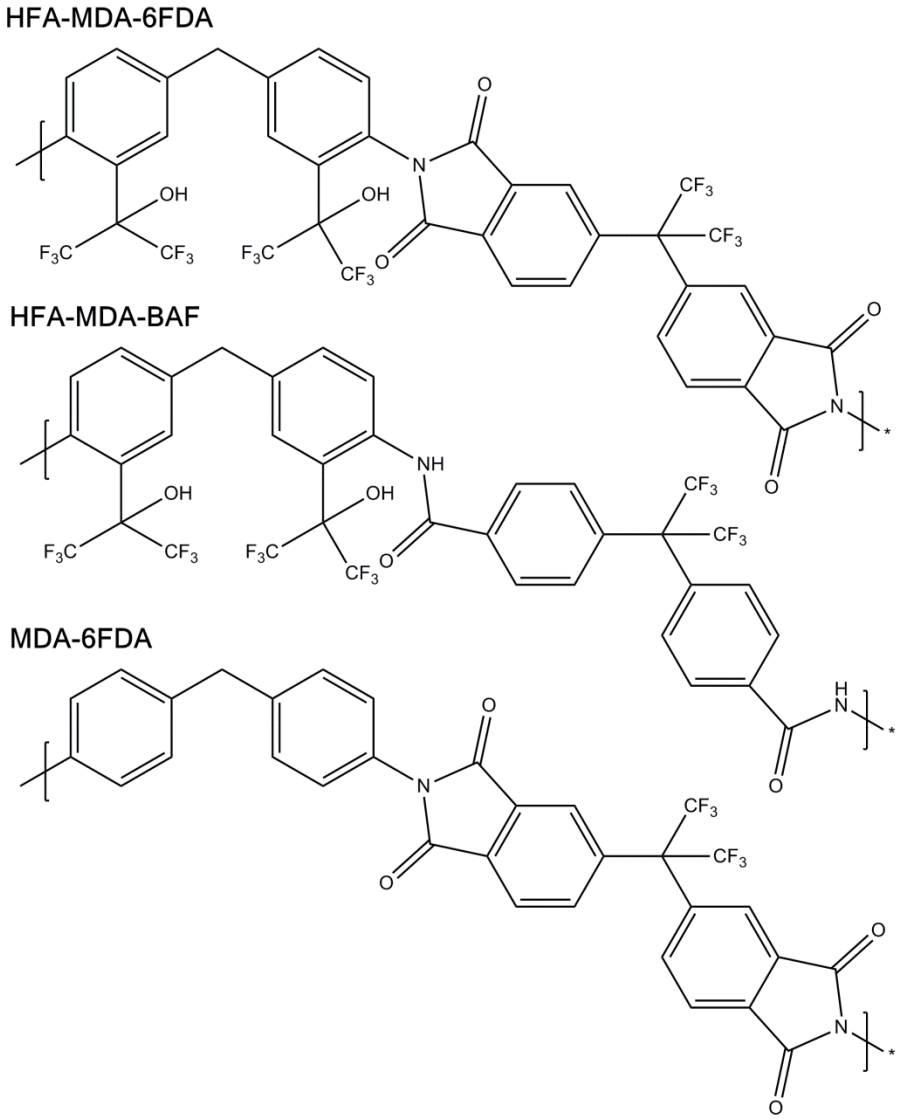

Figure 5.1 Chemical structures of polymers used in this study, HFA-MDA-6FDA and HFA-MDA-BAF, and the reference material, MDA-6FDA.

5.2.2 Glass Transition Temperature

HFA-MDA-6FDA's glass transition temperature was determined using a Q100 differential scanning calorimeter (DSC) from T.A. Instruments using a dry N_2 purge. Polymer samples weighing approximately 5 mg were loaded in aluminum pans and thermally equilibrated in the instrument at 40°C for at least 15 minutes. The samples

were then heated at 10°C/minute to 150°C and held for 30 minutes to remove sorbed water. The sample was then quench cooled at 30°C/minute to 40°C. Finally, the samples were heated at 10°C/minute to 350°C three times with quench cools at 30°C/minute to 40°C between each heat. The T_g is reported as the midpoint of the step change in heat capacity for the first heating scan as the sample degraded at temperatures above T_g.

5.2.3 Thermal Stability

The thermal stability of HFA-MDA-6FDA and HFA-MDA-BAF were evaluated by thermal gravimetric analysis (TGA) using a TA Instruments TGA Q500 with an N2 atmosphere with flow rates of 40 mL/min to the balance and 60 mL/min to the sample. A 10 mg sample was loaded into the sample pan and allowed to equilibrate in the furnace for 5 minutes at 25°C. The sample was then heated to 600°C at a rate of 5°C/minute. HFA-MDA-BAF was additionally tested in the high-resolution mode of the same TGA. High-resolution mode uses a dynamic heating rate which automatically slows when the sample is losing mass.

Finally, HFA-MDA-6FDA samples were also tested using isothermal TGA. The samples were prepared in the same way, using the same gas flows as described above. The method began with a 5°C/minute ramp to 150°C with an isothermal hold for 30 minutes to remove sorbed water. The sample was then heated at 5°C/minute to the desired hold temperature and held isothermally for 10 hours. The data are displayed with the time axis zero point set to the beginning of the ramp to the final temperature to capture mass loss during the heating ramp as well as during the high temperature hold.

5.3 RESULTS

5.3.1 HFA-MDA-6FDA Characterization

The basic characterization of HFA-MDA-6FDA is summarized in Table 5.1 along with literature data for MDA-6FDA.[26,27] HFA-MDA-6FDA's density is higher than that of similar polyimides, including MDA-6FDA[26,27], due to the large number of heavy fluorine atoms in the HFA-MDA-6FDA structure. Despite the higher density, the fractional free volume of HFA-MDA-6FDA is higher than these same polyimides, indicating that the HFA groups disrupted the chain packing.

Polymer	Density (g/cm^3)	Fractional Free Volume	Glass Transition (°C)	Water Uptake
HFA-MDA-6FDA	1.547	17.3%	290°C	1.57%
MDA-6FDA (Hirayama)[26]	1.417	15.5%	296°C	
MDA-6FDA (Coleman)[27]	1.400	16.00%	304°C	

Table 5.1 Summary of basic characterization of HFA-MDA-6FDA and reported values for MDA-6FDA.[26,27]

It is possible for polyimides to crosslink, especially when synthesized via solid-state imidization.[28] Crosslinked polymers have been shown to have improved selectivity and also resistance to physical changes due to the presence of highly sorbing penetrants,

i.e., plasticization. However, HFA-MDA-6FDA does not contain significant crosslinking as the sample dissolved in boiling NMP during a gel fraction test.

The glass transition of HFA-MDA-6FDA (Table 5.1) was measured on the first heat because the material undergoes a chemical reaction above its glass transition such that subsequent heats show progressively lower T_gs. This glass transition temperature is very high and indicates that the polymer is deep in the glassy state during all of the measurements reported here. The thermal stability is evaluated using TGA (Figure 5.2). HFA-MDA-6FDA is thermally stable up to its T_g. Above T_g, the polymer demonstrates two distinct mass loss regions which will be discussed in more detail in Section 5.3.6.

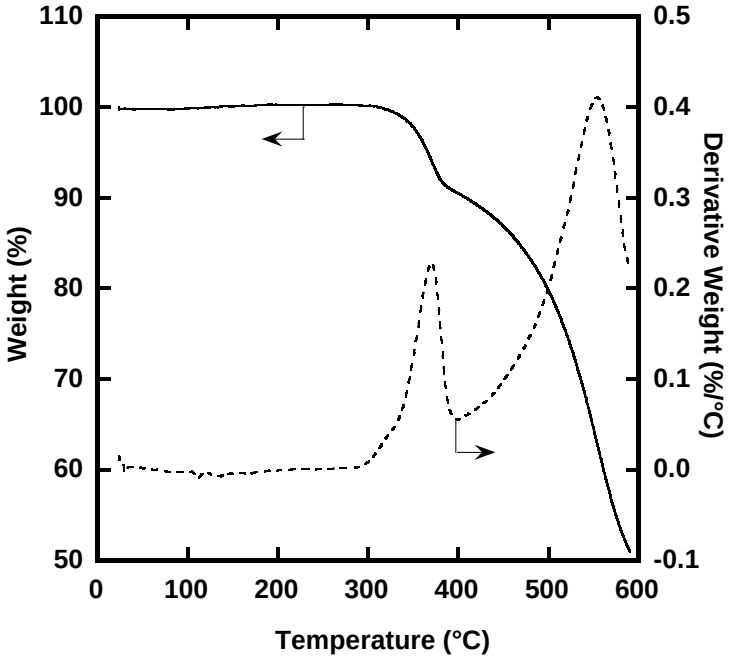

Figure 5.2 Thermogravimetric analysis for HFA-MDA-6FDA. Heating rate was 5°C/min with N_2 atmosphere.

5.3.2 Hydrogen-Bonding in the HFA Group

The transmission FT-IR spectrum of HFA-MDA-6FDA (Figure 5.3) indicates that the film is too thick to allow for quantitative analysis. However, the nature of the HFA group can be evaluated qualitatively. The alcohol in a free HFA group, one with no hydrogen bonding, shows a sharp peak at 3590-3610 cm^{-1},[15,18,20,29] while hydrogen bonded HFA groups have much broader absorption bands that range from 2900-3520 cm^{-1}.[15,18,20,29] HFA-MDA-6FDA shows both a sharp band at 3600 cm^{-1} and a very broad band from ~2900-3550 cm^{-1}, which indicates that many of the HFA groups are hydrogen bonding, likely with the imide carbonyls, but there are some that are not hydrogen-bonded. The presence of hydrogen-bonding could increase the stability of the polymer film in plasticizing environments.

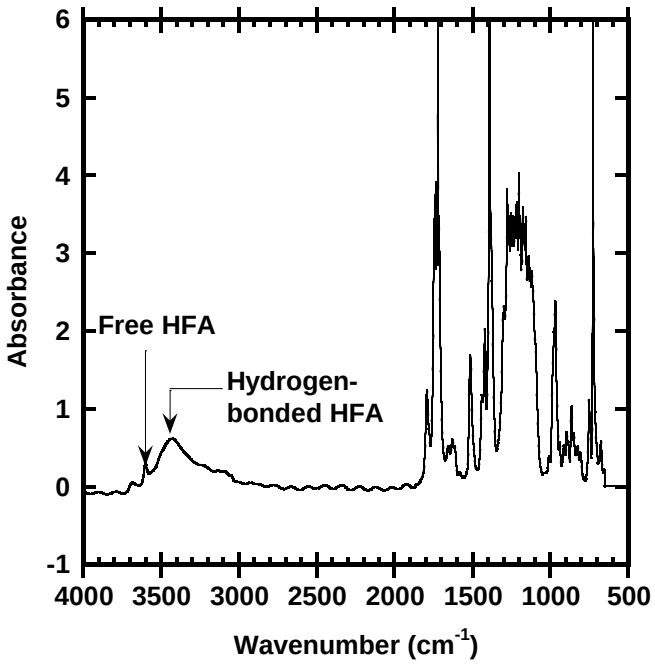

Figure 5.3 Transmission FT-IR spectrum of HFA-MDA-6FDA.

5.3.3 Pure Gas Permeability for Non-Plasticizing Gases

The pure gas permeability coefficients of He, O_2, N_2 and CH_4 at 35°C are shown as a function of pressure ranging from 2 to 20 atm (Figure 5.4). The permeability increases as the penetrant size decreases, which suggests that transport in HFA-MDA-6FDA is primarily limited by the diffusion of gas through the polymer. Furthermore, O_2, N_2, and CH_4 show a slight decrease in permeability with pressure as expected from the dual-mode behavior of glassy materials.[24] Permeability coefficients at 10 atm were interpolated from nearby data and these results are summarized in Table 5.2.

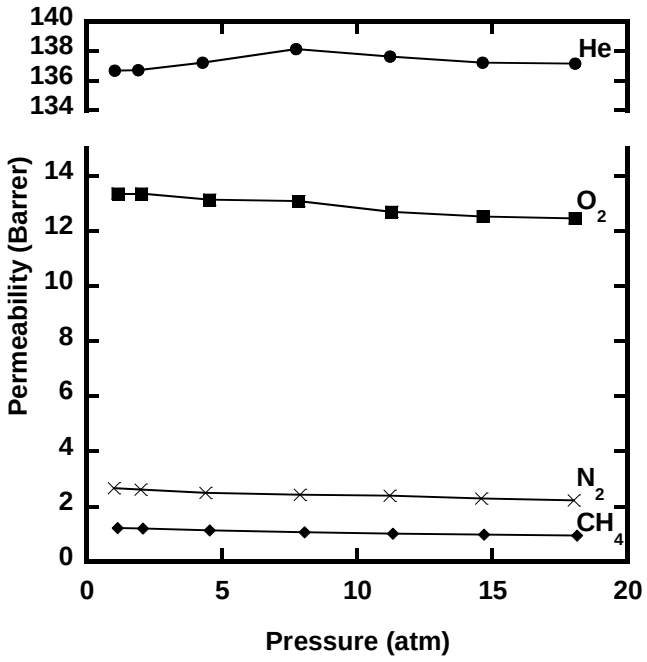

Figure 5.4 Permeability of He, O_2, N_2 and CH_4 in HFA-MDA-6FDA at 35°C as a function of upstream pressure.

Permeability (Barrer)					Ideal Selectivity		
CO_2	CH_4	N_2	O_2	He	CO_2/CH_4	CO_2/N_2	O_2/N_2
51.87	1.1	2.4	12.84	137.3	47	22	5.4

Table 5.2 Permeability at 10 atm and 35°C for HFA-MDA-6FDA. Pure gas selectivity at 35°C and 10 atm for selected gas pairs.

5.3.4 CO_2 Plasticization in HFA-MDA-6FDA

Plasticization is a phenomenon caused by highly sorbing penetrants, such as CO_2, which sorb to such an extent that the polymer matrix swells.[30] Furthermore, in glassy polymers, the structural changes caused by plasticizing penetrants can persist for long times after the penetrant is removed, an effect called conditioning.[31] To test the CO_2 plasticization and conditioning of HFA-MDA-6FDA, the pure gas permeability at 35°C was tested as a function of pressure according to the protocol shown in Figure 5.5a. A film sample was first exposed to step-wise increases in pressure to 30 atm with a 10 minute hold at each pressure. The permeability was measured in the last 90 seconds of the pressure hold. The time-lag of the material is less than 1 minute for CO_2 so the sample is at steady state for these measurements. The sample was then held at the maximum pressure for approximately 30 minutes before the pressure was decreased in the same manner. The sample was then held at 2 atm of CO_2 for approximately 1 day before the pressure was again cycled according to the same protocol except that the pressure was held at 30 atm for 2 days before the pressure was decreased.

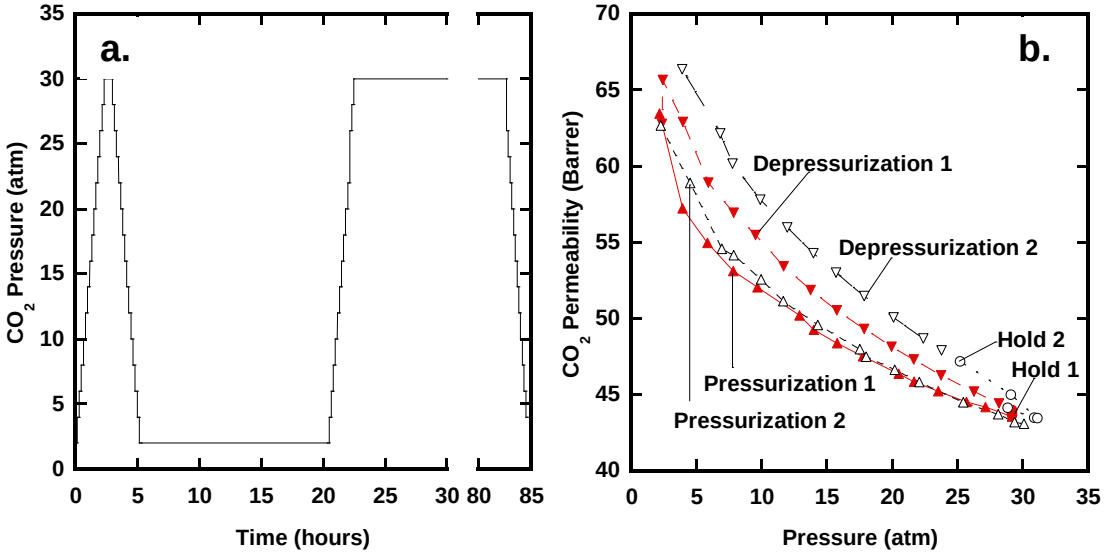

Figure 5.5 a. Upstream CO_2 pressure during the plasticization experiment. b. CO_2 permeability at 35°C in HFA-MDA-6FDA. Red (filled) symbols are the first pressure cycle. Blue (open) symbols are the second pressure cycle. Arrows pointing up indicate a pressurization step; circles indicate high pressure hold; arrows pointing down indicate a depressurization step.

The first pressurization (Figure 5.5b) does not show a minimum in the permeability versus pressure curve that would be expected if the film were undergoing plasticization.[24] The minimum in the permeability vs. pressure curve is termed the "plasticization pressure" and is typically assumed to be where plasticization begins to be significant.[32] In HFA-MDA-6FDA, the CO_2 plasticization pressure is above 30 atm which is higher than that of many other polymers.[30] However, the depressurization curve shows a somewhat higher CO_2 permeability than the pressurization curve. This hysteresis indicates that the polymer has undergone some plasticization-induced swelling and, due to the polymer being in the glassy state, this swelling cannot fully relax on the timescale of the experiment. Evidence of plasticization below the plasticization pressure has been previously reported.[32]

Because the second pressurization curve overlays the first, it can be assumed that the plasticization-induced swelling was not very significant or was able to relax during the overnight hold at low pressures. The longer hold time at high pressures causes additional plasticization, as shown by the higher permeability at 30 atm, and increased conditioning, as shown by the increased hysteresis in the depressurization curve.

According to published PALS results, during CO_2 plasticization of a glassy polymer, the average free volume element size becomes larger and the distribution of element sizes becomes broader.[33] The consequences of these changes in free volume are different for each penetrant gas. As the free volume increases, the diffusivity of all gases increases, with larger gases being affected more strongly.[24] Furthermore, recent analyses have shown that solubility also increases with free volume, and again larger molecules are affected more strongly than smaller molecules.[34] Thus, the free volume changes due to plasticization would be expected to affect the CH_4 more strongly than CO_2. To track the polymer's structural recovery after the second CO_2 pressure cycle, the permeability of CH_4 and O_2 at 2 and 4 atm were tracked as a function of time (Figure 5.6). The time axis shows the number of days after the end of the CO_2 tests described above. Figure 5.6a shows both the O_2 and CH_4 permeability are higher after CO_2 exposure, although over time the permeabilities approach their initial value. The CH_4 increases by a larger amount relative to its pre-CO_2-exposure permeability (Figure 5.6b). CH_4 permeability's relatively long recovery time compared to CO_2, which recovered at low pressures overnight, is likely due to CH_4's greater sensitivity to changes in the polymer free volume due to its larger size. Since CO_2 and O_2, are significantly smaller then CH_4, they are less sensitive to small changes in free volume. Thus, CH_4 permeability's slow recovery indicates that the recovery of the polymer matrix is much slower than indicated by the

CO_2. Because the polymer is well below its T_g, its chain motion is limited, and thus it would be expected that structural relaxation would be slow.

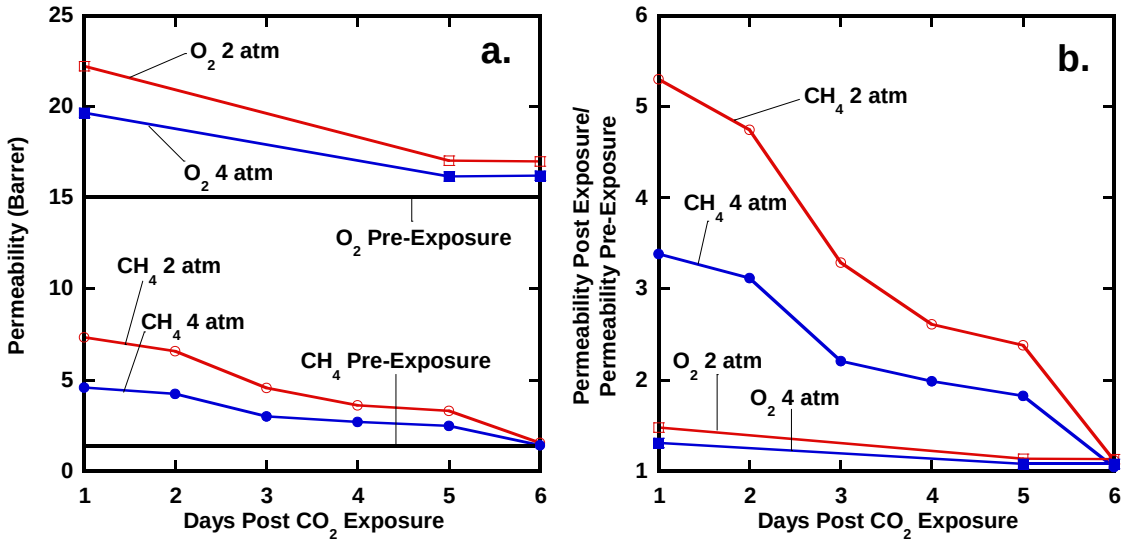

Figure 5.6 a. Permeability of O_2 and CH_4 as a function of time after CO_2 exposure. b. Permeability of O_2 and CH_4 normalized by pre-exposure permeability as a function of time post-CO_2 exposure.

5.3.5 Effect of HFA Group on Gas Solubility and Diffusivity

The gas sorption isotherms (Figure 5.7) are concave to the pressure axis, which demonstrates the expected dual-mode behavior.[24] The order of the gas sorption (S_{N_2}< S_{O_2}< S_{CH_4}< S_{CO_2}) follows the gases' condensability. Using the solubility at 10 atm and the permeability reported in section 5.3.3, the solution-diffusion model can be used to estimate the diffusion coefficient (Table 5.3). The reported permeabilities, solubilities and diffusivities of MDA-6FDA are listed for comparison.[26,27]

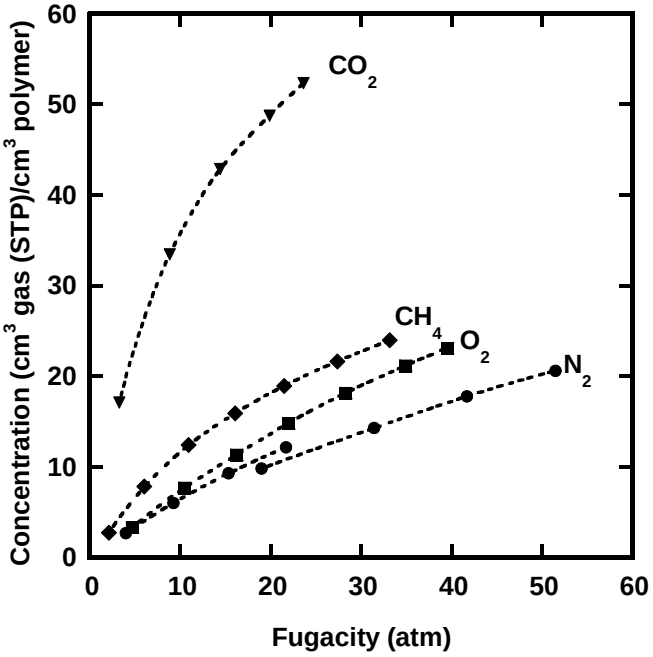

Figure 5.7 Sorption isotherms for N_2, O_2, CH_4 and CO_2 at 35°C for HFA-MDA-6FDA.

Permeability (Barrer)	CO_2	CH_4	O_2	N_2	CO_2/CH_4	O_2/N_2	CO_2/N_2
HFA-MDA-6FDA	51.87	1.1	12.84	2.4	47.2	5.4	21.6
MDA-6FDA (Hirayama)[26]	15.1	0.321	3.15	0.563	47.0	5.6	26.8
MDA-6FDA (Coleman)[27]	19.3	0.43	4.6	0.81	44.9	5.7	23.8
Diffusivity (10^{-9} cm^2/s)	CO_2	CH_4	O_2	N_2	CO_2/CH_4	O_2/N_2	CO_2/N_2
HFA-MDA-6FDA	140	9.3	180	37	15.1	4.9	3.8
MDA-6FDA (Hirayama)[26]	15.5	1.54	42.7	8.64	10.1	4.9	1.8
MDA-6FDA (Coleman)[27]	37	2.76	42.60	13.35	13.4	3.2	2.8
Solubility (cm^3(STP)/cm^3 polymer atm)	CO_2	CH_4	O_2	N_2	CO_2/CH_4	O_2/N_2	CO_2/N_2
HFA-MDA-6FDA	2.86	0.9	0.56	0.49	3.2	1.1	5.8
MDA-6FDA (Hirayama)[26]	7.40	1.58	0.56	0.50	4.7	1.1	14.9
MDA-6FDA (Coleman)[27]	3.96	1.18	0.82	0.46	3.4	1.8	8.6

Table 5.3 Permeability, diffusivity and solubility for HFA-MDA-6FDA and MDA-6FDA.[26,27]

HFA-MDA-6FDA's permeability to all gases is 2.5 - 4 times higher than MDA-6FDA's reported permeabilities, which is consistent with the higher calculated free volume in the HFA structure. The HFA structure's higher free volume is also consistent with the higher diffusivities relative to MDA-6FDA. In almost all cases, HFA-MDA-6FDA's diffusion coefficient is more than 3 times that of MDA-6FDA. The relatively large disagreement between the Coleman and Hirayama values for MDA-6FDA is likely due to their different measurement techniques. Hirayama et al.[26] measured the diffusivity using the time lag method[35] and then used the solution-diffusion model to calculate solubility. Coleman et al.[27] used the same methods described here, i.e. measuring

sorption coefficients and calculating diffusivity. The variation between the two diffusion coefficients reported for MDA-6FDA is, however, much smaller than the difference between either of these values and the HFA-MDA-6FDA diffusion coefficient. The solubility coefficient shows a similar variation in the literature values for MDA-6FDA. However, for all gases, HFA-MDA-6FDA has a similar or lower solubility coefficient than MDA-6FDA.

The increase in diffusion coefficient is expected for a higher free volume polymer; however, what are unexpected are the unchanging ideal selectivities between several gas pairs (Table 5.3). In many polymers, a trade-off relationship exists between permeability and selectivity such that increases in permeability cause proportional losses in selectivity.[36,37] This trade-off relationship is most clearly seen in the so-called Robeson upper bound plots (Figure 5.8). [36,37] Typically, a simple increase in free volume will cause the polymer to move parallel to the upper bound towards higher permeability.[38] However, HFA-MDA-6FDA moves almost horizontally relative to MDA-6FDA. It is not clear from these results why the HFA group does not follow the typical trade off behavior. Hexafluoroisopropylidene units have been hypothesized to increase free volume, while hindering chain rotation, which causes a similar type of non-trade-off behavior.[3] Additionally, the highly hydrogen-bond-acidic HFA groups may hydrogen bond with the carbonyls of the imide group to additionally increase the rigidity of the structure and increase selectivity relative to the unhydrogen-bonded structure.

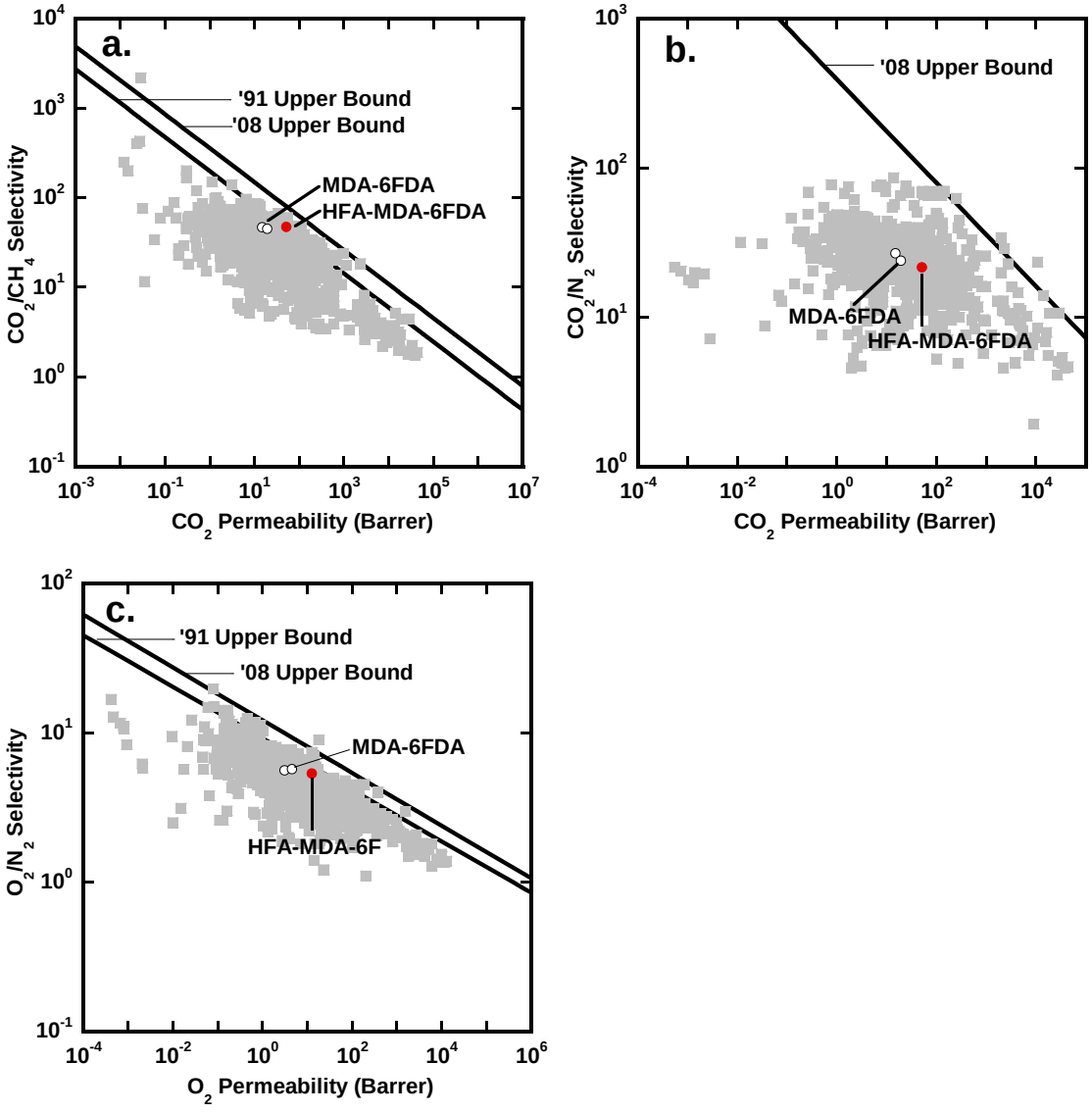

Figure 5.8 Upper bound plots for a. CO_2/CH_4, b. CO_2/N_2 and c. O_2/N_2. HFA-MDA-6FDA is a red, filled circle. MDA-6FDA data are open circles.[26,27] Grey symbols indicate data from the original upper bound plots.[37]

5.3.6 High Temperature Reaction in HFA-MDA-6FDA and HFA-MDA-BAF

5.3.6.1 TGA Results for HFA-MDA-6FDA

The TGA of HFA-MDA-6FDA (Figure 5.2) has an unusual two-step mass loss under N_2, which indicates a high-temperature reaction or partial degradation with a stable

product. This two-step mass loss is similar to the TGA results seen for the TR precursor hydroxyimides.[39] A benzoxazine product similar to the TR benzoxazole[39] can be proposed for HFA-MDA-6FDA (Figure 5.9).

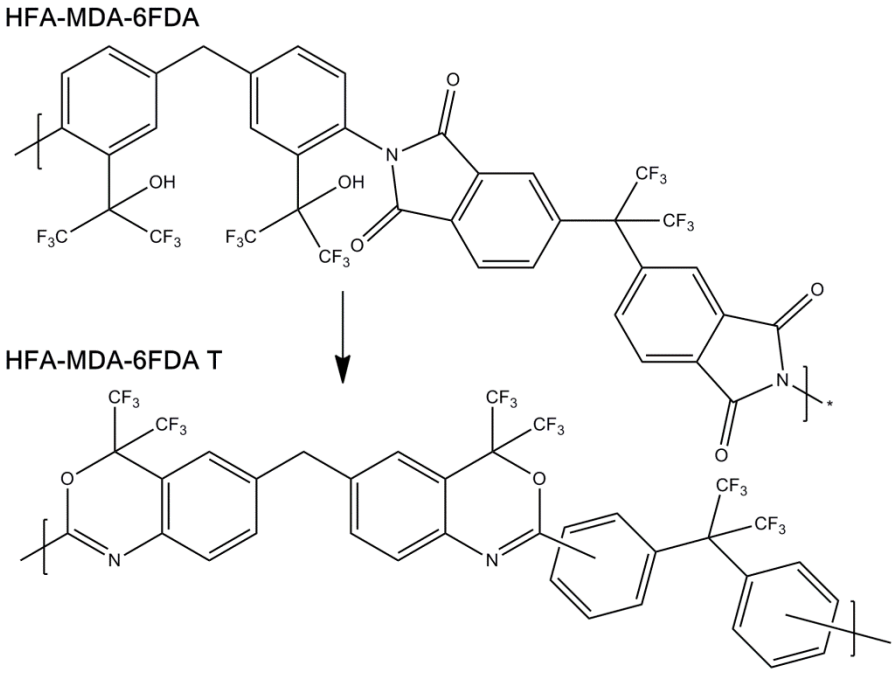

Figure 5.9 Chemical structures of HFA-MDA-6FDA and the proposed product, HFA-MDA-6FDA T.

With a given starting material and product, the theoretical percent mass loss can be calculated as follows:

$$Theoretical\ Mass\ Loss = \frac{(M_{initial} - M_{theoretical})}{M_{initial}} * 100\% \qquad (5.1)$$

where $M_{initial}$ is the starting material's repeat unit molecular weight and $M_{theoretical}$ is the predicted structure's repeat unit molecular weight. The theoretical mass loss for HFA-MDA-6FDA to the benzoxazine product is 9.4%, which is similar to the mass loss measured by TGA.

To attempt to understand the maximum possible mass loss, HFA-MDA-6FDA was also tested via high temperature, isothermal TGA (Figure 5.10). In these tests, the sample was held at the listed temperature for 10 hours to observe the evolution of the mass loss. In all samples, as soon as the temperature reached 310°C, approximately 30 minutes after the start of the temperature ramp, the mass rapidly decreases by about 10%. After the rapid initial mass loss, all samples experience a slow downward drift that continues for the entire 10 hour hold and becomes more pronounced at higher hold temperatures. This result may indicate that there are two reactions occurring in these samples, the first reaction happens rapidly once the sample has sufficient thermal energy, while the other is a much slower reaction that occurs over very long times. Similar results have been found in the TR polymers.[40] In those systems, the rapid mass loss is attributed to the TR reaction, while the slow mass loss is assumed to be degradation.[40]

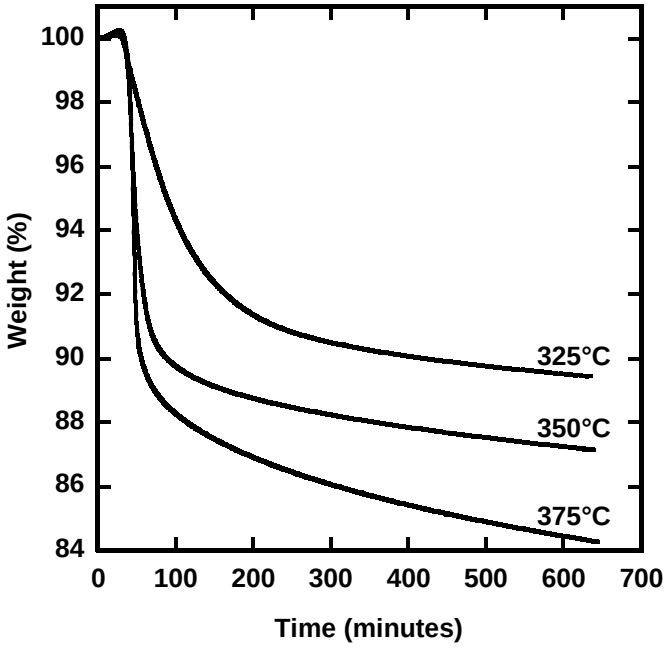

Figure 5.10 Isothermal TFA results for HFA-MDA-6FDA. Samples were first held at 150°C for 30 minutes (not shown). Time zero was set to the beginning of the 5°C/minute ramp to the listed temperature.

5.3.6.2 TGA Results for HFA-MDA-BAF and Evaluation of Solvent Removal

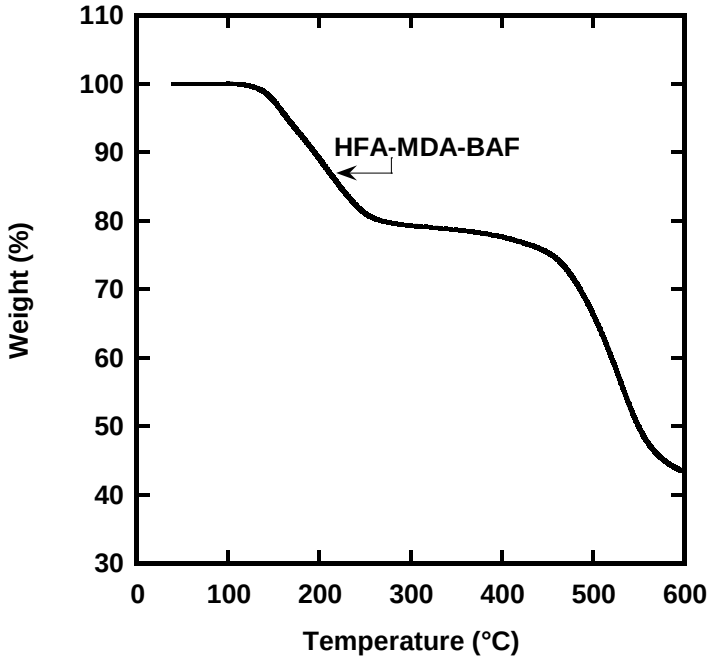

Figure 5.11 TGA of HFA-MDA-BAF using a 5°C/minute heating rate under a N_2 purge

HFA-MDA-BAF was also tested via TGA and showed a two-step mass loss similar to HFA-MDA-6FDA, but at lower temperatures (i.e., 150-250°C) (Figure 5.11). Given the reaction proposed in 5.3.6.1, the predicted product for HFA-MDA-BAF is shown in Figure 5.12. However, the theoretical mass loss (Equation 5.1) for HFA-MDA-BAF to the proposed product is only 4.1%, while the actual mass loss observed in the TGA results is approximately 20%.

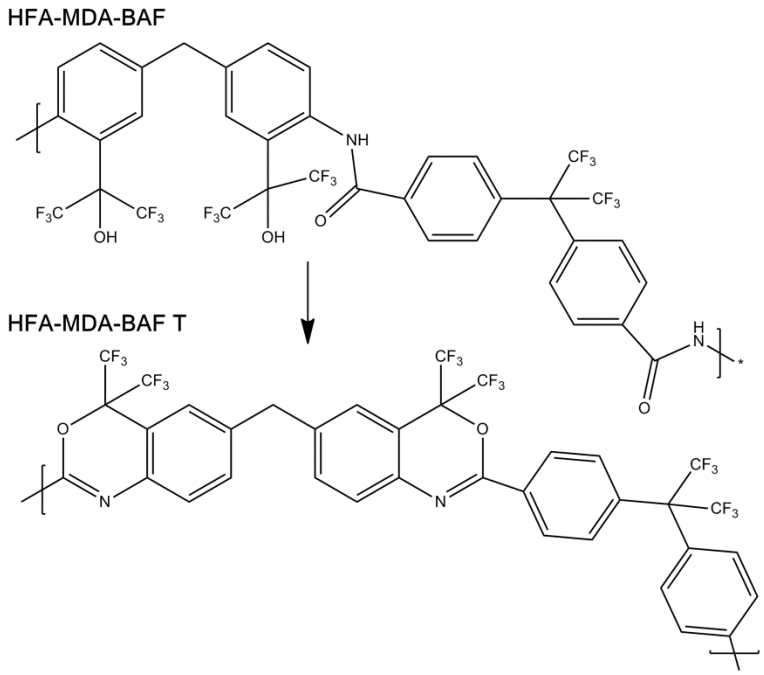

Figure 5.12 Chemical structures of HFA-MDA-BAF and proposed product, HFA-MDA-BAF T

To examine the mass loss of HFA-MDA-BAF in more detail, the experiment was repeated using high-resolution TGA (Figure 5.13), which slows the heating rate during periods of mass loss. High-resolution TGA helps isolate thermal events which occur at similar temperatures. The high resolution TGA shows two mass loss events in the range of 150-250°C as shown by the two peaks in the derivative mass loss. However, as the two events are still overlapping, it is impossible to assign the proper mass losses to each event.

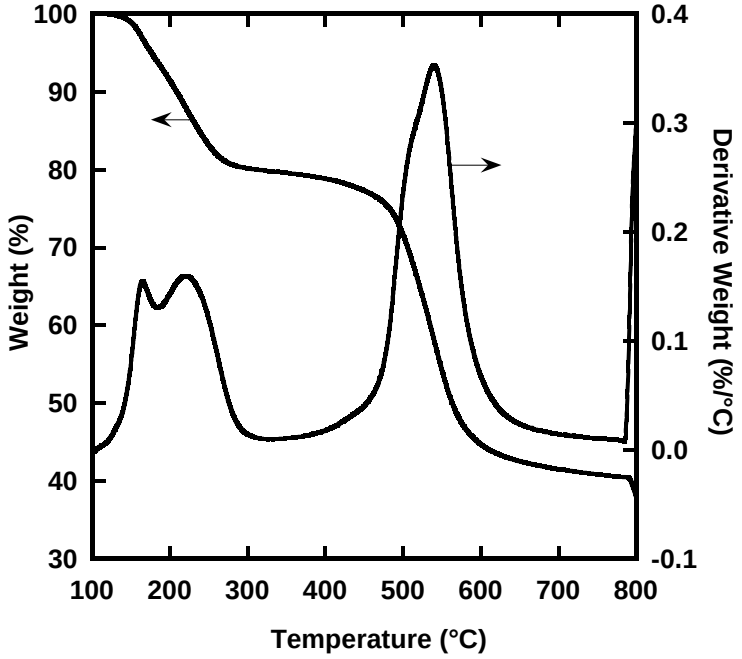

Figure 5.13 High resolution TGA results for HFA-MDA-BAF and the derivative of the mass loss curve.

One explanation for the higher than predicted mass loss for HFA-MDA-BAF is that these samples may have formed a stable HFA-THF complex that cannot be removed by the drying process used here (i.e., under vacuum at 100°C for several days). THF can form stable 1:1 complexes with secondary and tertiary fluoroalcohols such as 1,1,1,2,2,2-hexafluoro-2-propanol (HFIP, i.e., a small molecule analog of the HFA group).[25] The HFIP-THF complex is stable at its normal boiling point, which is approximately 100°C (i.e., more than 30°C above the boiling point of either THF or HFIP).[25] A similar complex could form between THF and the tertiary HFA group in HFA-MDA-6FDA, and it would be difficult to determine solely from the mass loss results.

FTIR analysis of an HFA-MDA-BAF film cast from THF (cf. Figure 5.15) can be compared with reported shifts in the alcohol peak of HFIP due to complexation with THF.[25] However, the HFA-THF peak would appear at approximately the same

wavenumber as the –NH peak of the amide group and other possible hydrogen-bonded HFA signals (i.e., hydrogen bonding with water or the amide group).[15,18,20,29] With the number of overlapping potential peaks, it is not possible to discern a clear signal for HFA-THF. Furthermore, the THF peaks cannot be separated from the HFA-MDA-BAF spectrum. The CH_2 peaks of THF overlap the –OH/-NH signal and the ether peak and five-membered ring stretch of THF overlap the CF_3 and amide functionality of HFA-MDA-6FDA. Thus, due to the complexity of HFA-MDA-BAF's FTIR spectrum, it is impossible to definitively demonstrate either the presence or lack of THF in the film.

The potential for an HFA-THF complex complicates the interpretation of the mass loss in TGA. Like the HFIP-THF complex, [25] an HFA-THF complex would likely be stable at 100°C, and being bound to the polymer would prevent the HFA-THF from vaporizing. However, for the proposed reaction to occur, any HFA-THF complexes would have to degrade first. The double event indicated by the high resolution TGA is consistent with first, the degradation of the HFA-THF complexes, and then the conversion to HFA-MDA-BAF T. The mass loss for the conversion from (HFA-THF)-MDA-6FDA to the proposed product is 20.3%, which is consistent with the mass loss observed by TGA. However, instead of the proposed reaction, the structure could be undergoing some form of degradation. The chemical structure HFA-MDA-BAF T will be examined further using FTIR in Section 5.3.6.4.

5.3.6.3 Changes in T_g of HFA-MDA-6FDA

As reported above (Section 5.3.1), the reported T_g of HFA-MDA-6FDA was determined on the first heat because the polymer clearly begins to react just above T_g (Figure 5.14). Immediately after passing through T_g, an exothermic event begins. After reaching 350°C, the sample was quench cooled (30°C/minute) to 40°C before being

heated again. With each subsequent heat to 350°C, the T_g decreases and, by the third heat, the T_g was almost 25°C lower. The decrease in T_g as the reaction occurs indicates that the structure is becoming more flexible as the reaction proceeds.

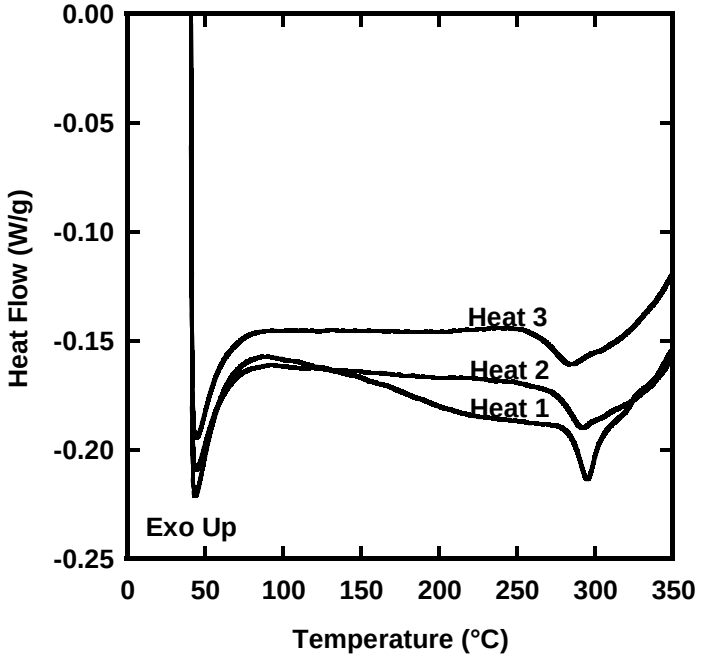

Figure 5.14 3 sequential DSC scan results for HFA-MDA-6FDA. Sample dried in DSC at 150°C for 30 minutes (not shown). Heats performed at 10°C/minute with quench cools at 30°C/minute (not shown) between heats.

5.3.6.4 Chemical Analysis by FT-IR

Film samples were studied via FT-IR to observe the changes in chemical structure due to the high temperature reaction. Specifically, films of HFA-MDA-6FDA and HFA-MDA-BAF were tested via transmission FT-IR. Additionally, films of HFA-MDA-BAF and HFA-MDA-6FDA were thermally treated under a N_2 purge in a Carbolite Three Zone Hinged Tube Furnace (Model HZS 12/-/600, Watertown, WI, USA). The 6FDA film was treated at 400°C for 3 hours (HFA-MDA-6FDA-T); and the HFA-MDA-BAF film was treated at 300°C for 1 hour (HFA-MDA-BAF-T). The thermal conditions used

to prepare the thermally treated samples were based on preliminary results provided by Central Glass Co., Ltd. The HFA-MDA-BAF-T film was also tested via transmission FT-IR; however, the HFA-MDA-6FDA-T was tested by Attenuated Total Reflectance (ATR).

The FT-IR spectrum of MDA-6FDA has been reported[41] and can be used to identify the peaks in the HFA-MDA-6FDA spectrum (Figure 5.15). The peak from 3000-3500 cm^{-1} contains the –OH signal, any residual N-H from incomplete imidization and signals for the C-H bonds. This region has been previously analyzed (5.3.2) as membrane hydrogen bonding can influence the gas transport properties. Other important peak assignments include: C=O (1790 and 1720 cm^{-1}), phenyl ring (1630 and 1510 cm^{-1}), C-N (1380 cm^{-1}), and one of the imide peaks (723 cm^{-1}). Additionally, in the range of 1130 to 1300 cm^{-1}, peaks corresponding to the C-F bonds, C-N bonds and imides all appear, but are impossible to distinguish due to their high absorption and peak overlap. Finally, the peak at 969 cm^{-1} may be associated with the C-O stretch in the HFA group, although primary alcohols typically appear at slightly higher wavenumbers (1025-1060 cm^{-1}).[42]

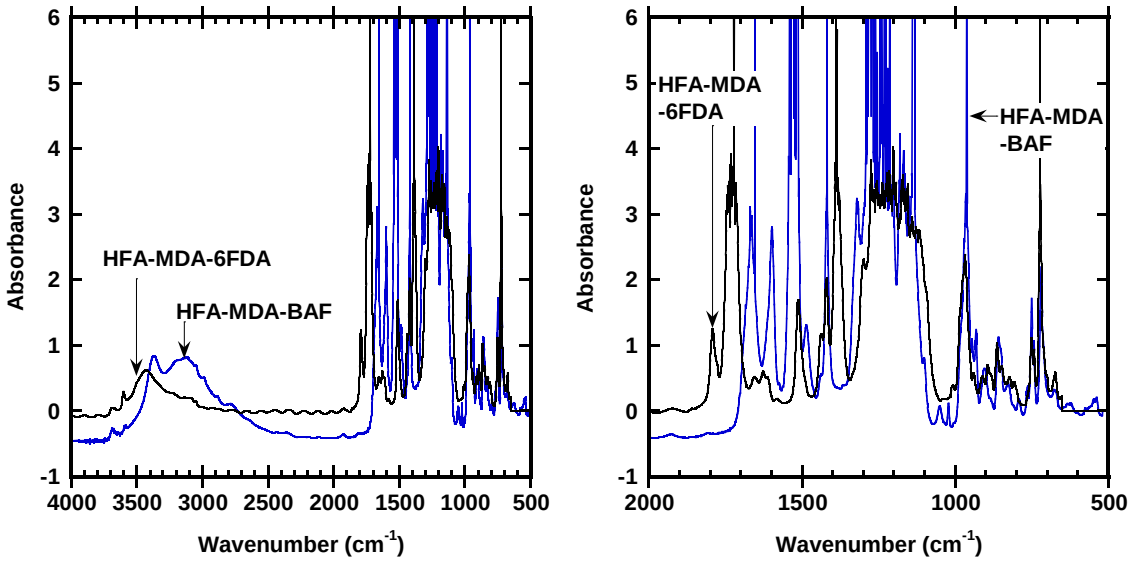

Figure 5.15 FT-IR spectra for HFA-MDA-6FDA and HFA-MDA-BAF

The HFA-MDA-BAF's spectrum can then be assessed relative to the HFA-MDA-6FDA spectrum (Figure 5.15). The region from 3000-3500 cm^{-1} shows a difference in shape, but this is expected based on the presence of an additional -NH group in the polyamide (HFA-MDA-BAF) structure which will contribute to this signal and can also participate in hydrogen bonding. The changes in the C=O and imide regions are also consistent with a switch from an imide structure to an amide structure. Alternatively, changes in both the –OH region and in the range of 900-1100 cm^{-1} could be due to an HFA-THF complex.[25,43]

Comparing the HFA-MDA-6FDA spectrum with the HFA-MDA-6FDA-T spectrum shows some interesting changes (Figure 5.16). The most obvious change is the lack of the broad –OH absorbance in the HFA-MDA-6FDA-T spectrum that indicates that the high temperature reaction has caused the loss of the hydroxyl units. In the region below 2000cm^{-1}, there are several significant changes. First, several imide peaks decay including: C=O (1790 and 1720 cm^{-1}), C-N (1380 cm^{-1}) and imide peak (723).

Unfortunately, the disappearance of these groups only indicates that the imide structure may be disappearing, but does not indicate if the structure is degrading or changing into the benzoxazine structure. Additionally, there are changes in the region from 1130-1300, but due to the overlap in these peaks, it is impossible to interpret what is occurring. If the benzoxazine structure were forming, two new peaks would be expected. First, a C-O-C peak for the ether would be expected in the range of 1070-1150 cm^{-1},[42] which is, unfortunately in the region with several other peaks. Second, a peak relating to the C=N group would be expected. The C=N in carboximidates (R-C(=NR')OR") tend to appear at approximately 1690-1645cm^{-1},[44] and having the carbon and the nitrogen bonded to phenyl rings tends to lower the wavenumber beyond that range.[44] The HFA-MDA-6FDA-T sample has a new peak at 1600 cm^{-1}, but it isn't clear if this is just a result of shifting in the nearby benzene ring stretch. Thus, these FT-IR results show some of the expected changes for the benoxazine reaction, but do not conclusively rule out degradation.

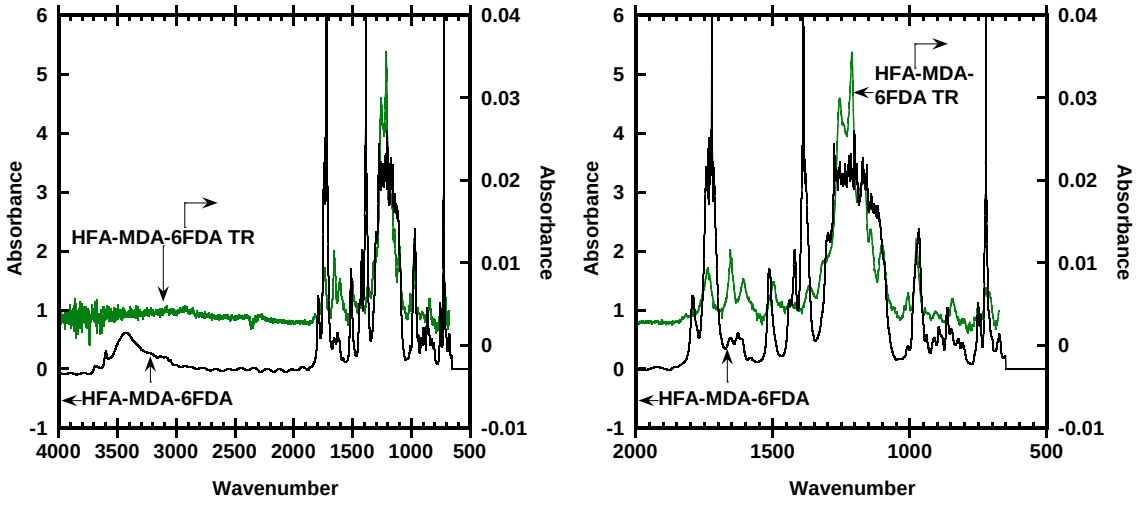

Figure 5.16 FT-IR spectra for HFA-MDA-6FDA and the thermal treated sample, HFA-MDA-6FDA-T

Comparing the HFA-MDA-BAF and HFA-MDA-BAF-T spectra (Figure 5.17), a similar result emerges. Again, the structure loses the –OH and –NH peaks above 2500 cm^{-1}. There are changes in the C=O peaks (1650 and 1600 cm^{-1}), although the changes seem more like shifts in wavenumber, rather than disappearing as in the HFA-MDA-6FDA-T spectrum. Additionally, there is a new peak in the HFA-MDA-BAF-T spectra at 1565, which likely corresponds to -NH deformation. The C-N peak at 1420 cm^{-1} seems to be decaying. Again, it is impossible to sort out the region containing the CF_3 groups, but there do seem to be some new peaks at 1100 and 1020 cm^{-1}, which could correspond to amines and ethers. Unfortunately, the FT-IR results are inconclusive. Some possible evidence of benoxazine formation can be found, but the results could also indicate some form of degradation. Further chemical characterization would be required to evaluate the thermally treated materials' structures.

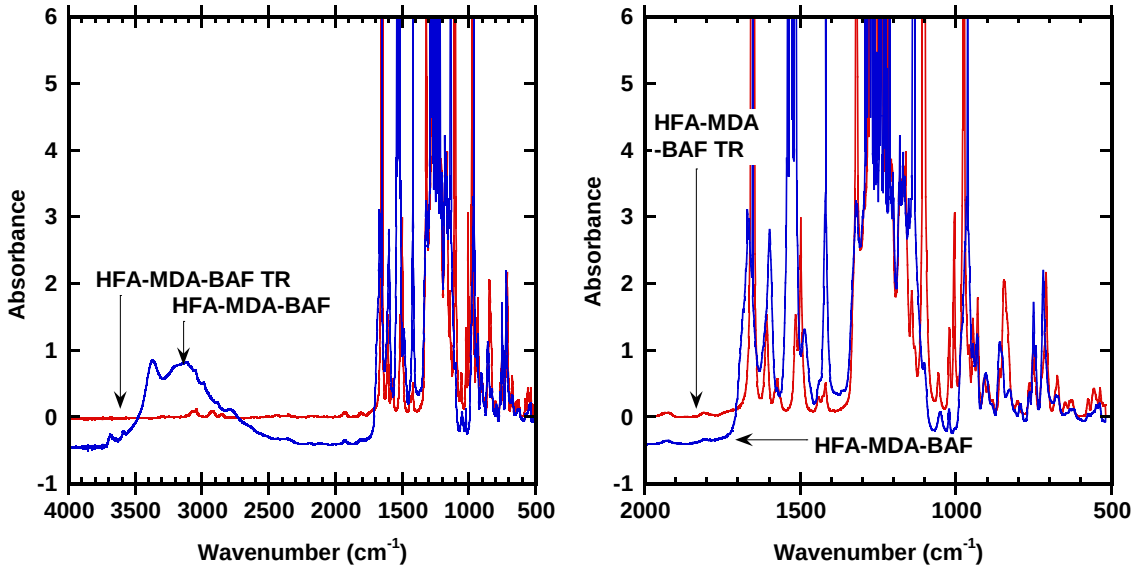

Figure 5.17 FT-IR spectra of HFA-MDA-BAF and the thermally treated sample, HFA-MDA-BAF-T.

5.4 CONCLUSIONS

Introducing the HFA group to the MDA-6FDA structure caused an increase in the fractional free volume of the material which increased the permeabilities of all gases. However, this increase in permeability is not accompanied by the expected decrease in selectivity. Although the causes of the unusual transport behavior cannot be described definitively, these changes are similar to those seen when hexafluoroisopropylidene units are introduced to the backbone of other polymers.

The TGA of both HFA-MDA-6FDA and HFA-MDA-BAF both show an unusual double mass loss at high temperatures. Unfortunately, due to overlapping peaks and complex chemical structure, it is not possible to use FT-IR to determine the chemical structure of the products. However, in the HFA-MDA-6FDA, the increase in chain flexibility combined with the high reaction temperature make it likely that the sample has undergone at least some degradation. The HFA-MDA-BAF structure undergoes its transition at lower temperature, which reduces the chance of degradation; however, potential formation of HFA:THF complexes makes analysis difficult.

5.5 REFERENCES

(1) Bhole, Y. S.; Karadkar, P. B.; Kharul, U. K. *J. Polym. Sci. Part B Polym. Phys.* **2007**, *45*, 3156–3168.

(2) Dai, Y.; Guiver, M. D.; Robertson, G. P.; Kang, Y. S.; Lee, K. J.; Jho, J. Y. *Macromolecules* **2004**, *37*, 1403–1410.

(3) Hellums, M. W.; Koros, W. J.; Husk, G. R.; Paul, D. R. *J. Memb. Sci.* **1989**, *46*, 93–112.

(4) Kumbharkar, S. C.; Karadkar, P. B.; Kharul, U. K. *J. Memb. Sci.* **2006**, *286*, 161–169.

(5) Mohr, J. M.; Paul, D. R.; Tullos, G. L.; Cassidy, P. E. *Polymer* **1991**, *32*, 2387–2394.

(6) Morisato, A.; Ghosal, K.; Freeman, B. D.; Chern, R. T.; Alvarez, J. C.; de la Campa, J. G.; Lozano, A. E.; de Abajo, J. *J. Memb. Sci.* **1995**, *104*, 231–241.

(7) Allen, R. D.; Na, Y.-H.; Sooriyakumaran, R.; Fujiwara, M.; Yamanaka, K. *J. Photopolym. Sci. Technol.* **2010**, *23*, 741–747.

(8) Allen, R. D.; Young-Hye, N.; Sooriyakumaran, R.; Fujiwara, M.; Yamanaka, K. Polyamide Membranes with Fluoroalcohol Functionality. US 2010/0216899 A1, 2010.

(9) La, Y.-H.; Sooriyakumaran, R.; Miller, D. C.; Fujiwara, M.; Terui, Y.; Yamanaka, K.; McCloskey, B. D.; Freeman, B. D.; Allen, R. D. *J. Mater. Chem.* **2010**, *20*, 4615.

(10) Hall, D. S.; Osborn, B.; Patterson, K.; Burns, S. D.; Willson, C. G. In *Advances in Resist Technology and Processing XVIII*; Houlihan, F. M., Ed.; 2001; Vol. 4345, pp. 1066–1072.

(11) Kishimura, S.; Endo, M.; Sasago, M. *J. Photopolym. Sci. Technol.* **2002**, *15*, 625–628.

(12) Fender, N.; Brock, P. J.; Chau, W.; Bangsaruntip, S.; Mahorowala, A. P.; Wallraff, G. M.; Hinsberg, W. D.; Larson, C. E.; Ito, H.; Breyta, G.; Burnham, K.; Truong, H. D.; Lawson, P.; Allen, R. D. In *Advances in Resist Technology and Processing XVIII*; Houlihan, F. M., Ed.; 2001; Vol. 4345, pp. 417–427.

(13) Lee, S. H.; Kim, J. W.; Kim, J. W.; Oh, S. K.; Park, C. S.; Lee, J. Y.; Kim, S. S.; Lee, J. W.; Kim, D.; Kim, J.; Ban, K. Do; Bok, C. K.; Moon, S. C. In *Advances in Resist Materials and Processing Technology XXIV*; Lin, Q., Ed.; 2007; Vol. 6519, pp. 1–9.

(14) Allen, A. D.; Breyta, G.; Brock, P.; DiPietro, R.; Sanders, D.; Sooriyakumaran, R.; Sundberg, L. K. *J. Photopolym. Sci. Technol.* **2006**, *19*, 569–572.

(15) Snow, A. W.; Sprague, L. G.; Soulen, R. L.; Grate, J. W.; Wohltjen, H. *J. Appl. Polym. Sci.* **1991**, *43*, 1659–1671.

(16) Grate, J. W.; Kaganove, S. N.; Patrash, S. J.; Craig, R.; Bliss, M. *Chem. Mater.* **1997**, *9*, 1201–1207.

(17) Grate, J. W. *Chem. Rev.* **2008**, *108*, 726–745.

(18) Masser, K. A.; Runt, J. *Macromolecules* **2010**, *43*, 6414–6421.

(19) Yang, X.; Painter, P. C.; Coleman, M. M.; Pearce, E. M.; Kwei, T. K. *Macromolecules* **1992**, *25*, 2156–2165.

(20) Sturgill, G. K.; Stanley, C.; Rezac, M. E.; Beckham, H. W. *Macromolecules* **2001**, *34*, 8730–8734.

(21) Gandler, J. R.; Jencks, W. P. *J. Am. Chem. Soc.* **1982**, *104*, 1937–1951.

(22) Li, J.; Zhang, Y.; Carr, P. W. *Anal. Chem.* **1993**, *65*, 1969–1979.

(23) Ito, H.; Hinsberg, W. D.; Rhodes, L. F.; Chang, C. In *Advances in Resist Technology and Processing XX*; Fedynyshyn, T. H., Ed.; 2003; Vol. 5039, pp. 70–79.

(24) Matteucci, S.; Yampolskii, Y. P.; Freeman, B. D.; Pinnau, I. In *Materials Science of Membranes for Gas and Vapor Separations*; Yampolskii, Y.; Pinnau, I.; Freeman, B. D., Eds.; John Wiley & Sons, Ltd: Chichester, 2006; pp. 1–47.

(25) Middleton, W. J.; Lindsey, R. V. *J. Am. Chem. Soc.* **1964**, *86*, 4948–4952.

(26) Hirayama, Y.; Yoshinaga, T.; Kusuki, Y.; Ninomiya, K.; Sakakibara, T.; Tamari, T. *J. Memb. Sci.* **1996**, *111*, 169–182.

(27) Coleman, M. R.; Koros, W. J. *J. Memb. Sci.* **1990**, *50*, 285–297.

(28) Husk, G. R.; Cassidy, P. E.; Gebert, K. L. *Macromolecules* **1988**, *21*, 1234–1238.

(29) Barlow, J. W.; Cassidy, P. E.; Lloyd, D. R.; You, C.-J.; Chang, Y.; Wong, P. C.; Noriyan, J. *Polym. Eng. Sci.* **1987**, *27*, 703–715.

(30) Bos, A.; Pünt, I. G. M.; Wessling, M.; Strathmann, H. *J. Memb. Sci.* **1999**, *155*, 67–78.

(31) Wonders, A.; Paul, D. R. *J. Memb. Sci.* **1979**, *5*, 63–75.

(32) Horn, N. R.; Paul, D. R. *Polymer* **2011**, *52*, 1619–1627.

(33) Tanaka, K.; Ito, M.; Kita, H.; Okamoto, K.; Ito, Y. *Bull. Chem. Soc. Jpn.* **1995**, *68*, 3011–3017.

(34) Robeson, L. M.; Smith, Z. P.; Freeman, B. D.; Paul, D. R. *J. Memb. Sci.* **2014**, *453*, 71–83.

(35) Lin, H.; Freeman, B. D. In *Springer Handbook of Materials Measurement Methods*; Czichos, H.; Saito, T.; Smith, L., Eds.; Springer: New York, 2006; pp. 371–387.

(36) Robeson, L. M. *J. Memb. Sci.* **1991**, *62*, 165–185.

(37) Robeson, L. M. *J. Memb. Sci.* **2008**, *320*, 390–400.

(38) Freeman, B. D. *Macromolecules* **1999**, *32*, 375–380.

(39) Smith, Z. P.; Sanders, D. F.; Ribeiro, C. P.; Guo, R.; Freeman, B. D.; Paul, D. R.; McGrath, J. E.; Swinnea, S. *J. Memb. Sci.* **2012**, *415-416*, 558–567.

(40) Sanders, D. F.; Smith, Z. P.; Ribeiro, C. P.; Guo, R.; McGrath, J. E.; Paul, D. R.; Freeman, B. D. *J. Memb. Sci.* **2012**, *409-410*, 232–241.

(41) Xiao, S.; Feng, X.; Huang, R. Y. M. *Macromol. Chem. Phys.* **2007**, *208*, 2665–2676.

(42) Lambert, J. B.; Shurvell, H. F.; Cooks, R. G. In *Introduction to Organic Spectroscopy*; Macmillan Publication: New York, 1987; pp. 174–177.

(43) Larkin, P. *Infrared and Raman Spectroscopy: Principles and Spectral Interpretation*; Elsevier Science, 2011.

(44) Colthup, N. In *Introduction to Infrared and Raman Spectroscopy*; Elsevier Science, 2012; Vol. 166, pp. 325–327.

Chapter 6 Characterization, Physical Aging and Plasticization in Cellulose Triacetate

6.1 Overview

The purpose of this study was to evaluate the physical aging and CO_2 plasticization response of thin cellulose triacetate (CTA) films relative to their thick film counterparts. To evaluate the properties of thick and thin CTA films, it was also necessary to perform supporting characterization of the morphology and thermal properties of the CTA films.

6.2 Experimental Details

6.2.1 Materials

This project focused on cellulose triacetate (CTA) graciously provided as a powder by Cameron International. This CTA polymer has a degree of substitution (DS) of 2.99 and is semi-crystalline, with crystallinities that range from 20%$_{wt}$ to over 70%$_{wt}$ depending on the sample preparation.

6.2.2 Casting Details

Thick CTA films (>10 μm) were prepared using a 9:1 (mass:mass) mixture of dichloromethane and ethanol as a solvent. The polymer solution was cast on a glass plate using a glass casting ring and the solvent evaporated at room temperature in a fume hood. After a solid film was formed, the sample was additionally dried between glass plates at 120°C overnight under full vacuum to complete the solvent removal.

Thin CTA films were spin coated on a silicon wafer from an n-methylpyrrolidone (NMP) solution. CTA has limited solubility in NMP and the maximum stable solution was approximately 2%$_{wt}$. To vary the film thickness, it was necessary to either spin multiple coats on the same wafer or reduce the spinning speed. Spin casting was done

with a Laurell Technologies spin coater, and typical spin casting parameters used in this study are: spinning speed of 700 RPM, Acceleration 11 and a spinning time of 4 minutes. The four minute spin time was insufficient to allow the NMP to fully dry so the wafers were additionally dried on a hot plate at 70°C for another four minutes. At this point, the films' thicknesses were measured, even though the films still contain some NMP. The films were then lifted on to wire support frames for annealing as described elsewhere.[1] The annealing process reset the thermal history and completed the solvent removal. Finally, to correct for any thickness changes that occur during this final annealing and solvent removal step, a representative sample was placed back on to a silicon wafer and the thickness was again measured. The percent change in thickness for this sample between the pre- and post-annealing measurement was used to adjust the thickness of the permeability samples, whose thicknesses could not be remeasured.

6.2.3 Crystallinity Determination

Crystallinity in all samples was determined by differential scanning calorimetry (DSC). Specifically, following the procedures in Chapter 3, a dry sample was heated to 305°C at 20°C/minute. Using the Universal Analysis software provided by TA Instruments, the area of the melting peak and the crystallization peak, if any, could be calculated. The percent crystallinity is then given by the following equation:[2]

$$\%\ crystallinity = \frac{\Delta H_m - \Delta H_c}{\Delta H^0} * 100\% \qquad 6.1$$

where ΔH_m is the area of the melting endotherm (J/g sample), ΔH_c is the area of the crystallization exotherm (J/g sample) and ΔH^0 is the heat of melting a 100% crystalline sample which is taken to be 34.3 J/g.[3]

6.3 RESULTS

6.3.1 Initial Characterization and Comparison with Literature

6.3.1.1 Density

A membrane's density is closely tied to the material's free volume and, thus, with its transport. The density of CTA was measured by two different methods. First, the density was measured using a benchtop density kit as described in Chapter 3.3.1. The second method used a magnetic suspension balance from Rubotherm. This technique measures the mass of the sample under vacuum before automatically measuring the mass change upon pressurization with increasing pressures of helium, which has a low sorption in polymers. The density of the He gas was calculated using the Virial Equation of State.[4] From the slope of the sample mass versus density of He, the volume of the sample can be obtained (Figure 6.1). The sample volume can then be combined with the sample mass to give the density. The density values obtained by analytical balance method and the magnetic suspension balance method were 1.287 g/cm^3 and 1.294 g/cm^3, respectively. These densities are compared against literature values[3,5] in Figure 6.2. The density of this CTA sample (DS 2.99) agrees reasonably with the literature data.

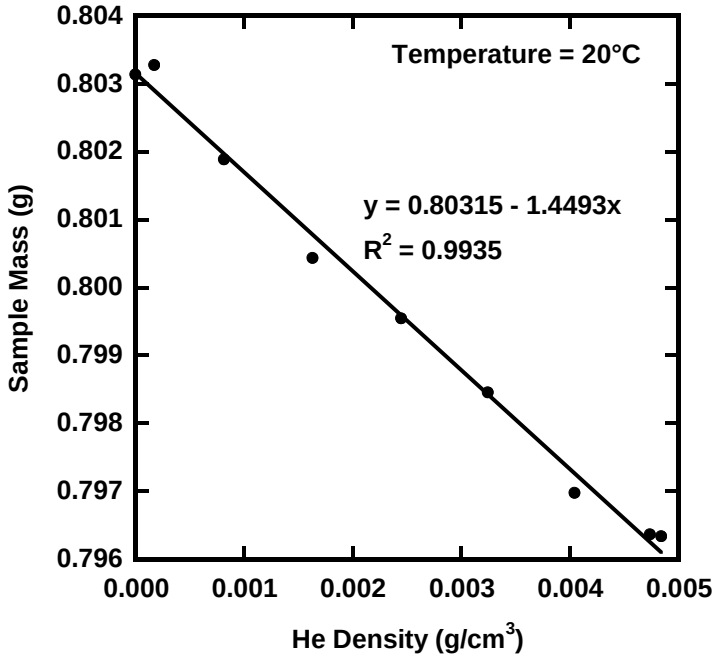

Figure 6.1 Magnetic Suspension Balance sample mass versus surrounding Helium density. Sample mass taken from intercept (i.e., under vacuum) and sample volume taken from the slope of the best fit line.

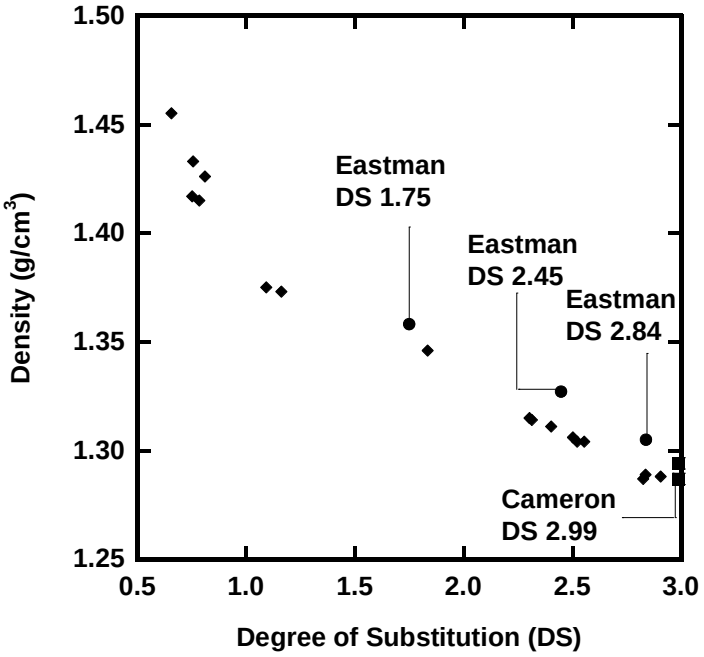

Figure 6.2 Density of Cameron CTA (DS 2.99), Eastman samples of varying DS[3] and other literature values[5]

6.3.1.2 Thermal Stability

The thermal stability of CTA was evaluated by TGA using a 5°C/minute heating rate (Figure 6.3). CTA is not stable above 300°C, even for short times. By doubling the heating rate to 10°C/minute, the decomposition temperature can be increased to approximately 305°C. However, hold times at these temperatures must be avoided to prevent degrading the samples.

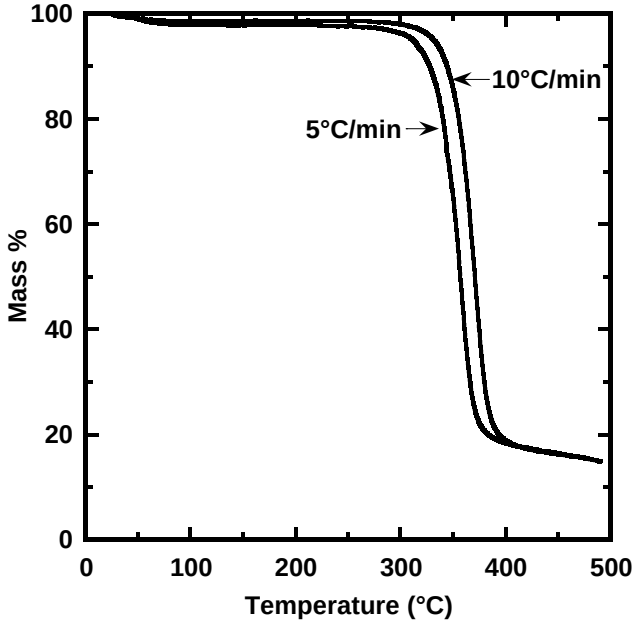

Figure 6.3 Thermal stability of CTA measured by TGA using a 5°C/minute and a 10°C/minute heating rate.

6.3.1.3. Wide Angle X-Ray Diffraction

Wide angle X-ray diffraction (WAXD) is a spectroscopic technique frequently used to study the crystal structure of polymers. WAXD was measured on both a powdered CTA sample and a film sample with very different results. The powder result (Figure 6.4a) shows a typical WAXD result for a polymer sample. The scattering results were fit to two broad amorphous scattering peaks to account for the non-crystalline regions of the polymer. The residual peaks after the amorphous scattering is accounted for are then attributed to the crystalline scattering. The relative area of the two types of scattering patterns provides a measure of the fraction of crystalline domains.

The results for the film sample (Figure 6.4b) are very different. The entire spectra can be fitted with three crystalline peaks. These crystalline peaks are so broad, however, that they could also be interpreted as amorphous scattering.[6] The ambiguity of these

results leads to the conclusion that the sample is either 100% crystalline or 100% amorphous. However, the DSC results for this same sample indicate that the sample is approximately $44\%_{wt}$ crystalline, and thus should show both crystal and amorphous scattering. These contradictory results could be explained by very small crystalline domains in the film sample. [6] As the crystal domains get smaller, the corresponding WAXD peaks become broader. If the crystallites are small enough it can be difficult to distinguish between amorphous and crystalline scattering.[6] Due to these results, crystallinity is determined by DSC throughout the rest of this work.

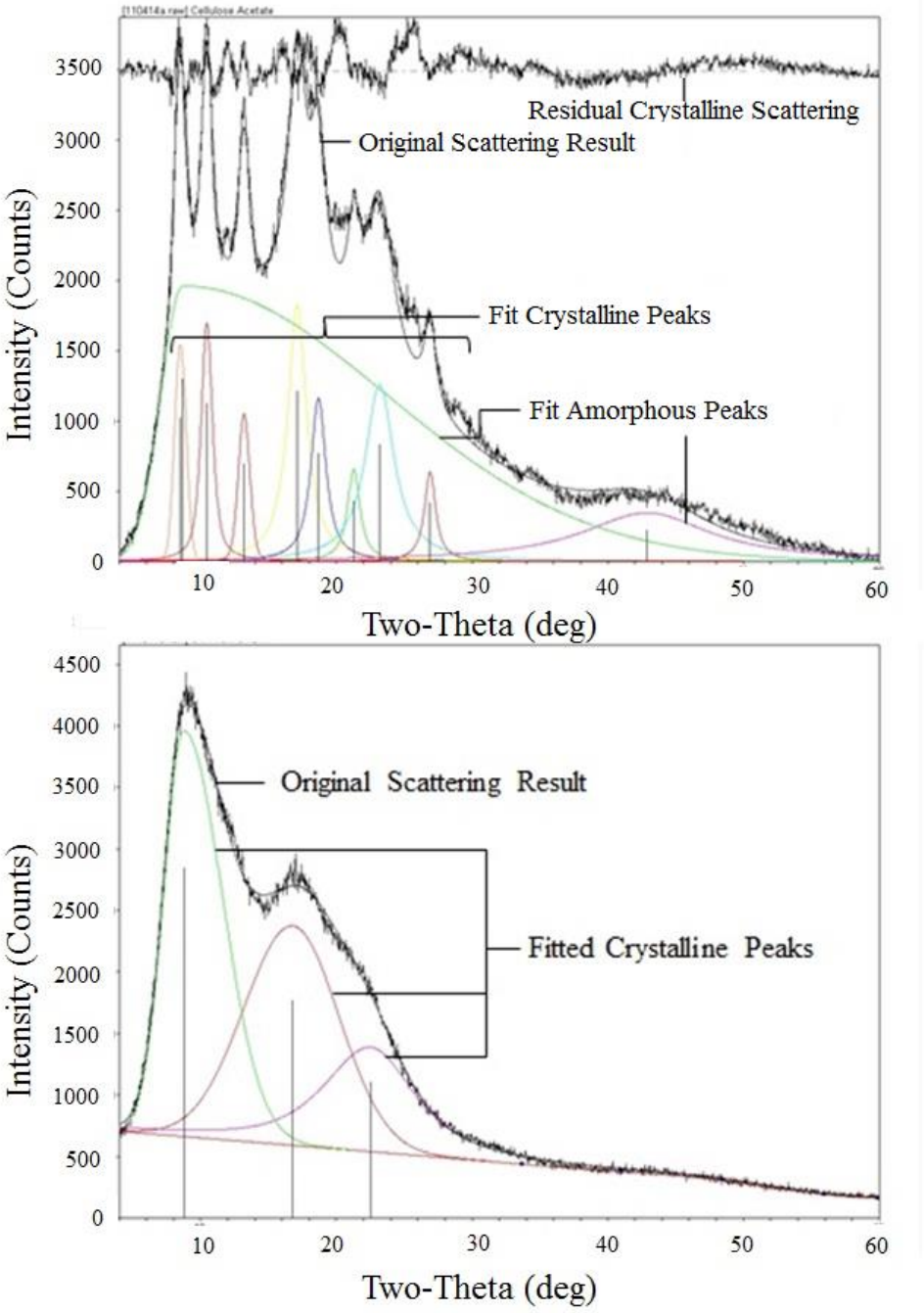

Figure 6.4 WAXD of CTA a. powder and b. 20 μm film sample. Tests were performed by Dr. Steven Swinnea at the Texas Materials Institute.

6.3.1.4 Effect of Sample Form on Thermal Characteristics

Several different CTA samples were studied by DSC (Table 6.1). Samples included: CTA hollow fibers generously provided by Cameron International, the CTA powder from which the hollow fibers were made, and a representative thick film cast by the author from the powder sample, which was heated to 210°C for 20 minutes to remove solvent. Each sample was first heated in the DSC to 120°C and held isothermally for 1 hour to remove any sorbed water. The sample was then cooled to 40°C before being heated to 305°C at 20°C/minute. It is important to note that the hollow fiber signal seen by DSC will be representative of the porous support layer rather than the selective surface layer. The T_g of the powder sample, measured as received, was too broad to show a clear step change and could not be determined. The film sample has a higher T_g than the hollow fibers, though the crystallinity is similar. The melting temperatures of the hollow fibers and the film are similar, which indicates that the crystals are similar in size, though the shape and distribution of the crystallites cannot be determined.[2,7] The powder sample likely has smaller crystals as the melting temperature is 10°C lower.[2,7] Furthermore, the film sample undergoes a similar amount of crystallization to the hollow fibers during heating, though the film does not begin to crystallize until a higher temperature. However, the film, has a similar crystallinity and melting point as the hollow fibers, which implies that the samples have similar morphology.[7]

	T_g (°C)	T_c (°C)	ΔH_c (J/g)	T_m (°C)	ΔH_m (J/g)	% Crystallinity
Hollow Fiber	181	211	2.65	296	19.12	48.0%
Film	191	220	2.97	292	21.35	53.6%
Powder	-	-	-	284	17.26	50.3%

Table 6.1 Thermal properties of CTA hollow fiber, thick film and powder. T_c is the temperature of the crystallization peak, ΔH_c is the enthalpy of crystallization, T_m is the temperature of melting and ΔH_m is the enthalpy of melting.

6.3.1.5 Permeability of CTA at 10 atm Compared to Literature

CTA's permeability to several gases is summarized in Table 6.2 along with literature data for a selection of Eastman Chemical Company cellulose acetate samples reported by Puleo et al.[3] The Eastman samples show monotonically increasing crystallinity and permeability to all gases as the degree of substitution is increased. However, the Cameron CTA sample does not follow this trend. The crystallinity of the Cameron CTA film is lower than that for Eastman DS 2.84. The permeability of CTA also does not follow with the trends established by the Puleo paper, with the helium permeability being particularly low. Because the Cameron CTA film does not follow the Eastman CA trend, it is likely that there are differences beyond those captured by a simple degree of substitution. For example, the acetyl distribution, both within the repeat unit (i.e., distribution of acetylation at each of the three sites) and along the chain (i.e., if the acetylation is distributed evenly down the length of the chain), could influence the permeation and crystallization characteristics of the membrane without changing the degree of substitution. The average acetyl distribution within the repeat unit could be evaluated by NMR, but this was not done as the aging studies on CTA took precedence.

	Eastman			Cameron
Degree of Substitution	1.75	2.45	2.85	2.99
Crystallinity ($\%_{mass}$)	27%	37%	52%	44%
CH_4 Permeability (Barrer)	0.052	0.15	0.20	0.19
CO_2 Permeability (Barrer)	1.84	4.75	6.56	5.59
He Permeability (Barrer)	9.34	16	19.6	13.5
O_2 Permeability (Barrer)	0.32	0.82	1.46	0.88
N_2 Permeability (Barrer)	0.057	0.15	0.23	0.16

Table 6.2 Permeability of several gases in Cameron CTA and Eastman samples[3]

6.3.1.6 Solubility

At least one contributing factor for the lower permeability of the CTA film than expected is that CTA has a lower intrinsic solubility to both CH_4 and CO_2 than would be expected based on the degree of substitution trend noted by Puleo et al.[3] If it is assumed that gas is only sorbed in the amorphous regions of the polymer, measured gas concentration in the polymer (expressed as cm^3 (STP)/cm^3 polymer) can be re-expressed based on the amorphous phase mass by the following equation:

$$C\left(\frac{cm^3(STP)}{g\ amorphous\ polymer}\right) = \frac{C\left(\frac{cm^3(STP)}{cm^3 polymer}\right)}{x_a * \rho} \qquad 6.2$$

where C is the concentration of gas in the film in the given units, x_a is the amorphous mass fraction of the polymer and ρ is measured density.

The sorption isotherms for CO_2 and CH_4, expressed based on total polymer volume and based on amorphous mass, are shown for CTA and the same Eastman samples discussed above (Figure 6.5 and 6.6).[3] The intrinsic sorption of CH_4 in CTA is lower than in any of the Eastman cellulose acetates. The CO_2 sorption of CTA is similar

to the DS 1.45 sample and lower than the DS 2.84 sample. As with the permeability results, the sorption data do not correlate with DS in any monotonic or simple way.

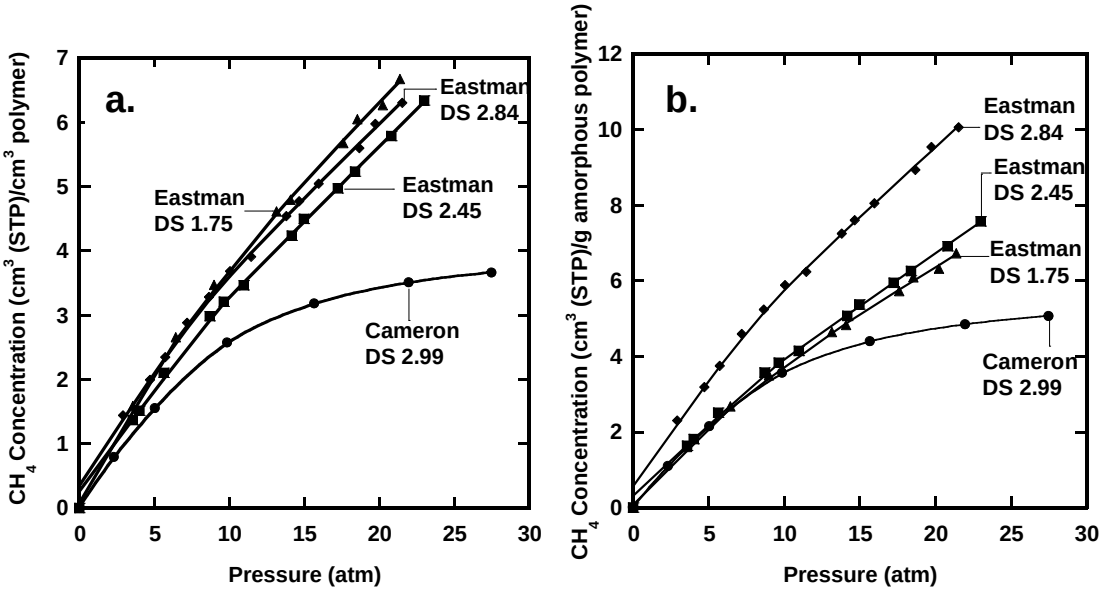

Figure 6.5 CH_4 sorption isotherms for Eastman[3] and Cameron cellulose acetate thick film samples. Sorption isotherms have been calculated on the basis of a. total polymer volume and b. mass of amorphous polymer (Equation 6.2).

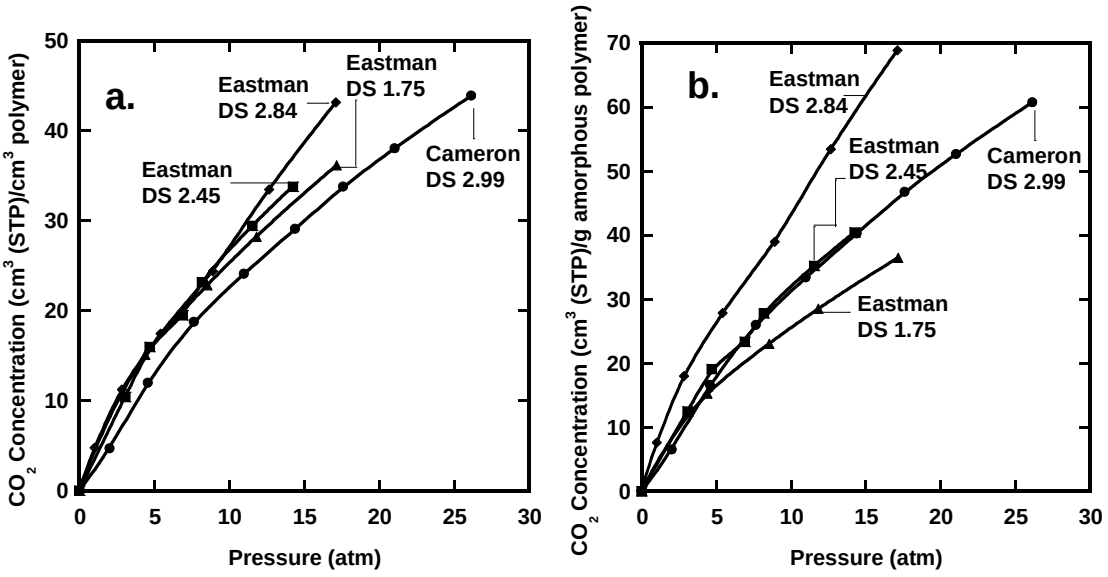

Figure 6.6 CO_2 sorption isotherms in Eastman[3] and Cameron cellulose acetate thick film samples. Sorption isotherms have been calculated on the basis of a. total polymer volume and b. mass of amorphous polymer (Equation 6.2).

6.3.1.7 Plasticization of CTA Relative to Literature

Finally, the extent of plasticization in the CTA sample relative to the Eastman samples[3] has been studied. Given the lower intrinsic CO_2 sorption in the CTA sample, it would be expected for the polymer to have lower plasticization. Indeed, as shown in Figure 6.7, the plasticization pressure curves (PPC) of the Eastman DS 2.84 and Cameron CTA samples show that the Eastman sample has a higher extent of plasticization. It is difficult to determine the plasticization pressure in the CTA sample. Due to the difference in absolute permeabilities, the permeabilities of the other CA samples are shown on a plot of permeability normalized by the lowest pressure permeability. Again on this plot, CTA shows a lower extent of plasticization than the Eastman DS 2.84, though it may plasticize somewhat more than the lower DS samples.[3]

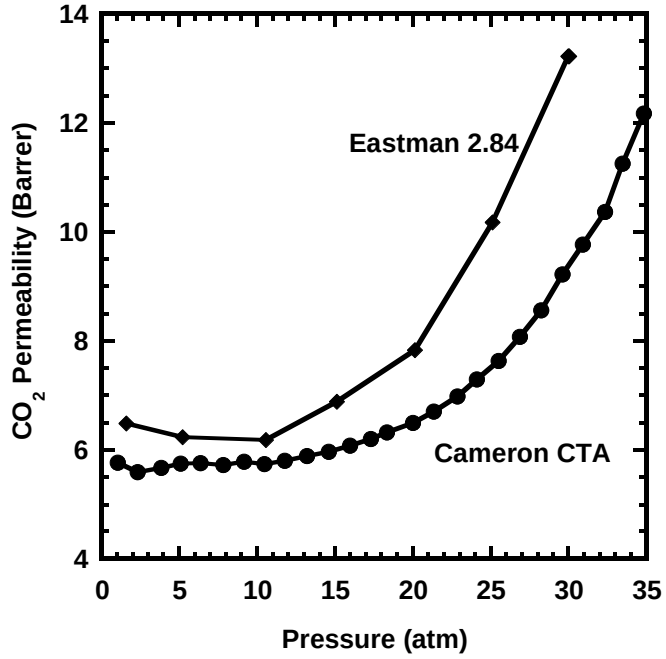

Figure 6.7 Plasticization pressure curves for Cameron CTA and Eastman DS 2.84[3]

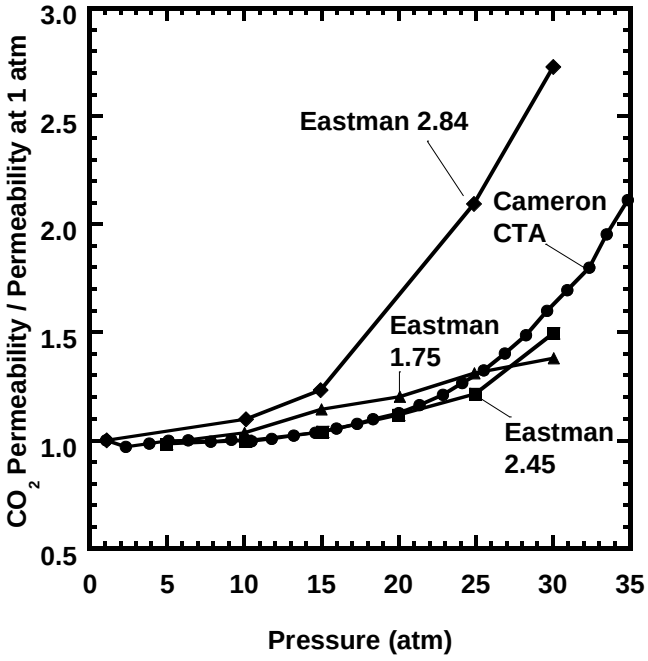

Figure 6.8 CO_2 plasticization pressure curves normalized by initial permeability at 1 atm for Eastman cellulose acetates[3] and Cameron CTA.

6.3.1.8 Methane Plasticization

A CH_4 hysteresis experiment was performed to test the suggestion to the author that CTA might be plasticized by CH_4. Due to the increased time-lag of CH_4, it was necessary to modify the hysteresis experiment described in Chapter 3. Specifically, instead of holding at each pressure for 10 minutes, hold times at each pressure were 4 hours except at the highest pressure, which was held for 12 hours. The resulting pressurization and depressurization curves (Figure 6.9) show very good agreement. Between the lack of hysteresis between pressurization and depressurization and the lack of a plasticization pressure point, it would appear that up to a pressure of 40 atm at these timescales, methane does not plasticize the CTA membrane.

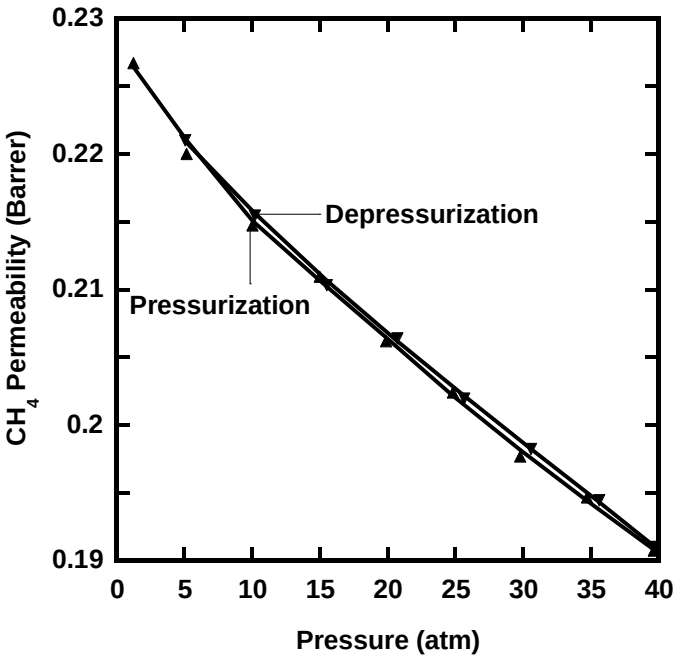

Figure 6.9 CH_4 plasticization pressure curve in CTA.

6.3.2 Determination of Proper Annealing Conditions for CTA

An aging experiment typically begins by annealing the sample above T_g to erase any thermal, aging and casting history (e.g. solvent, orientation, etc.).[1] Typically, a film sample is annealed at least 15°C above T_g for a minimum of 15 minutes.[1] Initial work with CTA used DSC to determine the T_g (Figure 6.10). The T_g shown here was calculated from the second heat because the step change in the heat flow of the first heat was too small and broad to calculate T_g. As measured here, the T_g is 167°C so an annealing temperature of 185°C would be appropriate. However, the T_g indicated by DSC does not register any rigid amorphous fraction present, it only registers the T_g of the bulk sample.[7] Thus, the T_g determined by DSC may not be representative of the entire sample. If only part of the sample is annealed above T_g, instead of resetting the aging process with a simple, known history, the sample is left with a very complex, unknown history as part of the sample was properly annealed and part of the sample may have undergone rapid, near-T_g aging.

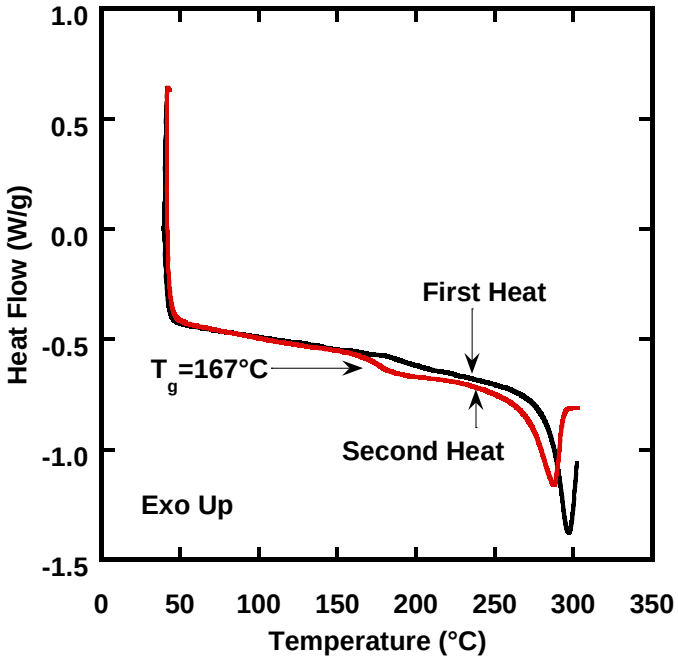

Figure 6.10 DSC results for the first and second heat of CTA.

The tan δ peak of a dynamic mechanical analysis (DMA) measurement provides different insight about the T_g of a material. The tan δ is sensitive to the thermal transitions of even small fractions of the polymer and thus the breadth of the tan δ peak corresponds to the distribution of T_gs throughout a sample.[7,8] The high temperature edge of the tan δ peak of CTA (Figure 6.11) does not occur until the sample is over 200°C. The annealing temperature chosen for this work based on the DMA results was 250°C, over 60°C higher than the annealing temperature chosen based on DSC.

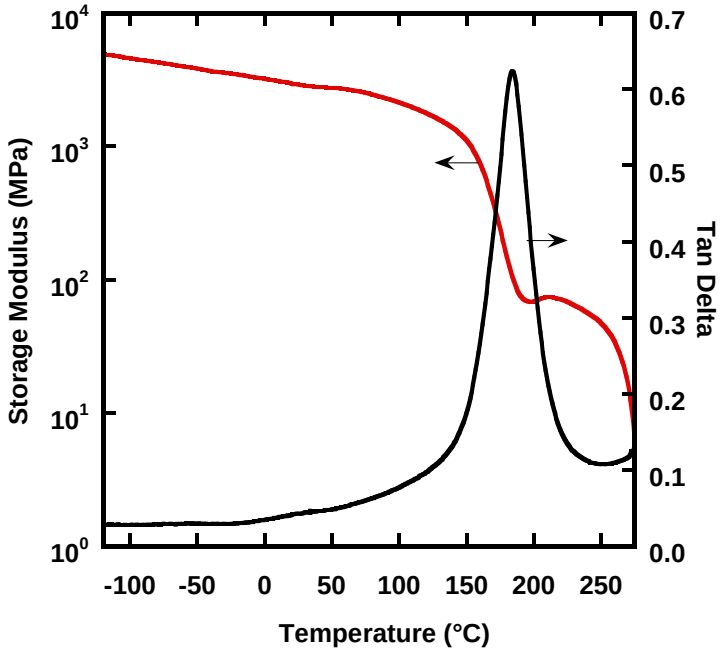

Figure 6.11 Storage and tan δ results for CTA using testing conditions described in Chapter 3.

The thermal stability of CTA at 250°C was confirmed by TGA (Figure 6.12). Although CTA is clearly not stable for long times at 250°C, the degradation is very slow so the mass loss during the initial 15 minutes was less than 0.2% Thus, CTA is stable enough to use 250°C as the annealing temperature, although multiple heats above T_g should be avoided and the annealing time rigorously controlled to 15 minutes to ensure repeatable results. An annealing temperature of 250° has been used for the majority of this work, though some comparisons with films annealed at 185°C have be done.

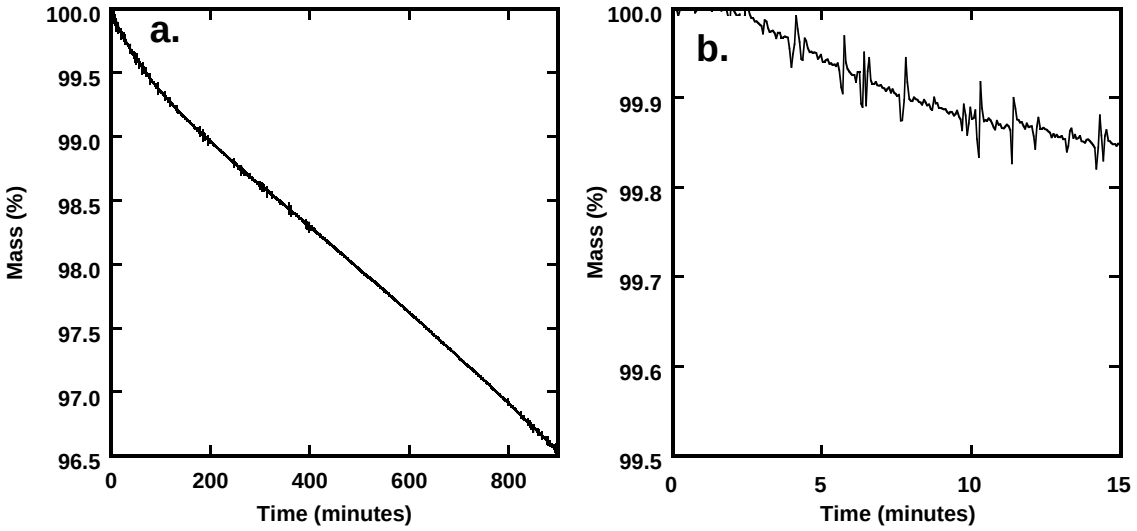

Figure 6.12 CTA mass loss during isothermal hold at 250°C for a. 15 hours and b. 15 minutes.

6.3.3 Effect of Annealing on Crystallinity and Thermal Behavior of CTA

DSC studies were done on thick (Figure 6.13) and thin (Figure 6.14) film samples to evaluate the effect of annealing on the crystallinity and thermal transitions in CTA. Three different thermal treatments are compared in thick films from the same film casting. The first sample, unannealed film, was dried under vacuum at 100°C for a sufficient time to remove the water and casting solvents. The second sample was dried in the same manner and then was additionally treated in the DSC with an annealing program of 250°C for 15 minutes. The annealing process caused several structural changes. First, the crystallization peak in the unannealed sample is not present in the annealed sample. The presence of the crystallization peak implies that the sample was solidified during casting before the equilibrium crystal content was reached.[7] The annealing process at 250°C is sufficient to allow the crystallization to occur, so the annealed sample does not undergo additional crystallization during the heating ramp. Furthermore, the annealed sample has slightly higher crystallinity. Finally, the 250°C, 15 minute annealing process

has caused the sample to develop two different crystal populations with distinct melting points. Because the new melting point is at a lower temperature, the new crystals in the annealed sample are smaller than the crystals present before annealing.[7]

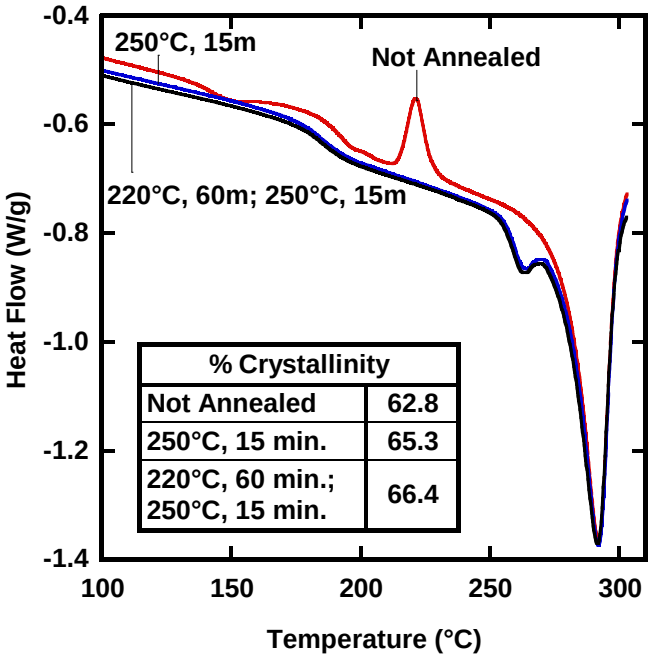

Figure 6.13 DSC results demonstrating the effect of different annealing conditions on thick film thermal behavior and crystallinity.

To create samples with higher crystallinity, a two-step annealing process was tested. Specifically, the sample was first annealed at 220°C for 60 minutes to allow crystallization and then annealed at 250°C for 15 minutes to remove the thermal history of the amorphous region. Unfortunately, as shown in Figure 6.13, the sample annealed in two steps has an identical thermal response to the sample that was only annealed at 250°C. Thus, the crystallinity of CTA cannot be increased via thermal techniques in a film annealed at 250°C. Because CTA degrades above its melting temperature, the crystallinity also cannot be reduced by quench cooling a sample from the melt.

The annealing of the thin CTA samples was done on the silicon wafer casting surface in a vacuum oven. To load the thin film samples into the DSC pan requires crumpling the sample and, if the sample is heated above T_g in this form, the sample would collapse and no longer be representative of a thin film. The thin CTA films show very similar thermal changes due to annealing (Figure 6.14). As in the thick films, the unannealed thin film sample shows a crystallization peak at about 220°C, which does not occur in the annealed sample. The annealed thin film also shows a new, lower temperature melting peak which corresponds to smaller crystals.

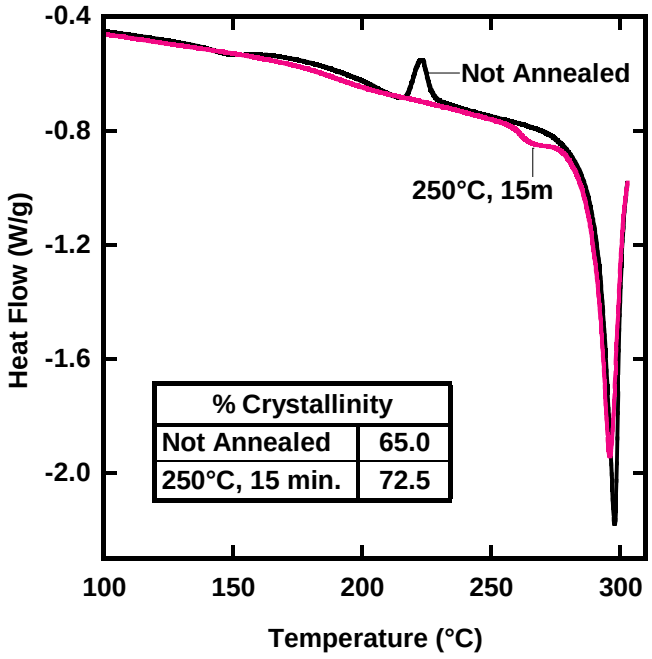

Figure 6.14 DSC results demonstrating the effect of different annealing conditions on thin film thermal behavior and crystallinity.

6.3.4 Effect of Casting Procedure on Crystallinity and Thermal Behavior of CTA

In previous aging studies, the samples were annealed above T_g, not just to reset the physical aging history, but also to erase the differences in casting history, particularly

between thin and thick films.[1] To create films that probe the full thicknesses range of interest (100 nm – 50 μm), it is necessary to use different casting techniques (i.e., spin coating vs. solution casting) and, frequently, different solvents.[1] Each of these factors can influence the morphology of the polymer which can, in turn, influence the gas transport behavior. DSC was used to study the effect of casting conditions on the morphology of thick and thin CTA films.

Unannealed thick and thin films (Figure 6.15) are fairly similar in thermal response up to temperatures of 275°C. The melting peak, on the other hand, shows significant differences between the thick and thin films. The thick film has a lower melting point and a broader melting peak. The lower melting point typically corresponds to smaller crystallites and the broader melting peak to a wider distribution of crystallite size.[7] Thus, spin coating the sample at 200 nm induces larger, more regular crystallites.

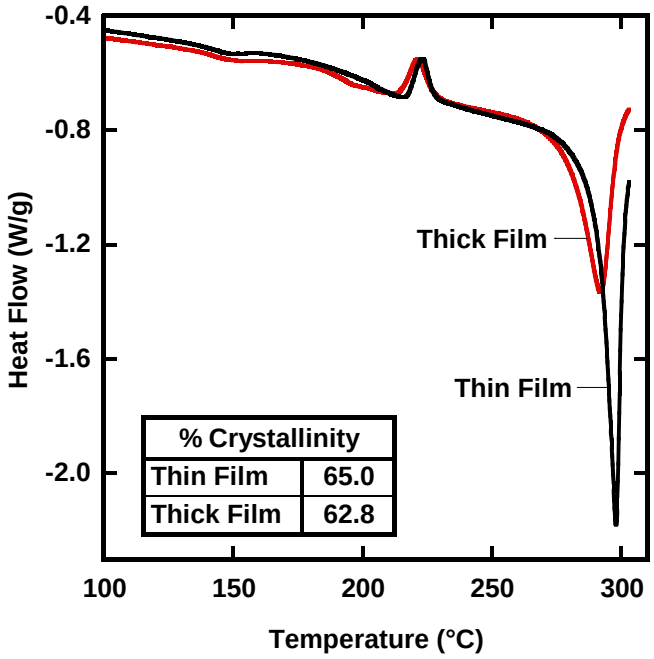

Figure 6.15 DSC results demonstrating the effect of thickness on the thermal behavior and crystallinity of unannealed films. The thicknesses of the thick and thin films were 60 µm and 200 nm respectively.

The results of the annealed films (Figure 6.16) are very similar to the unannealed results. The thermal response of the annealed films below the melting peak is very similar between thin and thick films, but the structure of the melting peak indicates morphological differences. Specifically, the thick film still has smaller, less regular crystallites than the thin film. Additionally the amount of small crystals, those associated with the lower temperature melting peak, is larger in the thick film than the thin film. Finally, the thin film has a higher crystallinity than the thick film and gains more crystallinity during the annealing process. The critical result of this analysis is that the morphology of the thin and thick films are different, and the annealing process cannot erase these differences.

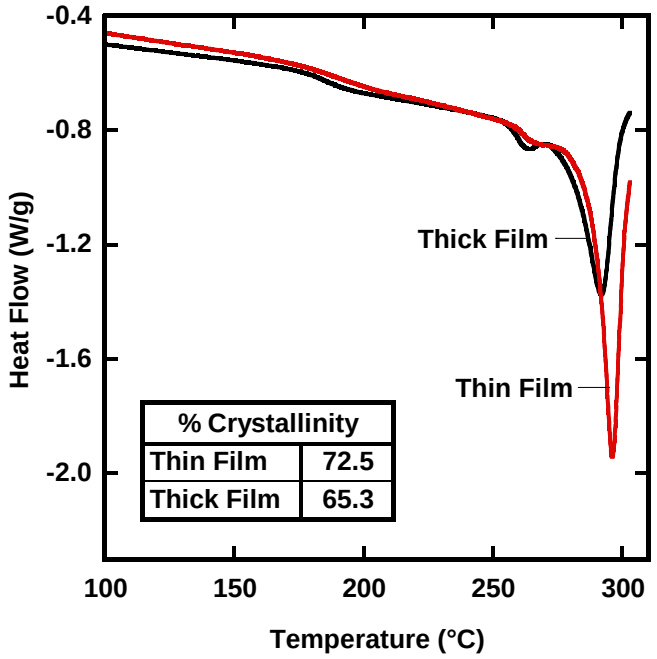

Figure 6.16 DSC results demonstrating the effect of thickness on the thermal behavior and crystallinity of annealed films. The thicknesses of the thick and thin films were 60 µm and 200 nm respectively.

6.3.5 Effect of Annealing Temperature on Permeability and Aging of CTA

Preliminary aging data on a 280 nm thin film annealed at 185°C are compared with data from a 190 nm film annealed at 250°C (Figure 6.17). The absolute permeability of the sample annealed at 250°C is approximately 30% lower the sample annealed at 185°C, likely due to the increase in crystallinity after the 250°C annealing (see Section 6.3.3). However, the aging rate is similar between the two samples. This is likely due to the fact that the bulk of the material is above the glass transition at 185°C, and therefore has a similar history regardless of the annealing temperature. However, for consistency in the remaining data, all samples were annealed at 250°C.

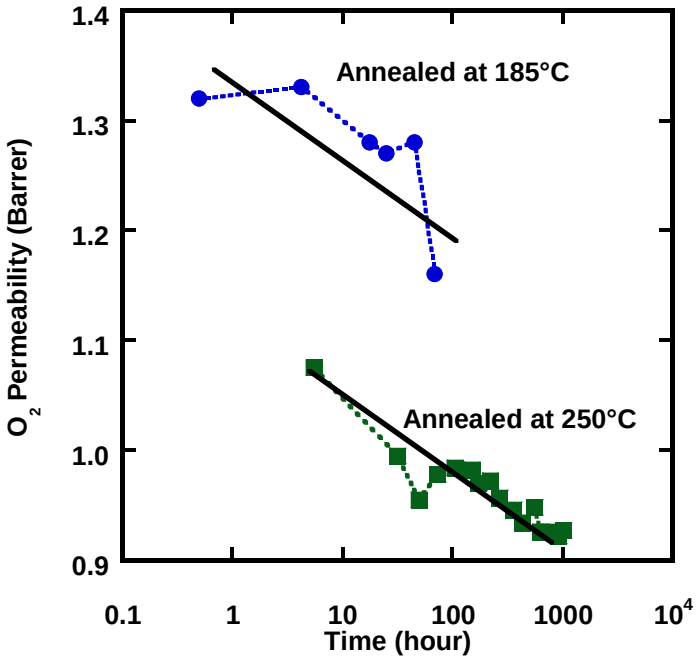

Figure 6.17 O_2 permeability as a function of time in CTA thin films annealed at 185°C and 250°C. Solid lines are drawn to guide the eye and have the same slope.

6.3.6 Effect of Thickness on Permeability and Aging

An aging experiment was performed with thin film samples ranging in thickness from 190 nm to 390 nm and a 60 μm thick film sample. All of the samples were annealed at 250°C for 15 minutes with the thin films on wire supports as described elsewhere[1] and the thick films free-standing. As described in Section 6.2.2, the thickness of the thin film samples has been adjusted for the thickness changes that occur during annealing. The sample thicknesses, casting details and crystallinity are summarized in Table 6.3. Insufficient sample remained of the 310nm film to collect DSC results to determine crystallinity.

Film	Casting	% Crystallinity	ℓ_0	ℓ_a
190 nm	R700,A11,T4m	73%	220nm	191 nm
310 nm	R700,A11,T4m x3		360nm	313 nm
390 nm	R300,A11,T4m	77%	443nm	385 nm
60 micron	Solution Cast	63%	60 μm	

Table 6.3 Casting conditions where R stands for spinning speed in RPM, A is acceleration on a Laurell Technologies Spin Coater and T is spinning time in minutes. The 310nm sample used the listed spinning conditions sequentially three times. ℓ_0 is the thickness measured prior to annealing and ℓ_a is the adjusted film thickness

The aging data for the CTA films are plotted here in terms of absolute permeability (Figures 6.18 – 6.20). The noise in the data is likely due to variations in the leak rate of the system, which, particularly in the 60 μm N_2 data, is over 10%. The thinner films, which have higher fluxes, are less noisy because the flux is higher relative to the leak rate. The oxygen data (Figure 6.18) show that the 60 μm film has the highest permeability which corresponds to having the lowest crystallinity. The thin films have higher crystallinity and correspondingly lower permeability. The aging rate of these films seems to be similar as evidenced by the slope of the permeability versus time. There is no evidence of accelerated aging in the O_2 permeability results of the thinner films. The nitrogen data (Figure 6.19) show very similar results, although the data are noisier due to the lower N_2 permeability. Again, there is no evidence of accelerated aging. The CH_4 data (Figure 6.20) show a slightly different result. The 200 nm film

seems to be aging more quickly than the 310 nm and 390 nm samples. At the time of the 60 µm aging experiment, CH_4 gas was unavailable, so the data were not collected.

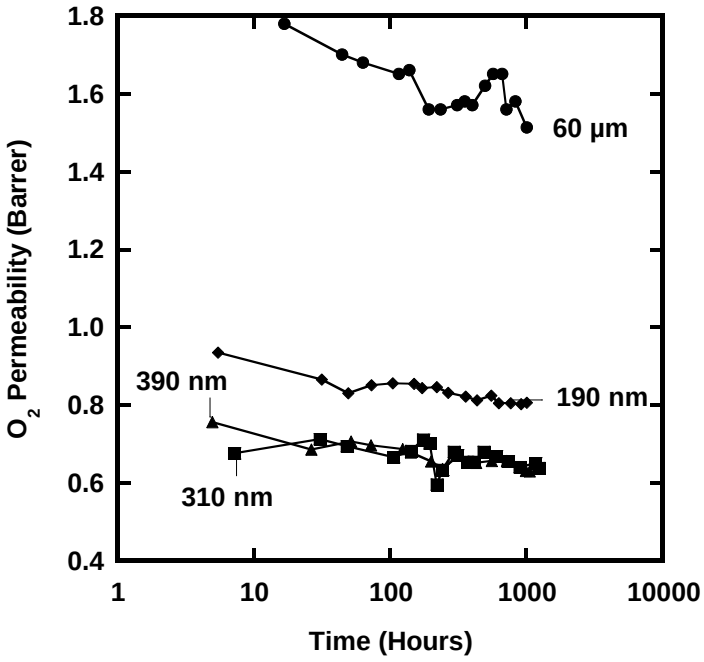

Figure 6.18 O_2 permeability in thick and thin CTA films as a function of time.

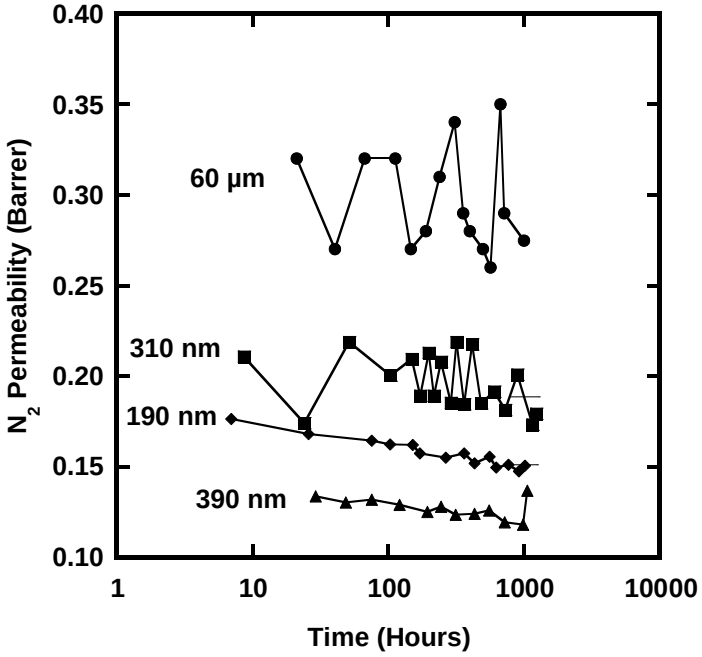

Figure 6.19 N_2 data as a function of thickness and aging time.

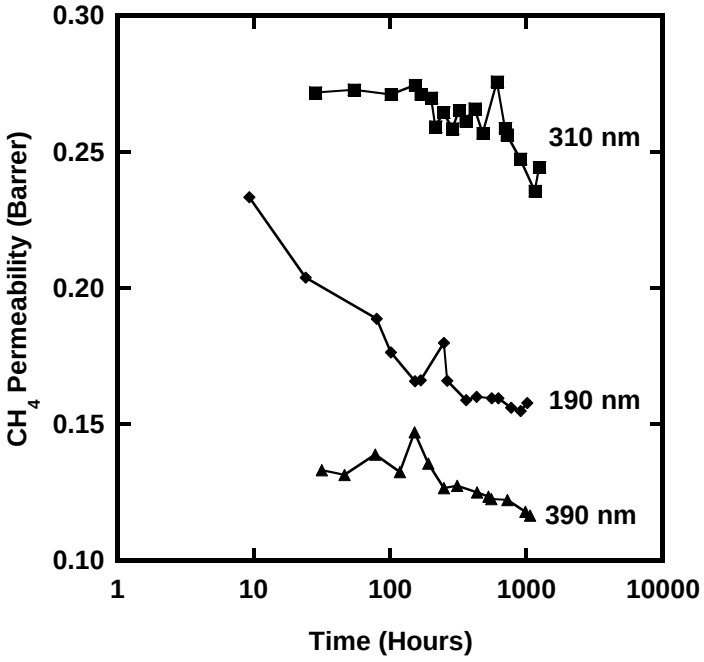

Figure 6.20 CH_4 permeability in CTA as a function of thickness and aging time

To isolate the aging rates of the samples from the variation in initial permeability, the data have also been plotted on the basis of relative permeability (Equation 6.3).

$$Relative\ Permeability\ at\ time, t = \frac{P_t}{P_i} \qquad 6.3$$

where P_t is the permeability at time, t, and P_i is the permeability measured at the earliest time. (Figures 6.21-6.23)

The relative O_2 permeability confirms the observation that thick and thin films are aging at similar rates. The results are essentially identical. The N_2 data are similar to the O_2 results; however, the CH_4 data are somewhat different. The relative CH_4 permeability data show that the 200 nm film is aging more rapidly than the 310 nm and 390 nm films. CH_4 is a larger molecule than N_2 or O_2, and as a result it is much more sensitive to the changes in free volume than the smaller molecules.[9,10] The CH_4 results imply that accelerated aging could be happening in the thinnest sample, but that the structural changes are too small to influence the O_2 and N_2 permeabilities.

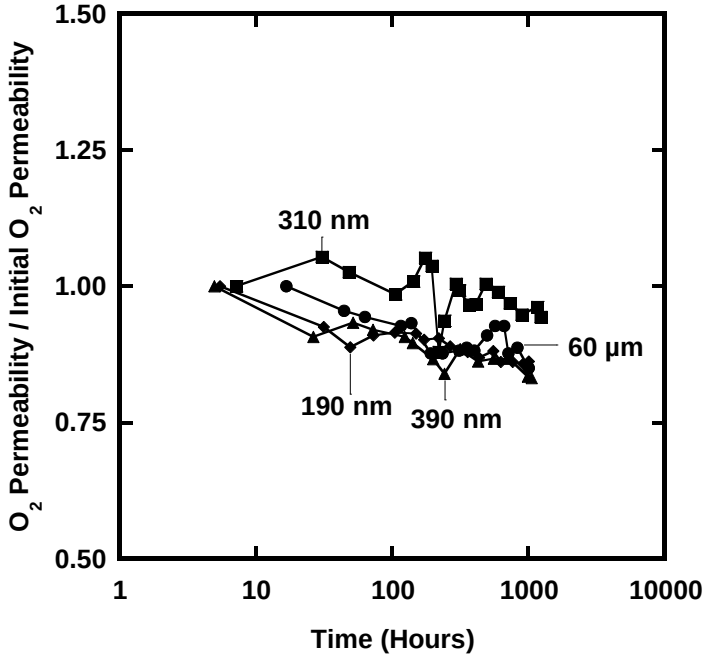

Figure 6.21 O_2 permeability in CTA normalized by initial permeability as a function of aging time and film thickness

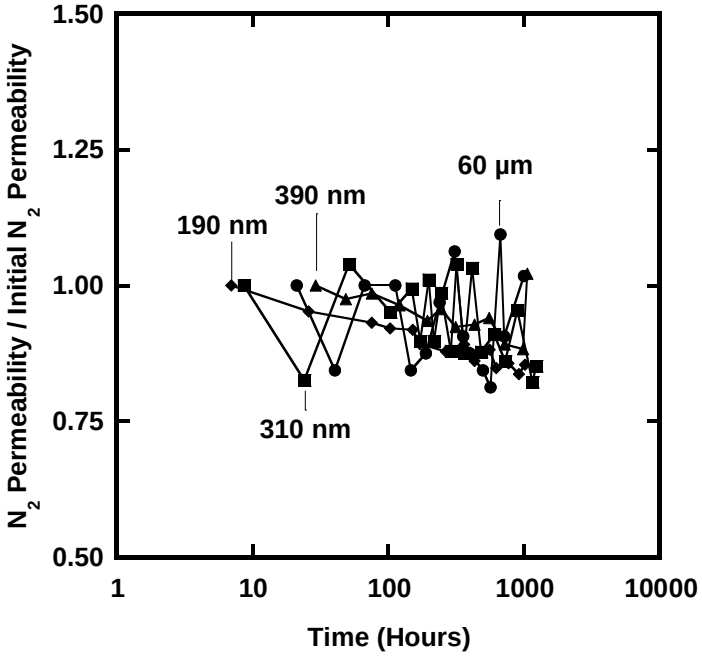

Figure 6.22 N_2 permeability in CTA normalized by the initial permeability as a function of film thickness and aging time.

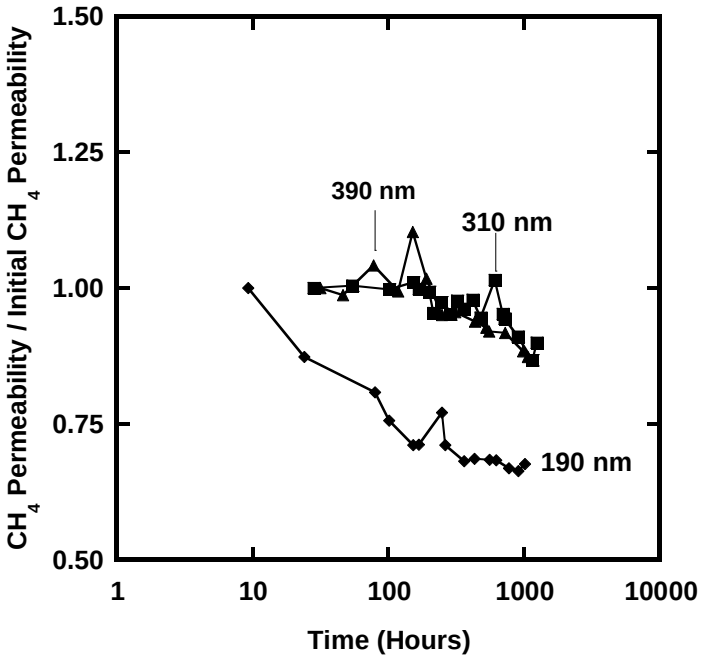

Figure 6.23 CH_4 permeability of CTA normalized by the initial permeability as a function of aging time and film thickness.

The CTA data are compared to the literature results on other polymers in Figure 6.24 in terms of relative O_2 permeability (Equation 6.3) for bulk polysulfone (PSF), [11] poly(phenylene oxide) (PPO), [11] and Matrimid[11] as well as the CTA data for the 200 nm and 60 µm films. The aging rate of both CTA samples is comparable to the bulk PPO results (i.e., CTA is aging faster than PSF and slower than Matrimid). Most significantly, the 200 nm film does not drop off faster than the bulk samples, but ages very similarly to them.

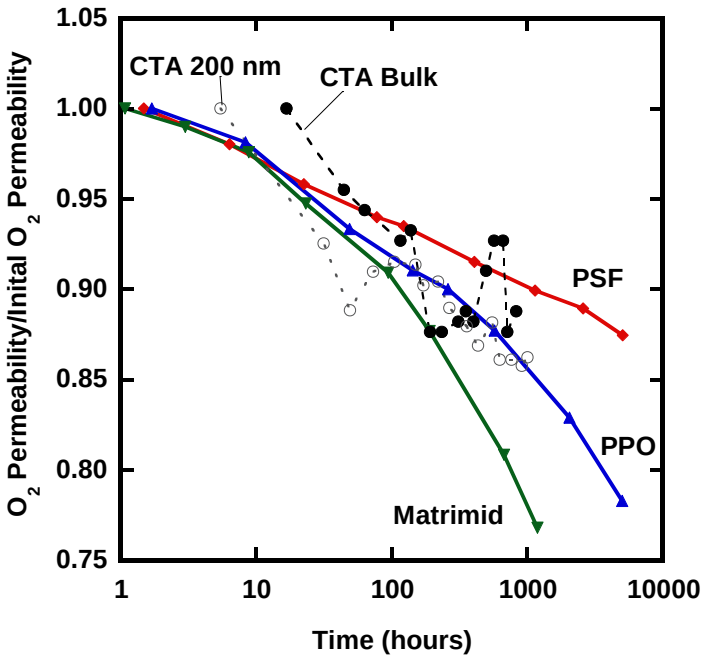

Figure 6.24 O_2 permeability normalized by initial permeability for CTA films and bulk PSF,[11] PPO[11] and Matrimid[11] as a function of aging time.

Finally, to capture the behavior of all the polymers for a range of thicknesses, the data are presented as the relative permeability at 500 and 1000 hours versus 1/film thickness (Figures 6.25 and 6.26). These plots compare the effect of thickness on the

amount of aging that has occurred at the given time. It is apparent that the CTA film is much less sensitive to thickness than the previously tested films.[11,12] In the data shown here, the sensitivity of aging to film thickness increases as the polymer's bulk density decreases (i.e., $\rho_{PPO} < \rho_{PSF}$ and relative O_2 permeability of PPO at a given time and thickness is less than that of PSF). This observation does not agree with the aging rates indicated for the bulk films in Figure 6.24, but this might be because of the relative thinness of the Matrimid bulk sample (3.5 μm). In Figure 6.25, it appears that a thicker Matrimid film might have a permeability at 500 hours that is higher than that of PPO, the opposite of the trend shown in Figure 6.24.

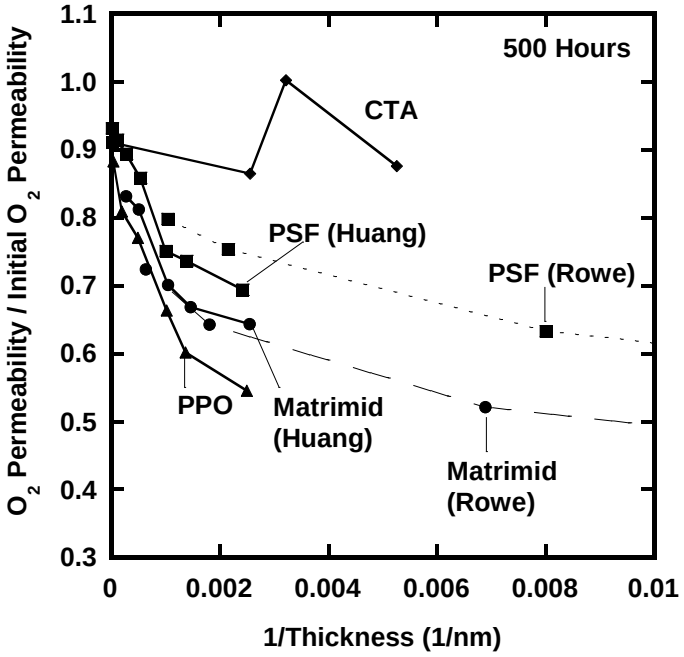

Figure 6.25 Relative O_2 permeability at 500 hours as a function of 1/thickness in CTA and polymers reported by Huang et al.[11] and Rowe et al.[12]

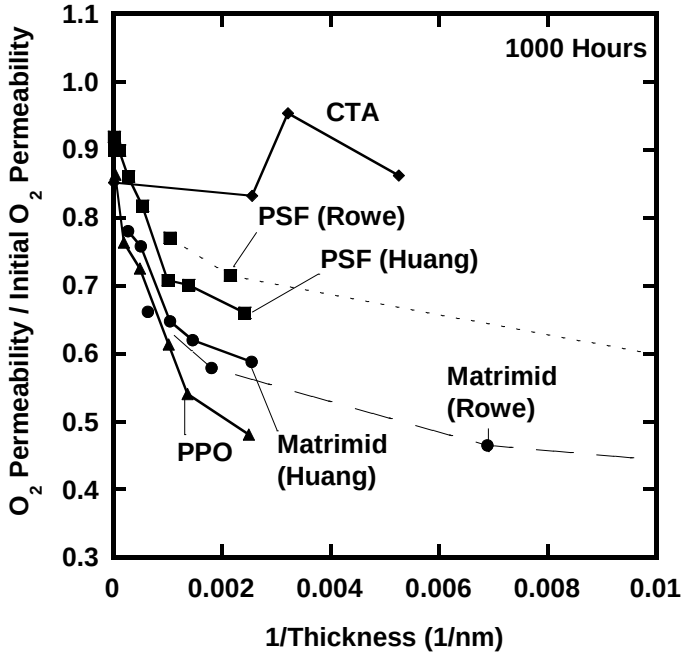

Figure 6.26 Relative O_2 permeability at 500 hours as a function of 1/thickness in CTA and polymers reported by Huang et al.[11] and Rowe et al.[12]

It is difficult to definitively explain the lack of accelerated aging in the O_2 and N_2 data for CTA thin films. The CH_4 data imply that accelerated aging may occur in the thinnest films to a minor extent. Perhaps the critical thickness for observing accelerated aging in CTA is below 200 nm, but thinner films would be needed to probe this possibility.

Alternatively, the origin of the reduced aging could be explained as the crystallites effectively trapping the chains in the non-equilibrium state. Although the CTA bulk samples age at a similar rate to the other polymers, perhaps the higher crystallinity and larger crystals in the thin films reduces their aging rate. Tant and Wilkes have shown reduced aging with increasing crystallinity in poly(ethylene terephthalate) (PET) with crystallinities ranging from 0-51%$_{wt}$, for which they give three possible explanations.[13] First, the increase of crystallinity reduces the fraction of the polymer

undergoing aging, which reduces the observed aging rate. However, for the CTA data, this would imply that the thin film aging rate was balanced between the increased rate due to thickness, as seen in amorphous polymers,[11,12] and the reduced aging rate due to crystallinity. [13] However, the crystallinity of the 190 nm is similar to the 390 nm film, but the aging rate is unchanged despite the reduction in film thickness by a factor of two. Tant and Wilkes' second proposal is that by broadening T_g towards higher temperature, the crystallinity effectively increases the distance between the aging temperature and T_g, which reduces aging. Again, this proposal is unsatisfactory for the CTA aging data presented here because, if a significant difference in T_g exists between the thick and thin films, the thin film sample has a lower T_g and higher crystallinity (cf. Figure 6.16). However, this difference in T_g is probably not significant considering the CTA samples are being aged over 140°C below T_g.[8] Tant and Wilkes' final proposal is that the crystals reduce the mobility of the amorphous chains that are near the crystallites.[13] Furthermore, recent work by Krishnaswamy et al. demonstrates that the morphology of the polymer, not just the amount of crystallinity, can influence the physical aging behavior of poly(phenylene sulfide).[14] Specifically, crystallization techniques which resulted in higher rigid amorphous fractions also resulted in higher aging rates as indicated by enthalpy recovery in DSC. [14] In the case of CTA, this would imply that the differences in morphology (i.e., thinner films having larger crystals) are significant to the resulting aging rate. The methods used by Krishnaswamy et al. to demonstrate this effect (i.e., generating samples with similar crystal fractions, but different rigid amorphous fraction via different crystallization temperatures) was not feasible with CTA due to the close overlap of the T_g and the decomposition temperature and the difficulty decoupling film thickness and morphology.

6.3.7 Effect of Thickness on CO_2 Plasticization

A CO_2 plasticization pressure curve was measured for films that had been annealed at 185°C and aged for 100 hours prior to the experiment. These results (Figure 6.27) are very different from the results seen in previous work.[15] In CTA, the thin film sample has a higher plasticization pressure and a lower overall extent of plasticization. The combination of these two factors indicates that the thin film is less sensitive to CO_2 plasticization than the thicker films.

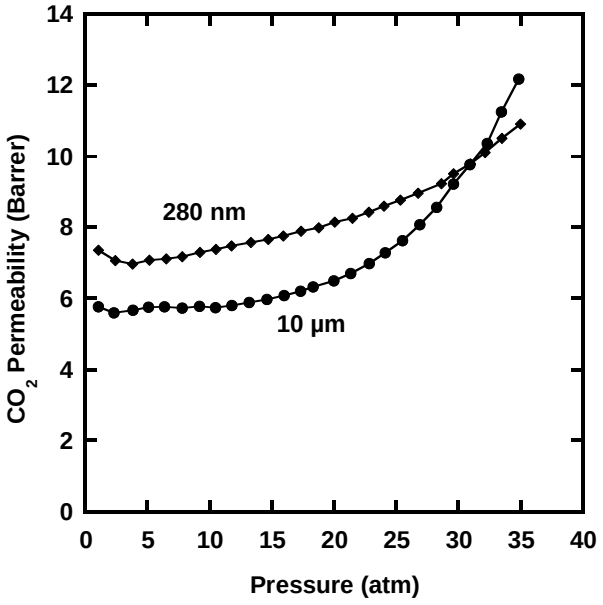

Figure 6.27 Plasticization pressure curve for 280 nm and 10 µm CTA films annealed at 185°C and aged for 100 hours prior to experiment.

To confirm these results, the CO_2 permeability of films annealed at 250°C for 15 minutes were measured with 2 hour holds at each pressure. The pressures chosen, 1, 4, 8, 16, 24 and 32 atm, start below the plasticization pressure, but probe up to the maximum pressures of interest for natural gas separations. The results of the 2 hour plasticization experiment are shown in Figure 6.28. For consistency, each film was aged for 100 hours

prior to the beginning of the CO_2 experiment. As with the other gases, the absolute CO_2 permeability of the CTA thick film is higher than the thin film. Unexpectedly, the plasticization of the thick film, as shown by the increase in permeability, is also higher. This result is the opposite of the trend observed in Matrimid (Figure 6.28).[15] However, plasticization results are strongly dependent on the polymer as shown in Figure 6.29. All of these films are slightly less than 200 nm, but each exhibits very different behavior in the presence of increasing CO_2 pressure.

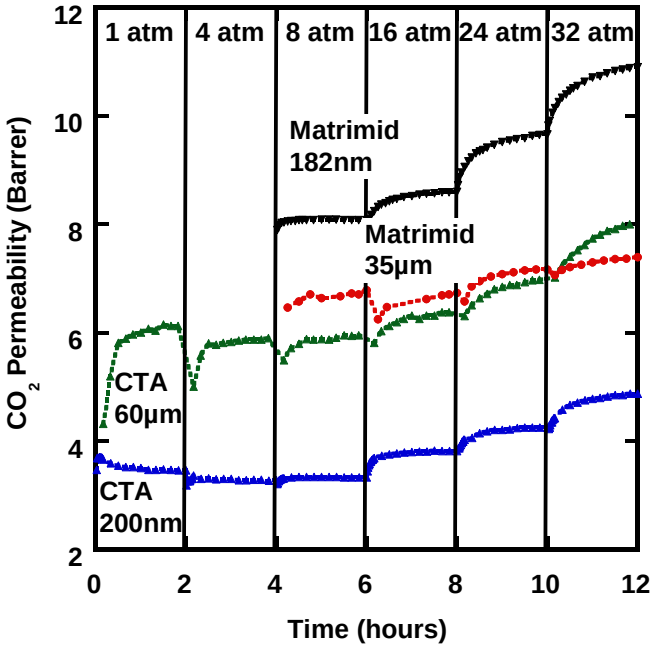

Figure 6.28 CO_2 permeability in CTA and Matrimid[15] with 2 hour holds at each pressure.

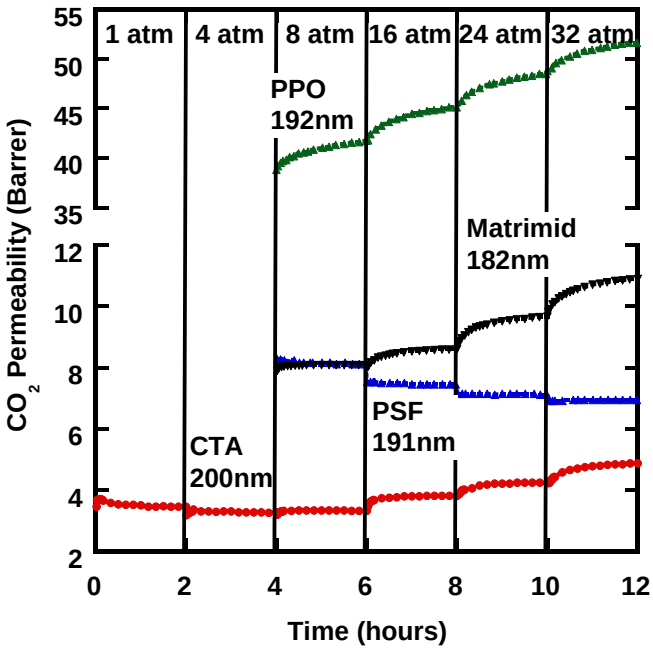

Figure 6.29 Plasticization behavior of CTA and report polymer thin films[15] during a 2 hour pressure step experiment.

The reduced plasticization in the CTA thin film may be a result of the crystallinity of the polymer. If the polymer chains are tied together by the crystallites, it may prevent their ability to swell and reduce the CO_2 uptake relative to where it would be in a purely amorphous polymer.

6.4 CONCLUSIONS

Cellulose acetates are a complicated family of materials. Gas transport in these materials seems to be dependent on more than simple crystallinity and chemical structure analysis captured by DS. Furthermore, due to CTA's thermal instability in the melt and limitations due to the thermal annealing process, it is difficult to control the morphology of these materials independently of chemical structure and film thickness. Thermal analysis indicated that the Cameron CTA has a very broad T_g and that a 250°C annealing temperature is necessary to equilibrate the film. Unfortunately, this heat treatment instills

maximum crystallinity in the film, which cannot be reduced without degrading the sample. Furthermore, the crystallites formed by spin coating are different from the crystallites formed by solution casting, and these differences persist through the annealing process. The differences in the morphology of the thick and thin films can be seen in the reduced permeability of the thin films, which is consistent with their higher crystal fractions. The difference in morphology makes the aging data more difficult to interpret as the film thickness is not decoupled from the crystallinity. However, these CTA samples do not show the accelerated aging in films as thin as 200 nm, as seen in materials studied by this method previously. Finally, the plasticization response of the thin CTA films is suppressed relative to the thicker films. This could be due to the increased crystallinity in the thin films preventing them from swelling, but to definitively determine the origin of the aging behavior will require decoupling thickness and crystallinity, which has thus far proven difficult.

6.5 REFERENCES

(1) Huang, Y.; Paul, D. R. *J. Memb. Sci.* **2004**, *244*, 167–178.

(2) Groenewoud, W. M. *Characterization of Polymers by Thermal Analysis*; 1st ed.; Elsevier Science B. V.: Amsterdam, 2001.

(3) Puleo, A. C.; Paul, D. R.; Kelley, S. S. *J. Memb. Sci.* **1989**, *47*, 301–332.

(4) Dymond, J. H.; Marsh, K. N.; Wilhoit, R. C.; Wong, K. C. *The Virial Coefficients of Pure Gases and Mixtures*; Frenkel, M.; Marsh, K. N., Eds.; Landolt-Bornstein: Darmstadt, 2001.

(5) Zugenmaier, P. *Macromol. Symp.* **2004**, *208*, 81–166.

(6) Kasai, N.; Kakudo, M. *X-Ray Diffraction by Macromolecules*; Castleman Jr., A. W.; Toennies, J. P.; Zinth, W., Eds.; Kodansha Ltd and Springer: Tokyo, 1995.

(7) *Principles and Applications of Thermal Analysis*; Gabbot, P., Ed.; 1st ed.; Blackwell Publishing: Oxford, 2008.

(8) Struik, L. C. E. *Physical Aging in Amorphous Polymers and Other Materials*; Elsevier Scientific Publishing Company: Amsterdam, The Netherlands, 1978; Vol. 54.

(9) Matteucci, S.; Yampolskii, Y. P.; Freeman, B. D.; Pinnau, I. In *Materials Science of Membranes for Gas and Vapor Separations*; Yampolskii, Y.; Pinnau, I.; Freeman, B. D., Eds.; John Wiley & Sons, Ltd: Chichester, 2006; pp. 1–47.

(10) Robeson, L. M.; Smith, Z. P.; Freeman, B. D.; Paul, D. R. *J. Memb. Sci.* **2014**, *453*, 71–83.

(11) Huang, Y.; Paul, D. R. *Polymer* **2004**, *45*, 8377–8393.

(12) Rowe, B. W.; Freeman, B. D.; Paul, D. R. *Polymer* **2009**, *50*, 5565–5575.

(13) Tant, M. R.; Wilkes, G. L. *J. Appl. Polym. Sci.* **1981**, *26*, 2813–2825.

(14) Krishnaswamy, R. K.; Geibel, J. F.; Lewis, B. J. *Macromolecules* **2003**, *36*, 2907–2914.

(15) Horn, N. R.; Paul, D. R. *Polymer* **2011**, *52*, 1619–1627.

Chapter 7: Conclusions and Recommendations

The work detailed in this dissertation evaluated the potential of novel membrane materials and investigated the physical aging and plasticization of cellulose acetate. Below is a brief summary of the most important conclusions arising from this work followed by recommendations for future work.

7.1 CONCLUSIONS

7.1.1 Ethanol Dehydration

The purpose of the work detailed in Chapter 4: Ethanol Dehydration with Thermally Rearranged Polyimides was to evaluate the ethanol dehydration potential of TR materials. To this end, a series of pervaporation measurements were made on a representative material, HAB-6FDA TR. HAB-6FDA TR's water and ethanol permeability decreased as temperature increased. However, due to the rapidly increasing driving force as temperature increases, the flux increases. Relative to reported values in the open literature,[1] HAB-6FDA TR's transport performance is not remarkable. The lower performance may be due to the relatively high temperatures (56°C to 76°C) used in this study, which, as previously stated, decrease the permeability of the material. However, the separation targeted by this work would require temperatures over 100°C and pressures of several bar.[2–7] Most of the reported membranes will degrade under these conditions, while TR materials should not. Finally, HAB-6FDA TR's membrane performance was compared to that of a commercial ethanol dehydration membrane from UBE Industries, Ltd.[8] If the materials are compared on a similar thickness basis, the HAB-6FDA TR shows water and ethanol permeances that are approximately an order of magnitude higher than the UBE material with a selectivity that is comparable to the UBE

material.[8] Based on these results, it was determined that the TR materials have potential as ethanol dehydration membranes.

7.1.2 Effect of Hexafluoroalcohol on Gas Transport

Chapter 5: Gas Transport and Thermal Stability of HFA-Containing Aromatic Polyimide evaluates the impact of the hexafluoroalcohol (HFA) moiety on the gas transport properties of an aromatic polyimide, MDA-6FDA, the properties of which have been previously reported. [9,10] Inclusion of the HFA moiety increased the fractional free volume of MDA-6FDA, which increased the permeability of all gases by at least 2.5 times. The permeability increases are due to diffusivity increases, as the solubilities remain unchanged by the inclusion of the HFA group.

However, the permeability increases due to the HFA group are not accompanied by the expected decreases in selectivities.[11] The selectivities of several gas pairs (e.g., CO_2/CH_4) are unchanged by the inclusion of the HFA group. A simple increase in fractional free volume would typically cause a material to move parallel to the upper bound towards higher permeability,[12] but HFA causes MDA-6DFA to move horizontally towards the upper bound. These results are similar to the results seen with hexafluoroisopropylidene units,[13–18] which are attributed to simultaneous increases in fractional free volume and chain stiffness.[15] The bulky HFA group can not only hinder backbone motion, it can also hydrogen bond with the imide groups[19] and further reduce chain motion.

Finally, the TGA of HFA-MDA-6FDA shows a two-step mass loss at 400°C, that is similar to the TGA results for TR polymers, and a similar product was proposed. Structural investigations by FTIR were not definitive, but there is some evidence of

benoxazine formation. However, the large number of overlapping peaks made analysis impossible.

7.1.3 Physical Aging and Plasticization in Cellulose Triacetate

The work detailed in Chapter 6: Characterization, Physical Aging and Plasticization of Cellulose Triacetate investigated the physical aging and plasticization of well-characterized cellulose triacetate (CTA) films as a function of film thickness. Due to results published by previous researchers,[20–22] it was expected that as the CTA film thickness was decreased below approximately 1 μm, the sample would show accelerated aging and increased plasticization in CO_2. However, permeability measurements tracking CTA's physical aging do not show accelerated aging in films as thin as 300 nm. In a 200 nm film, the aging tracked by O_2 and N_2 permeability is also identical to the thicker films, although the aging tracked by CH_4 permeability does show accelerated aging. Because CH_4 is a larger molecule than O_2 or N_2, it is more sensitive to small changes in free volume. [12,23] Thus, the accelerated aging indicated by the CH_4 data may indicate that the 200nm film is aging slightly faster than the thicker films, but not enough so that O_2 or N_2 are affected. Furthermore, the plasticization results in CTA show reduced plasticization in 200 nm CTA relative to a bulk film. Plasticization results, however, show far more variation with polymer structure than the physical aging results.[22]

The molecular origin for these results has not been determined, primarily due to the inability to decouple film thickness and crystallinity. Due to the thermal instability of CTA above its melting temperature, it is not possible to remove the crystallinity introduced by the casting and annealing processes. Differential scanning calorimetry (DSC) results show that the crystallinity of the thin films is higher and made up of larger, more regular crystals than the thick films. It is possible that the higher crystallinity in the

thin films reduces the chain motion, which would slow the physical aging and reduce the film's plasticization. However, according to the Struik model of aging in semi-crystalline polymers,[24,25] aging far below T_g should be unaffected by the presence of crystallites. Furthermore, previous studies using permeability to track physical aging in semi-crystalline poly(phenylene oxide) showed that although the absolute permeability was reduced by the presence of crystallites, the aging rate was unchanged from a sample without crystals.[26] To isolate the cause of the unusual aging behavior in CTA, a method for decoupling crystallinity and thickness is needed, and one was not found in the course of this work. A few ideas for decoupling thickness and crystallinity are presented in section 7.2.6.

7.2 Recommendations for Future Work

7.2.1 Chemical Structure Optimization for Ethanol Dehydration with TR Polymers

A complete structure/property study to optimize the chemical structure of the TR polymers for ethanol dehydration has not been done. Even within the TR platform, there are several potential avenues for increasing membrane productivity. For example, the gas transport properties of the rearranged polymer are dependent on the identity of the leaving group formed by the ortho-positioned functional group (e.g., the hydrogen of the ortho-alcohol).[27,28] In general, a larger ortho-functional leaving group results in higher permeability of the resulting TR structure, even when the nominal chemical structure is identical.[27,28] Additionally, the effects of changing the ortho-functionality from alcohols and esters to sulfur- and nitrogen-containing functional groups gives rise to TR structures that are polybenzthiazoles and polybenzimidazoles, respectively. The identity of the ortho-group will likely change the reactivity and kinetics of the TR reaction. By optimizing the reactivity of this reaction, it may be possible to utilize backbones that,

under the current platform, do not fully rearrange before degradation, which will increase the number of viable structures available.

Anther structural opportunity that has not been explored for ethanol dehydration with TR polymers is the use of copolymers. One avenue would be to use copolymers of multiple TR precursors to take advantage of particular characteristics of each polymer. For example, HAB-6FDA, detailed here, has the highest molecular weight and mechanical properties of the hydroxyl-based TR polymers studied; however, a TR polymer synthesized from 2,2'-Bis(3-amino-4-hydroxy phenyl) hexafluoropropane (APAF) and 6FDA, APAF-6FDA TR, typically has better gas permeation results.[29] Perhaps by copolymerizing the two monomers, some of the beneficial properties of each structure can be obtained. Furthermore, there are other polymer structures which may be stable at these use conditions, such as poly(dimethylsiloxane) (PDMS). PDMS is a rubbery polymer with very high permeability that has been copolymerized with aromatic polyimides.[30] The PDMS-imide copolymers are thermally stable above 400°C, which indicates that TR rearrangement of a copolymer would be possible, particularly with lower molecular weight PDMS.[30] By copolymerizing PDMS units into the TR structure, it may be possible to increase the permeability of the copolymer beyond the permeability of the TR polymers, though likely with some loss of selectivity.

Finally, a fundamental evaluation of the transport properties can give a deeper understanding of how these membranes work which, in turn, can give rise to new avenues of materials for this separation and an understanding for other separations these membranes might be useful for. One example is to evaluate not just the sorption and diffusivity components of the membranes, but how these change with temperature and pressure. This study could help determine if there are particular operating conditions under which the membranes are most efficient. Furthermore, a fundamental evaluation of

the feed induced swelling and plasticization would increase the understanding of the actual state of the membrane in use as well as increasing the understanding of these poorly understood phenomena.

7.2.2 Other High-Temperature, Chemically Aggressive Separations

In addition to ethanol dehydration, there are many other separations which could benefit from the high thermal and chemical stability coupled with the transport properties of TR materials. Membranes have been studied for the dehydration of numerous organics, including other alcohols.[1,6,31,32] Due to the strongly size sieving nature of TR polymers, the separation of water from most organics should be efficient.

Beyond the dehydration separations, other separations which benefit from higher temperature feeds, either from a transport perspective, or from a plant-design perspective could be areas where the TR polymers could be useful. For example, both pre- and post-combustion carbon capture require membranes that are stable well above room temperature. Post-combustion carbon capture requires CO_2 removal from N_2 at around 200°C and relatively low pressures.[33] Pre-combustion carbon capture requires CO_2 removal from H_2 at temperatures closer to 400°C and pressures close to 1000 psi.[33] Beyond the temperature stability, the membranes will need to be plasticization resistant and chemically stable to the possible contaminants in the streams.

Membrane reactors would be another area where the high thermal and chemical stability of TR materials could be very useful. Membrane reactors combine a traditional reactor design with a separation membrane in a single process step. Membrane reactors are of interest as they can reduce energy costs by combining reactions and separations, shift reaction equilibrium to increase production and reduce side reactions. The advantage of using polymer membranes for membrane reactors is the well-developed

ability to produce thin polymer films, however, polymers typically lack sufficient thermal and chemical stability.[34] While even TR materials are not stable up to the temperatures of some reactors (>600°C)[35], there are a few applications for which TR materials make likely candidates. For example, membrane-assisted catalysis for esterification has similar requirements to organic dehydration.[34] Esterification is an equilibrium-limited reaction which can be shifted towards products by the removal of water. Thus, a membrane that could selectively remove water from an acid-catalyzed mixture of organics would be able to increase the yield of the reaction. Membranes have been commercialized for this purpose, but these materials are limited in the reactions for which they are appropriate.[34]

7.2.3 HFA Moiety in Other Polymer Backbones

Given the positive influence the HFA group has on the gas transport properties of MDA-6DFA and the similar effect hexafluoroisopropylidene units have been shown to have on multiple backbones,[13–18] it would be interesting to expand this study to other HFA-containing polymers. There are numerous ways to incorporate the HFA moiety into a polymeric backbone. For example, combining the HFA-MDA monomer utilized in this work with other dianhydrides and diacid chlorides should yield additional polyimides and polyamides. Additionally, Central Glass Co., Ltd. has patented methods for producing dicarboxylic acids containing HFA groups.[36] Combined with the HFA-MDA used here, a polymer could be synthesized that contains HFA groups on both monomers. Alternatively, polymer backbones consisting of other backbone functionality (e.g., polyester) are possible. Testing the gas transport properties of these other structures will test the generalizability of these results and may find more promising materials.

7.2.4 High Temperature Reaction Products of HFA-MDA-6FDA and HFA-MDA-BAF

There are other techniques which have not yet been utilized to elucidate the high temperature reaction products of HFA-MDA-6FDA and HFA-MDA-BAF. For example, elemental analysis might help illuminate if the fluorine groups are stable or if they are potentially part of the degradation process. Unfortunately, due to the large number of potential products, it may be difficult to isolate the exact structure from just the elemental composition.

TGA can be coupled with mass spectroscopy to identify the chemicals which are being emitted by the sample as the heating rate occurs. In particular, it could be instructive to look for peaks associated with the predicted by-products of the proposed reaction (i.e., H_2O for HFA-MDA-BAF and CO_2 for HFA-MDA-6FDA). Alternatively, peaks containing fluorine or aromatic groups would indicate some level of degradation. Peaks which are not consistent with either of these scenarios would indicate that a different reaction was occurring.

Solution-state Nuclear Magnetic Resonance (NMR) analysis could provide additional insight into the chemical structure of HFA-MDA-6FDA-T and HFA-MDA-BAF-T. The first challenge would be to prepare an NMR solution. Prior to the thermal treatment, HFA-MDA-6FDA was only soluble in hot NMP, but this solvent was not tested for the HFA-MDA-6FDA-T samples. d_6-NMP is available, though expensive. If a suitable solvent could be found, there are several valuable NMR experiments that could be performed. First, simple ^{1}H and ^{13}C NMR provide the foundation for more advanced techniques which will likely be necessary due to the complexity of the structure and the relatively few protons. Additional techniques, such as correlation spectroscopy (COSY), heteronuclear single quantum correlation (HSQC) spectroscopy and heteronuclear

multiple bond correlation (HMBC) spectroscopy will likely be necessary to sort out the complicated heteronuclear, multicyclic structures. Solid-state NMR would avoid the need for a solvent, however, the resulting signals are frequently too broad to allow for detailed characterization of complex structures.

Another direction this study could go would be to utilize small-molecule analogs. This would require the synthesis of molecules that are very similar in structure to the region of the repeat unit near the imide linkage. The primary advantage of using the small molecule analog is the increased solubility of low molecular weight compounds, which may allow for more solution-based analysis techniques. This advantage is offset by the additional work necessary to demonstrate that any chemistry that occurs in the small molecules is representative of the polymers' reactions.

Finally, characterization of the gas transport properties of the high temperature reaction products could be interesting. Whether the final structure is a benzoxazine or a partial degradation, the loss of a large portion of the repeat unit could carve out large free volume elements. Research in TR polymers has demonstrated that larger leaving groups translate to higher permeability,[27] so the high temperature reaction products could have very high permeability.

7.2.5 Effect of Acetate Group Distribution on Transport Properties in Cellulose Acetates

As shown by the disagreement of the Cameron CTA with Puleo's work on the Eastman CA samples,[37] there seems to be more governing the morphology and transport in CA samples than is captured by DS. A study using samples prepared by different techniques could illuminate the source of this discrepancy. CA samples could be readily acquired from different sources, and additional samples could be created by deactylating high DS samples. The transport, thermal and morphological properties could then be

examined and correlated with the chemistry of each sample. A better understanding of the fundamental transport in CA could then be leveraged to understand the unusual aging and plasticization results found in this work.

7.2.6 Decouple Thickness and Crystallinity in Cellulose Acetates

One way to decouple crystallinity and thickness in CA samples is to compare these results with similar studies on samples with lower DS. As the DS of CA decreases, the crystallinity of the sample also decreases,[38] though as the DS approaches zero and the structure approaches cellulose, the crystallinity does begin to increase. However, in samples of DS that are reasonable for gas separations (i.e., DS 1.75 or higher), the crystallinity decreases monotonically as the DS decreases.[38] Producing thin films of similar thicknesses from these polymers will decouple the crystallinity from the film thickness, though the chemical structure will no longer be identical between samples. However, if the behavior of the lower DS samples is similar to the aging of polysulfone and the other polymers previously reported,[20,21] it would indicate that the morphology of these CTA films was critical to the aging results.

If the origin of the unusual physical aging behavior of CTA is due to its crystallinity, another semi-crystalline polymer with similar crystal structure might give similar results. Specifically, a polymer with similar levels of crystallinity that does not degrade above its melt temperature would allow for an almost complete decoupling of crystallinity and thickness. With a thermally stable polymer, thin films could be taken into the melt, and then cooled at different rates to prepare samples of approximately the same thickness with different crystallinities. The physical aging properties could then be measured and correlated with the film structure. However, to be tested by permeability measurements as described here, the polymer must also have a reasonable permeability

(i.e., not so low that large film areas are required to get measureable flux). One potential polymer fitting this description is syndiotactic polystyrene (SPS). Specifically, samples containing 0-43%$_{wt}$ β crystals have been prepared via thermal annealing.[39,40] The O_2 permeability of these samples is above 1.5 barrer, which should be reasonable for testing.[40] The aging behavior as measured by mechanical properties shows that far below T_g, SPS ages similarly to amorphous materials, but the crystallinity of the samples was not determined.[41] Furthermore, the physical aging measured via gas permeability of thin films of amorphous polystyrene has been reported.[42] The sensitivity of aging rate to film thickness is lower in polystyrene than Matrimid and polysulfone, though the reason is not determined. [42] The ability to have a control sample, without crystallinity, that shows qualitatively similar behavior to the previous PSF and Matrimid data is one advantage of using SPS. One downside to using polystyrene is the relatively low T_g (i.e., approximately 100°C),[39,40,42] meaning that the aging experiments at 35°C will be much closer to T_g, and the effect of this different driving force is not clear.

7.3 REFERENCES

(1) Chapman, P. D.; Oliveira, T.; Livingston, A. G.; Li, K. *J. Memb. Sci.* **2008**, *318*, 5–37.

(2) Côté, P.; Noël, G.; Moore, S. *Desalination* **2010**, *250*, 1060–1066.

(3) Côté, P.; Roy, C.; Bernier, N. *Sep. Sci. Technol.* **2009**, *44*, 110–120.

(4) Huang, Y.; Baker, R. W.; Aldajani, T.; Ly, J. Dehydration Processes Using Membranes with Hydrophobic Coating. US 2009/0057224 A1, 2009.

(5) Huang, Y.; Baker, R. W.; Vane, L. M. *Ind. Eng. Chem. Res.* **2010**, *49*, 3760–3768.

(6) Osora, H.; Seiki, Y.; Yukumoto, A.; Yukio, T.; Ogino, S.; Hiroshima-Ken, M. Membrane system for the dehydration of solvents. EP 2 263 783 A1, 2010.

(7) Vane, L. M.; Alvarez, F. R.; Huang, Y.; Baker, R. W. *J. Chem. Technol. Biotechnol.* **2009**, *85*, 502–511.

(8) Nakagawa, K.; Kusuki, Y.; Ninomiya, K. *Proc. Fourth Int. Congr. Pervaporation Process. Chem. Ind.* **1989**, 250–260.

(9) Hirayama, Y.; Yoshinaga, T.; Kusuki, Y.; Ninomiya, K.; Sakakibara, T.; Tamari, T. *J. Memb. Sci.* **1996**, *111*, 169–182.

(10) Coleman, M. R.; Koros, W. J. *J. Memb. Sci.* **1990**, *50*, 285–297.

(11) Freeman, B. D. *Macromolecules* **1999**, *32*, 375–380.

(12) Matteucci, S.; Yampolskii, Y. P.; Freeman, B. D.; Pinnau, I. In *Materials Science of Membranes for Gas and Vapor Separations*; Yampolskii, Y.; Pinnau, I.; Freeman, B. D., Eds.; John Wiley & Sons, Ltd: Chichester, 2006; pp. 1–47.

(13) Bhole, Y. S.; Karadkar, P. B.; Kharul, U. K. *J. Polym. Sci. Part B Polym. Phys.* **2007**, *45*, 3156–3168.

(14) Dai, Y.; Guiver, M. D.; Robertson, G. P.; Kang, Y. S.; Lee, K. J.; Jho, J. Y. *Macromolecules* **2004**, *37*, 1403–1410.

(15) Hellums, M. W.; Koros, W. J.; Husk, G. R.; Paul, D. R. *J. Memb. Sci.* **1989**, *46*, 93–112.

(16) Kumbharkar, S. C.; Karadkar, P. B.; Kharul, U. K. *J. Memb. Sci.* **2006**, *286*, 161–169.

(17) Mohr, J. M.; Paul, D. R.; Tullos, G. L.; Cassidy, P. E. *Polymer* **1991**, *32*, 2387–2394.

(18) Morisato, A.; Ghosal, K.; Freeman, B. D.; Chern, R. T.; Alvarez, J. C.; de la Campa, J. G.; Lozano, A. E.; de Abajo, J. *J. Memb. Sci.* **1995**, *104*, 231–241.

(19) Ito, H.; Hinsberg, W. D.; Rhodes, L. F.; Chang, C. In *Advances in Resist Technology and Processing XX*; Fedynyshyn, T. H., Ed.; 2003; Vol. 5039, pp. 70–79.

(20) Huang, Y.; Paul, D. R. *Polymer* **2004**, *45*, 8377–8393.

(21) Rowe, B. W.; Freeman, B. D.; Paul, D. R. *Polymer* **2009**, *50*, 5565–5575.

(22) Horn, N. R.; Paul, D. R. *Polymer* **2011**, *52*, 1619–1627.

(23) Robeson, L. M.; Smith, Z. P.; Freeman, B. D.; Paul, D. R. *J. Memb. Sci.* **2014**, *453*, 71–83.

(24) Struik, L. C. E. *Physical aging in amorphous polymers and other materials*; Elsevier Scientific Publishing Company: Amsterdam, The Netherlands, 1978; Vol. 54.

(25) Struik, L. C. E. *Polymer* **1987**, *28*, 1521–1533.

(26) Huang, Y. Physical Aging of Thin Glassy Polymer Films, The University of Texas at Austin, 2005.

(27) Sanders, D. F.; Guo, R.; Smith, Z. P.; Stevens, K. A.; Liu, Q.; McGrath, J. E.; Paul, D. R.; Freeman, B. D. *J. Memb. Sci.* **2014**, *In Press*.

(28) Sanders, D. F.; Guo, R.; Smith, Z. P.; Liu, Q.; Stevens, K. a.; McGrath, J. E.; Paul, D. R.; Freeman, B. D. *Polymer* **2014**, *55*, 1636–1647.

(29) Park, H. B.; Jung, C. H.; Lee, Y. M.; Hill, A. J.; Pas, S. J.; Mudie, S. T.; Van Wagner, E.; Freeman, B. D.; Cookson, D. J. *Science* **2007**, *318*, 254–258.

(30) Moon, Y. D.; Lee, Y. M. *J. Appl. Polym. Sci.* **1993**, *50*, 1461–1473.

(31) Badiger, H.; Shukla, S.; Kalyani, S.; Sridhar, S. *J. Appl. Polym. Sci.* **2014**, *131*.

(32) Huang, Y.; Ly, J.; Aldajani, T.; Baker, R. W. Liquid-phase and vapor-phase dehydration of organic/water solutions, 2008.

(33) Figueroa, J. D.; Fout, T.; Plasynski, S.; McIlvried, H.; Srivastava, R. D. *Int. J. Greenh. Gas Control* **2008**, *2*, 9–20.

(34) Vankelecom, I. F. J. *Chem. Rev.* **2002**, *102*, 3779–3810.

(35) Saracco, G.; Vesteeg, G. F.; van Swaaij, W. P. M. *J. Memb. Sci.* **1994**, *95*, 105–123.

(36) Narizuka, S.; Hagiwara, Y.; Nagamori, M.; Yamanaka, K. Novel Fluoroine-Containing Dicarboxylic Acids and Their Novel Polymer Compounds. US 2009/0030173 A1, 2009.

(37) Puleo, A. C.; Paul, D. R.; Kelley, S. S. *J. Memb. Sci.* **1989**, *47*, 301–332.

(38) Zugenmaier, P. *Macromol. Symp.* **2004**, *208*, 81–166.

(39) Hodge, K.; Prodpran, T.; Shenogina, N. B.; Nazarenko, S. *J. Polym. Sci. Part B Polym. Phys.* **2001**, *39*, 2519–2538.

(40) Prodpran, T. *Polymer* **2002**, *43*, 2295–2309.

(41) Beckmann, J.; McKenna, G. B.; Landes, B. G.; Bank, D. H.; Bubeck, R. A. *Polym. Eng. Sci.* **1997**, *37*, 1459–1468.

(42) Murphy, T. M.; Freeman, B. D.; Paul, D. R. *Polymer* **2013**, *54*, 873–880.

References

Aitken, C. L.; Koros, W. J.; Paul, D. R. *Macromolecules* **1992**, *25*, 3424–3434.

Aitken, C. L.; Koros, W. J.; Paul, D. R. *Macromolecules* **1992**, *25*, 3651–3658.

Al-Juaied, M.; Koros, W. J. *J. Memb. Sci.* **2006**, *274*, 227–243.

Allcock, H. R.; Lampe, F. W.; Mark, J. E. *Contemporary Polymer Chemistry*; 3rd ed.; Pearson Education, Inc.: Upper Saddle River, 2003.

Allen, A. D.; Breyta, G.; Brock, P.; DiPietro, R.; Sanders, D.; Sooriyakumaran, R.; Sundberg, L. K. *J. Photopolym. Sci. Technol.* **2006**, *19*, 569–572.

Allen, R. D.; Na, Y.-H.; Sooriyakumaran, R.; Fujiwara, M.; Yamanaka, K. *J. Photopolym. Sci. Technol.* **2010**, *23*, 741–747.

Allen, R. D.; Young-Hye, N.; Sooriyakumaran, R.; Fujiwara, M.; Yamanaka, K. Polyamide Membranes with Fluoroalcohol Functionality. US 2010/0216899 A1, 2010.

Anwand, D.; Muller, F. W.; Strehmel, B.; Schiller, K. *Die Makromol. Chemie* **1991**, *192*, 1981–1991.

Azeotropic Data - III; Horsley, L. H., Ed.; American Chemical Society, 1973.

Badiger, H.; Shukla, S.; Kalyani, S.; Sridhar, S. *J. Appl. Polym. Sci.* **2014**, *131*.

Baker, E. A.; Rittigstein, P.; Torkelson, J. M.; Roth, C. B. *J. Polym. Sci. Part B Polym. Phys.* **2009**, *47*, 2509–2519.

Baker, R. W. *Ind. Eng. Chem. Res.* **2002**, *41*, 1393–1411.

Baker, R. W. *Membrane Technology and Applications*; 2nd ed.; John Wiley & Sons, Ltd, 2004; pp. 1–538.

Baker, R. W.; Lokhandwala, K. *Ind. Eng. Chem. Res.* **2008**, *47*, 2109–2121.

Barlow, J. W.; Cassidy, P. E.; Lloyd, D. R.; You, C.-J.; Chang, Y.; Wong, P. C.; Noriyan, J. *Polym. Eng. Sci.* **1987**, *27*, 703–715.

Beckmann, J.; McKenna, G. B.; Landes, B. G.; Bank, D. H.; Bubeck, R. A. *Polym. Eng. Sci.* **1997**, *37*, 1459–1468.

Berens, A. R.; Hodge, I. M. *Macromolecules* **1982**, *15*, 756–761.

Bernardo, P.; Drioli, E.; Golemme, G. *Ind. Eng. Chem. Res.* **2009**, *48*, 4638–4663.

Bhole, Y. S.; Karadkar, P. B.; Kharul, U. K. *J. Polym. Sci. Part B Polym. Phys.* **2007**, *45*, 3156–3168.

Bondi, A. *J. Phys. Chem.* **1964**, *68*, 441–451.

Bondi, A. *Physical Properties of Molecular Crystals, Liquids, and Glasses*; John Wiley & Sons, Inc.: New York, 1968.

Bos, A.; Pünt, I. G. M.; Wessling, M.; Strathmann, H. *J. Memb. Sci.* **1999**, *155*, 67–78.

C. O'Brien, K.; Koros, W. J.; Husk, G. R. *J. Memb. Sci.* **1988**, *35*, 217–230.

Calle, M.; Chan, Y.; Jo, H. J.; Lee, Y. M. *Polymer* **2012**, *53*, 2783–2791.

Calle, M.; Doherty, C. M.; Hill, A. J.; Lee, Y. M. *Macromolecules* **2013**, *46*, 8179–8189.

Calle, M.; Lozano, A. E.; Lee, Y. M. *Eur. Polym. J.* **2012**, *48*, 1313–1322.

Chan, A. H.; Paul, D. R. *J. Appl. Polym. Sci.* **1980**, *25*, 971–974.

Chapman, P. D.; Oliveira, T.; Livingston, A. G.; Li, K. *J. Memb. Sci.* **2008**, *318*, 5–37.

Chiou, J. S.; Barlow, J. W.; Paul, D. R. *J. App. Poly. Sci.* **1985**, *30*, 2633–2642.

Chiou, J. S.; Paul, D. R. *J. Memb. Sci.* **1987**, *32*, 195–205.

Choi, J. I.; Jung, C. H.; Han, S. H.; Park, H. B.; Lee, Y. M. *J. Memb. Sci.* **2010**, *349*, 358–368.

Choji, N.; Pusch, W.; Satoh, M.; Tak, T.; Tanioka, A. *Desalination* **1985**, *53*, 347–361.

Coleman, M. R.; Koros, W. J. *J. Memb. Sci.* **1990**, *50*, 285–297.

Colthup, N. In *Introduction to Infrared and Raman Spectroscopy*; Elsevier Science, 2012; Vol. 166, pp. 325–327.

Côté, P.; Noël, G.; Moore, S. *Desalination* **2010**, *250*, 1060–1066.

Côté, P.; Roy, C.; Bernier, N. *Sep. Sci. Technol.* **2009**, *44*, 110–120.

Cui, L.; Qiu, W.; Paul, D. R.; Koros, W. J. *Polymer* **2011**, *52*, 5528–5537.

Dai, Y.; Guiver, M. D.; Robertson, G. P.; Kang, Y. S.; Lee, K. J.; Jho, J. Y. *Macromolecules* **2004**, *37*, 1403–1410.

Donohue, M.; Minhas, B.; Lee, S. *J. Memb. Sci.* **1989**, *42*, 197–214.

Dorkenoo, K. D.; Pfromm, P. H. *Macromolecules* **2000**, *33*, 3747–3751.

Dymond, J. H.; Marsh, K. N.; Wilhoit, R. C.; Wong, K. C. *The Virial Coefficients of Pure Gases and Mixtures*; Frenkel, M.; Marsh, K. N., Eds.; Landolt-Bornstein: Darmstadt, 2001.

Dymond, J. H.; Marsh, K. N.; Wilhoit, R. C.; Wong, K. C. *The Virial Coefficients of Pure Gases and Mixtures*; Frenkel, M.; Marsh, K. N., Eds.; Landolt-Bornstein: Darmstadt, 2001.

Echeverria, I.; Su, P.-C.; Simon, S. L.; Plazek, D. J. *J. Polym. Sci. Part B Polym. Phys.* **1995**, *33*.

Ellison, C. J.; Kim, S. D.; Hall, D. B.; Torkelson, J. M. *Eur. Phys. J. E. Soft Matter* **2002**, *8*, 155–166.

Evers, R. C.; Arnold, F. E.; Helminiak, T. E. *Macromolecules* **1981**, *14*, 925–930.

Fender, N.; Brock, P. J.; Chau, W.; Bangsaruntip, S.; Mahorowala, A. P.; Wallraff, G. M.; Hinsberg, W. D.; Larson, C. E.; Ito, H.; Breyta, G.; Burnham, K.; Truong, H. D.; Lawson, P.; Allen, R. D. In *Advances in Resist Technology and Processing XVIII*; Houlihan, F. M., Ed.; 2001; Vol. 4345, pp. 417–427.

Figueroa, J. D.; Fout, T.; Plasynski, S.; McIlvried, H.; Srivastava, R. D. *Int. J. Greenh. Gas Control* **2008**, *2*, 9–20.

Finkelshtein, E. S.; Gringolts, M. .; Ushakov, N. .; Lakhtin, V. .; Soloviev, S. .; Yampol'skii, Y. . *Polymer* **2003**, *44*, 2843–2851.

Frank, C. W.; Rao, V.; Despotopoulou, M. M.; Pease, R. F. W.; Hinsberg, W. D.; Miller, R. D.; Rabolt, J. F. *Science* **1996**, *273*, 912–915.

Freeman, B. D. *Macromolecules* **1999**, *32*, 375–380.

Gandler, J. R.; Jencks, W. P. *J. Am. Chem. Soc.* **1982**, *104*, 1937–1951.

Ghosal, K.; Freeman, B. D. *Polym. Adv. Technol.* **1994**, *5*, 673–697.

Ghosal, K.; Freeman, B. D.; Chern, R.; Daly, W.; Negulescu, I. *Macromolecules* **1996**, *29*, 4360–4369.

Gleason, K. L.; Paul, D. R.; Freeman, B. D. Vapor Permeation of Ethanol and Water in Thermally Rearranged (TR) Polymers, 2013.

Gmehling, J.; Onken, U.; Arlt, W. *Vapor-Liquid Equilibrium Data Collection*; Dechema: Frankfurt, 1977.

Graham, T. *J. Memb. Sci.* **1995**, *100*, 27–31.

Grate, J. W. *Chem. Rev.* **2008**, *108*, 726–745.

Grate, J. W.; Kaganove, S. N.; Patrash, S. J.; Craig, R.; Bliss, M. *Chem. Mater.* **1997**, *9*, 1201–1207.

Groenewoud, W. M. *Characterization of Polymers by Thermal Analysis*; 1st ed.; Elsevier Science B. V.: Amsterdam, 2001.

Hall, D. S.; Osborn, B.; Patterson, K.; Burns, S. D.; Willson, C. G. In *Advances in Resist Technology and Processing XVIII*; Houlihan, F. M., Ed.; 2001; Vol. 4345, pp. 1066–1072.

Han, S. H.; Lee, J. E.; Lee, K.-J.; Park, H. B.; Lee, Y. M. *J. Memb. Sci.* **2010**, *357*, 143–151.

Haraya, K.; Obata, K.; Hakuta, T.; Yoshitome, H. *J. Chem. Eng. Japan* **1986**, *19*, 431–436.

Haraya, K.; Obata, K.; Hakuta, T.; Yoshitome, H. *J. Chem. Eng. Japan* **1986**, *19*, 464–466.

Hedesiu, C.; Demco, D. E.; Kleppinger, R.; Poel, G. Vanden; Remerie, K.; Litvinov, V. M.; Blümich, B.; Steenbakkers, R. *Macromol. Mater. Eng.* **2008**, *293*, 847–857.

Heinze, T.; Liebert, T. *Macromol. Symp.* **2004**, *208*, 167–238.

Hellums, M. W.; Koros, W. J.; Husk, G. R.; Paul, D. R. *J. Memb. Sci.* **1989**, *46*, 93–112.

Henis, J. M. S.; Tripodi, M. K. *Science* **1983**, *220*, 11–17.

Hirayama, Y.; Yoshinaga, T.; Kusuki, Y.; Ninomiya, K.; Sakakibara, T.; Tamari, T. *J. Memb. Sci.* **1996**, *111*, 169–182.

Hodge, I. M. *Macromolecules* **1983**, *16*, 898–902.

Hodge, I. M. *Macromolecules* **1987**, *20*, 2897–2908.

Hodge, I. M. *Science* **1995**, *267*, 1945–1947.

Hodge, I. M.; Berens, A. R. *Macromolecules* **1981**, *14*, 1598–1599.

Hodge, I. M.; Berens, A. R. *Macromolecules* **1982**, *15*, 762–770.

Hodge, I. M.; Berens, a. R. *Macromolecules* **1985**, *18*, 1980–1984.

Hodge, I. M.; Huvard, G. S. *Macromolecules* **1983**, *16*, 371–375.

Hodge, K.; Prodpran, T.; Shenogina, N. B.; Nazarenko, S. *J. Polym. Sci. Part B Polym. Phys.* **2001**, *39*, 2519–2538.

Horn, N. R.; Paul, D. R. *Macromolecules* **2012**, *45*, 2820–2834.

Horn, N. R.; Paul, D. R. *Polymer* **2011**, *52*, 1619–1627.

Horn, N. R.; Paul, D. R. *Polymer* **2011**, *52*, 1619–1627.

Huang, Y. Physical Aging of Thin Glassy Polymer Films, The University of Texas at Austin, 2005.

Huang, Y.; Baker, R. W.; Aldajani, T.; Ly, J. Dehydration Processes Using Membranes with Hydrophobic Coating. US 2009/0057224 A1, 2009.

Huang, Y.; Baker, R. W.; Vane, L. M. *Ind. Eng. Chem. Res.* **2010**, *49*, 3760–3768.

Huang, Y.; Ly, J.; Aldajani, T.; Baker, R. W. Liquid-phase and vapor-phase dehydration of organic/water solutions, 2008.

Huang, Y.; Ly, J.; Nguyen, D.; Baker, R. W. *Ind. Eng. Chem. Res.* **2010**.

Huang, Y.; Paul, D. R. *Ind. Eng. Chem. Res.* **2007**, *46*, 2342–2347.

Huang, Y.; Paul, D. R. *J. Memb. Sci.* **2004**, *244*, 167–178.

Huang, Y.; Paul, D. R. *J. Polym. Sci. Part B Polym. Phys.* **2007**, *45*, 1390–1398.

Huang, Y.; Paul, D. R. *Macromolecules* **2005**, *38*, 10148–10154.

Huang, Y.; Paul, D. R. *Macromolecules* **2006**, *39*, 1554–1559.

Huang, Y.; Paul, D. R. *Polymer* **2004**, *45*, 8377–8393.

Huang, Y.; Wang, X.; Paul, D. R. *J. Memb. Sci.* **2006**, *277*, 219–229.

Husk, G. R.; Cassidy, P. E.; Gebert, K. L. *Macromolecules* **1988**, *21*, 1234–1238.

Hutchinson, J. M. *Prog. Polym. Sci.* **1995**, *20*, 703–760.

Ismail, A. F.; Lorna, W. *Sep. Purif. Technol.* **2002**, *27*, 173–194.

Ito, H.; Hinsberg, W. D.; Rhodes, L. F.; Chang, C. In *Advances in Resist Technology and Processing XX*; Fedynyshyn, T. H., Ed.; 2003; Vol. 5039, pp. 70–79.

Jung, C. H.; Lee, J. E.; Han, S. H.; Park, H. B.; Lee, Y. M. *J. Memb. Sci.* **2010**, *350*, 301–309.

Kasai, N.; Kakudo, M. *X-Ray Diffraction by Macromolecules*; Castleman Jr., A. W.; Toennies, J. P.; Zinth, W., Eds.; Kodansha Ltd and Springer: Tokyo, 1995.

Khotimskii, V. S.; Filippova, V. G.; Bryantseva, I. S.; Bondar, V. I.; Shantarovich, V. P.; Yampolskii, Y. P. *J. Appl. Polym. Sci.* **2000**, *78*, 1612–1620.

Kim, J. H.; Koros, W. J.; Paul, D. R. *Polymer* **2006**, *47*, 3094–3103.

Kim, J. H.; Koros, W. J.; Paul, D. R. *Polymer* **2006**, *47*, 3104–3111.

Kim, J.; Koros, W. J.; Paul, D. R. *J. Memb. Sci.* **2006**, *282*, 32–43.

Kim, T. H.; Koros, W. J.; Husk, G. R.; O'Brien, K. C. *J. Memb. Sci.* **1988**, *37*, 45–62.

Kishimura, S.; Endo, M.; Sasago, M. *J. Photopolym. Sci. Technol.* **2002**, *15*, 625–628.

Klopffer, M. H.; Flaconnèche, B. *Oil Gas Sci. Technol.* **2001**, *56*, 223–244.

Koros, W. J.; Fleming, G. K. *J. Memb. Sci.* **1993**, *83*, 1–80.

Koros, W. J.; Paul, D. R. In *Proceedings 6th Annual Industrial Energy Conservation Technology Conference*; 1984; p. 525.

Koros, W. J.; Paul, D. R. In *Synthetic Membranes*; Chenoweth, M. B., Ed.; MMI Press, 1986; pp. 155–189.

Koros, W. J.; Paul, D. R. *Polym. Eng. Sci.* **1980**, *20*, 14–19.

Koros, W. J.; Paul, D. R.; Rocha, A. A. *J. Polym. Sci. Polym. Phys. Ed.* **1976**, *14*, 687–702.

Kostina, J.; Rusakova, O.; Bondarenko, G.; Alentiev, A.; Meleshko, T.; Kukarkina, N.; Yakimanskii, A.; Yampolskii, Y. P. *Ind. Eng. Chem. Res.* **2013**, *52*, 10476–10483.

Kraftschik, B.; Koros, W. J. *Macromolecules* **2013**, *46*, 6908–6921.

Krishnaswamy, R. K.; Geibel, J. F.; Lewis, B. J. *Macromolecules* **2003**, *36*, 2907–2914.

Kubota, T.; Nakanishi, R. *Polym. Lett.* **1964**, *2*, 655–659.

Kumazawa, H.; Sada, E.; Nakata, K.; Kawashima, N.; Kataoka, S.; Tada, K. *J. Appl. Polym. Sci.* **1994**, *53*, 113–119.

Kumbharkar, S. C.; Karadkar, P. B.; Kharul, U. K. *J. Memb. Sci.* **2006**, *286*, 161–169.

La, Y.-H.; Sooriyakumaran, R.; Miller, D. C.; Fujiwara, M.; Terui, Y.; Yamanaka, K.; McCloskey, B. D.; Freeman, B. D.; Allen, R. D. *J. Mater. Chem.* **2010**, *20*, 4615.

Lambert, J. B.; Shurvell, H. F.; Cooks, R. G. In *Introduction to Organic Spectroscopy*; Macmillan Publication: New York, 1987; pp. 174–177.

Larkin, P. *Infrared and Raman Spectroscopy: Principles and Spectral Interpretation*; Elsevier Science, 2011.

Lee, a; Feldkirchner, H.; Stern, S.; Houde, A.; Gamez, J.; Meyer, H. *Gas Sep. Purif.* **1995**, *9*, 35–43.

Lee, S. H.; Kim, J. W.; Kim, J. W.; Oh, S. K.; Park, C. S.; Lee, J. Y.; Kim, S. S.; Lee, J. W.; Kim, D.; Kim, J.; Ban, K. Do; Bok, C. K.; Moon, S. C. In *Advances in Resist Materials and Processing Technology XXIV*; Lin, Q., Ed.; 2007; Vol. 6519, pp. 1–9.

Lee, S. Y. S.; Minhas, B. S.; Donohue, M. D. In *AIChE Symposium Series*; 1988; Vol. 84, pp. 93–101.

Li, J.; Zhang, Y.; Carr, P. W. *Anal. Chem.* **1993**, *65*, 1969–1979.

Li, Q.; Simon, S. L. *Polymer* **2006**, *47*, 4781–4788.

Lin, H.; Freeman, B. D. In *Springer Handbook of Materials Measurement Methods*; Czichos, H.; Saito, T.; Smith, L., Eds.; Springer: New York, 2006; pp. 371–387.

Masser, K. A.; Runt, J. *Macromolecules* **2010**, *43*, 6414–6421.

Matteucci, S.; Yampolskii, Y. P.; Freeman, B. D.; Pinnau, I. In *Materials Science of Membranes for Gas and Vapor Separations*; Yampolskii, Y.; Pinnau, I.; Freeman, B. D., Eds.; John Wiley & Sons, Ltd: Chichester, 2006; pp. 1–47.

McCaig, M. .; Paul, D. R.; Barlow, J. . W. *Polymer* **2000**, *41*, 639–648.

McCaig, M. S.; Paul, D. R. *Polymer* **1999**, *40*, 7209–7225.

McCaig, M. S.; Paul, D. R. *Polymer* **2000**, *41*, 629–637.

McCrum, N. G.; Buckley, C. P.; Bucknall, C. B. *Principles of Polymer Engineering*; 2nd ed.; Oxford University Press: Oxford, 1997.

McHattie, J. S.; Koros, W. J.; Paul, D. R. *Polymer* **1991**, *32*, 840–850.

Middleton, W. J.; Lindsey, R. V. *J. Am. Chem. Soc.* **1964**, *86*, 4948–4952.

Mitchell, J. K. *J. Memb. Sci.* **1995**, *100*, 11–16.

Mohr, J. M.; Paul, D. R.; Tullos, G. L.; Cassidy, P. E. *Polymer* **1991**, *32*, 2387–2394.

Mondal, M. K.; Balsora, H. K.; Varshney, P. *Energy* **2012**, *46*, 431–441.

Moon, Y. D.; Lee, Y. M. *J. Appl. Polym. Sci.* **1993**, *50*, 1461–1473.

Morisato, A.; Ghosal, K.; Freeman, B. D.; Chern, R. T.; Alvarez, J. C.; de la Campa, J. G.; Lozano, A. E.; de Abajo, J. *J. Memb. Sci.* **1995**, *104*, 231–241.

Murphy, T. M.; Freeman, B. D.; Paul, D. R. *Polymer* **2013**, *54*, 873–880.

Murphy, T. M.; Langhe, D. S.; Ponting, M.; Baer, E.; Freeman, B. D.; Paul, D. R. *Polymer* **2011**, *52*, 6117–6125.

Murphy, T. M.; Offord, G. T.; Paul, D. R. In *Membrane Operations*; Drioli, E.; Giorno, L., Eds.; Wiley-VCH Verlag GmbH & Co. KGaA: Weinheim, Germany, 2009; pp. 63–82.

Muruganandam, N.; Koros, W. J.; Paul, D. R. *J. Polym. Sci. Part B Polym. Phys.* **1987**, *25*, 1999–2026.

Nagai, K.; Masuda, T.; Nakagawa, T.; Freeman, B. D.; Pinnau, I. *Prog. Polym. Sci.* **2001**, *26*, 721–798.

Nairn, K. M.; Walters, R. L.; Simon, G. P.; Hill, A. J. *Mater. Forum* **1992**, *16*, 167–172.

Nakagawa, K.; Kusuki, Y.; Ninomiya, K. *Proc. Fourth Int. Congr. Pervaporation Process. Chem. Ind.* **1989**, 250–260.

Narizuka, S.; Hagiwara, Y.; Nagamori, M.; Yamanaka, K. Novel Fluoroine-Containing Dicarboxylic Acids and Their Novel Polymer Compounds. US 2009/0030173 A1, 2009.

Nguyen, H. K.; Labardi, M.; Capaccioli, S.; Lucchesi, M.; Rolla, P.; Prevosto, D. *Macromolecules* **2012**, *45*, 2138–2144.

Nollet, J. A. *J. Memb. Sci.* **1995**, *100*, 1–3.

Odian, G. *Principles of Polymerization*; 4th ed.; John Wiley & Sons, Inc.: Hoboken, 2004.

Ohya, H.; Kudryavtsev, V. V.; Semenova, S. I. *Polyimide Membranes: Applications, Fabrications, and Properties*; Kodansha LTD. and Gordon and Breach Science Publishers S. A.., 1996.

Osora, H.; Seiki, Y.; Yukumoto, A.; Yukio, T.; Ogino, S.; Hiroshima-Ken, M. Membrane system for the dehydration of solvents. EP 2 263 783 A1, 2010.

Pan, C. Y.; Jensen, C.; Bielech, C.; Habgood, H. *J. Appl. Polym. Sci.* **1978**, *22*, 2307–2323.

Park, H. B.; Han, S. H.; Jung, C. H.; Lee, Y. M.; Hill, A. J. *J. Memb. Sci.* **2010**, *359*, 11–24.

Park, H. B.; Jung, C. H.; Lee, Y. M.; Hill, A. J.; Pas, S. J.; Mudie, S. T.; Van Wagner, E.; Freeman, B. D.; Cookson, D. J. *Science* **2007**, *318*, 254–258.

Patel, V. M.; Patel, K. C.; Patel, R. D. *Die Makromol. Chemie* **1978**, *179*, 2531–2539.

Paul, D. R. In *Comprehensive Membrane Science and Engineering, Volume 1*; Drioli, E.; Giorno, L., Eds.; Elsevier B.V., 2010; Vol. 1, pp. 75–90.

Pfromm, P.; Koros, W. J. *Polymer*, 1995, *36*, 2379–2387.

Pixton, M. R.; Paul, D. R. In *Polymeric Gas Separation Membranes*; Paul, D. R.; Yampolskii, Y. P., Eds.; CRC Press: Boca Raton, Fl, 1994; pp. 83–153.

Priestley, R. D. *Soft Matter* **2009**, *5*, 919.

Priestley, R. D.; Broadbelt, L. J.; Torkelson, J. M. *Macromolecules* **2005**, *38*, 654–657.

Priestley, R. D.; Rittigstein, P.; Broadbelt, L. J.; Fukao, K.; Torkelson, J. M. *J. Phys. Condens. Matter* **2007**, *19*, 205120–205132.

Principles and Applications of Thermal Analysis; Gabbot, P., Ed.; 1st ed.; Blackwell Publishing: Oxford, 2008.

Prodpran, T. *Polymer* **2002**, *43*, 2295–2309.

Puleo, A. C.; Paul, D. R.; Kelley, S. S. *J. Memb. Sci.* **1989**, *47*, 301–332.

Pye, J. E.; Rohald, K. A.; Baker, E. A.; Roth, C. B. *Macromolecules* **2010**, *43*, 8296–8303.

Pye, J. E.; Roth, C. B. *Macromolecules* **2013**, *46*, 9455–9463.

Qiu, Z.; Wang, J.; Zhang, Q.; Zhang, S.; Ding, M.; Gao, L. *Polymer* **2006**, *47*, 8444–8452.

Read, B. E.; Tomlins, P. E.; Dean, G. D. *Polymer* **1990**, *31*, 1204–1215.

Ribeiro Jr., C. P.; Borges, C. P. *Brazilian J. Chem. Eng.* **2004**, *21*, 629 – 640.

Robertson, C. G.; Monat, J. E.; Wilkes, G. L. *J. Polym. Sci., Part B Polym. Phys.* **1999**, *37*, 1931–1946.

Robeson, L. M. *J. Memb. Sci.* **1991**, *62*, 165–185.

Robeson, L. M. *J. Memb. Sci.* **2008**, *320*, 390–400.

Robeson, L. M.; Smith, Z. P.; Freeman, B. D.; Paul, D. R. *J. Memb. Sci.* **2014**, *453*, 71–83.

Roth, C. B.; Dutcher, J. R. *J. Electroanal. Chem.* **2005**, *584*, 13–22.

Rowe, B. W.; Freeman, B. D.; Paul, D. R. *Polymer* **2009**, *50*, 5565–5575.

Rowe, B. W.; Freeman, B. D.; Paul, D. R. *Polymer* **2010**, *51*, 3784–3792.

Rowe, B. W.; Pas, S. J.; Hill, A. J.; Suzuki, R.; Freeman, B. D.; Paul, D. R. *Polymer* **2009**, *50*, 6149–6156.

Sada, E.; Kumazawa, H.; Wang, J.-S.; Koizumi, M. *J. Appl. Polym. Sci.* **1992**, *45*, 2181–2186.

Sada, E.; Kumazawa, H.; Xu, P.; Wang, S. T. *J. Polym. Sci. Part B Polym. Phys.* **1990**, *28*, 113–125.

Sada, E.; Kumazawa, H.; Yoshio, Y.; Wang, S. T.; Xu, P. *J. Polym. Sci. Part B Polym. Phys.* **1988**, *26*, 1035–1048.

Sanders, D. F.; Guo, R.; Smith, Z. P.; Liu, Q.; Stevens, K. a.; McGrath, J. E.; Paul, D. R.; Freeman, B. D. *Polymer* **2014**, *55*, 1636–1647.

Sanders, D. F.; Guo, R.; Smith, Z. P.; Stevens, K. A.; Liu, Q.; McGrath, J. E.; Paul, D. R.; Freeman, B. D. *J. Memb. Sci.* **2014**, *In Press*.

Sanders, D. F.; Smith, Z. P.; Guo, R.; Robeson, L. M.; McGrath, J. E.; Paul, D. R.; Freeman, B. D. *Polymer* **2013**, *54*, 4729–4761.

Sanders, D. F.; Smith, Z. P.; Ribeiro, C. P.; Guo, R.; McGrath, J. E.; Paul, D. R.; Freeman, B. D. *J. Memb. Sci.* **2012**, *409-410*, 232–241.

Sanders, E. S. *Annu. Conv. Proc. - Gas Process. Assoc.* **2004**, *83*, 270–312.

Sanders, E. S. *Annu. Conv. Proc. - Gas Process. Assoc.* **2004**, *83*, 270–312.

Sanders, E. S. *J. Memb. Sci.* **1988**, *37*, 63–80.

Saracco, G.; Vesteeg, G. F.; van Swaaij, W. P. M. *J. Memb. Sci.* **1994**, *95*, 105–123.

Scientific Instruments Training Institute: Fundamentals of Analysis Manual; ThermoScientific.

Shao, L.; Chung, T.; Goh, S.; Pramoda, K. *J. Memb. Sci.* **2005**, *256*, 46–56.

Shao, P.; Huang, R. Y. M. *J. Memb. Sci.* **2007**, *287*, 162–179.

Shimazu, A.; Miyazaki, T.; Matsushita, T.; Maeda, M.; Ikeda, K. *J. Polym. Sci. Part B Polym. Phys.* **1999**, *37*, 2941–2949.

Shindo, R.; Amanuma, S.; Kojima, K.; Sato, S.; Kanehashi, S.; Nagai, K. *Polym. Eng. Sci.* **2013**.

Simon, S. L.; Park, J.-Y.; McKenna, G. B. *Eur. Phys. J. E. Soft Matter* **2002**, *8*, 209–216.

Sissine, F. *Energy Independence and Security Act of 2007: a summary of major provisions*; Library of Congress: Washington, 2007.

Smith, Z. P.; Sanders, D. F.; Ribeiro, C. P.; Guo, R.; Freeman, B. D.; Paul, D. R.; McGrath, J. E.; Swinnea, S. *J. Memb. Sci.* **2012**, *415-416*, 558–567.

Snow, A. W.; Sprague, L. G.; Soulen, R. L.; Grate, J. W.; Wohltjen, H. *J. Appl. Polym. Sci.* **1991**, *43*, 1659–1671.

Sridhar, S.; Smitha, B.; Aminabhavi, T. M. *Sep. Purif. Rev.* **2007**, *36*, 113–174.

Stannett, V. T.; Koros, W. J.; Paul, D. R.; Lonsdale, H. L.; Baker, R. W. In *Advances in Polymer Science*; Advances in Polymer Science; Springer Berlin Heidelberg: Berlin, Heidelberg, 1979; Vol. 32, pp. 69–121.

Stannett, V.; Szwarc, M. *J. Polym. Sci.* **1955**, *16*, 89–91.

Stern, S. A. *J. Memb. Sci.* **1994**, *94*, 1–65.

Struik, L. C. E. *Physical Aging in Amorphous Polymers and Other Materials*; Elsevier Scientific Publishing Company: Amsterdam, The Netherlands, 1978; Vol. 54.

Struik, L. C. E. *Polymer* **1987**, *28*, 1521–1533.

Struik, L. C. E. *Polymer* **1987**, *28*, 1534–1542.

Struik, L. C. E. *Polymer* **1989**, *30*, 799–814.

Struik, L. C. E. *Polymer* **1989**, *30*, 815–830.

Sturgill, G. K.; Stanley, C.; Rezac, M. E.; Beckham, H. W. *Macromolecules* **2001**, *34*, 8730–8734.

Tanaka, K.; Ito, M.; Kita, H.; Okamoto, K.; Ito, Y. *Bull. Chem. Soc. Jpn.* **1995**, *68*, 3011–3017.

Tant, M. R.; Wilkes, G. L. *J. Appl. Polym. Sci.* **1981**, *26*, 2813–2825.

Tompkins, H. G.; McGahan, W. A. *Spectroscopic Ellipsometry and Relectometry*; John Wiley & Sons, Inc.: New York, 1999.

Tullos, G.; Mathias, L. *Polymer* **1999**, *40*, 3463–3468.

Van Krevelen, D. W. *Properties of Polymers: Their Correlation with Chemical Structure; Their Numerical Estimation and Prediction from Additive Group Contributions*; 3rd ed.; Elsevier: Amsterdam, 1990.

Vane, L. M.; Alvarez, F. R.; Huang, Y.; Baker, R. W. *J. Chem. Technol. Biotechnol.* **2009**, *85*, 502–511.

Vankelecom, I. F. J. *Chem. Rev.* **2002**, *102*, 3779–3810.

Wang, X.-Y.; in't Veld, P. J.; Lu, Y.; Freeman, B. D.; Sanchez, I. C. *Polymer* **2005**, *46*, 9155–9161.

White, L. S. In *Membrane Gas Separation*; Yampolskii, Y.; Freeman, B., Eds.; John Wiley & Sons, Ltd: Chichester, UK, 2010; pp. 313–332.

Wijmans, J.; Baker, R. W. *J. Memb. Sci.* **1995**, *107*, 1–21.

Wind, J. D.; Paul, D. R.; Koros, W. J. *J. Memb. Sci.* **2004**, *228*, 227–236.

Wonders, A.; Paul, D. R. *J. Memb. Sci.* **1979**, *5*, 63–75.

Xiao, S.; Feng, X.; Huang, R. Y. M. *Macromol. Chem. Phys.* **2007**, *208*, 2665–2676.

Xu, W.; Paul, D. R.; Koros, W. J. *J. Memb. Sci.* **2003**, *219*, 89–102.

Yampol'skii, Y. P.; Volkov, V. V. *J. Memb. Sci.* **1991**, *64*, 191–228.

Yampolskii, Y. P. *Macromolecules* **2012**, *45*, 3298–3311.

Yang, X.; Painter, P. C.; Coleman, M. M.; Pearce, E. M.; Kwei, T. K. *Macromolecules* **1992**, *25*, 2156–2165.

Zugenmaier, P. *Macromol. Symp.* **2004**, *208*, 81–166.

Vita

Katrina Marie Czenkusch grew up just north of Austin in Round Rock, Texas. She graduated from Round Rock High School in 2003 and moved on to Texas Lutheran University. At TLU, she spent her summers doing research in the chemistry department. In 2007, she acquired a Bachelors of Science in Chemistry with minors in Math and the Business of Science. In the fall of 2007, Katrina began pursuing her Ph.D. in Chemical Engineering at the University of Texas at Austin. She graduated in May 2014. Katrina will pursue a career at Celanese with their Technology and Innovation Leadership Program.

Permanent Email: czenkusch@gmail.com

This dissertation was typed by the author.